AD-A123 630 CERTAIN EFFECTS OF PLASMA JETTING ACROSS AND ALONG MAGNETIC FIELDS(U) JAYCOR SAN DIEGO CA J L SPERLING ET AL. 30 APR 81 JAYCOR-J510-81-028 1/2

UNCLASSIFIED DNA-5740F DNA001-79-C-0050 F/G 4/1 NL

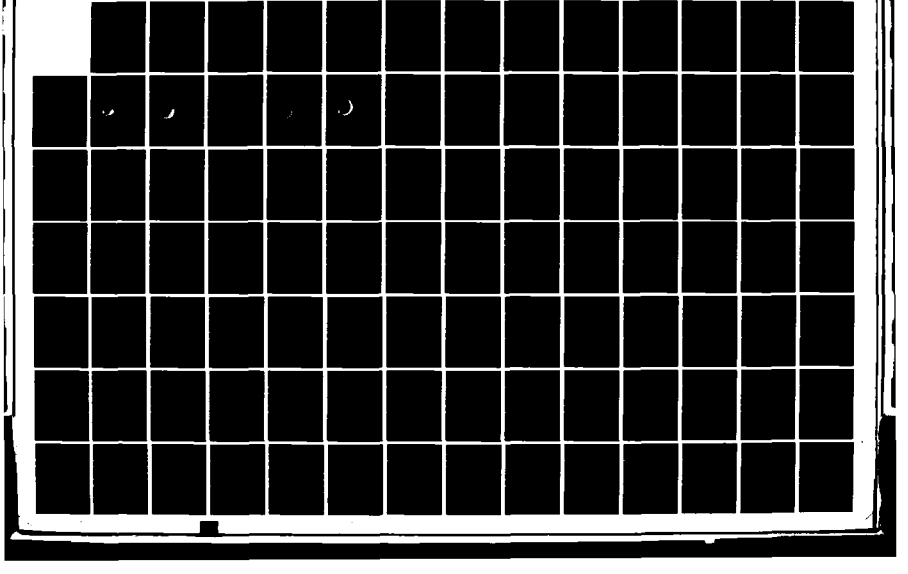

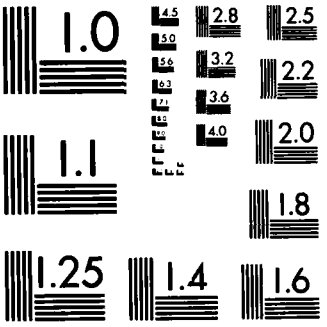

(12)

DNA 5740F

CERTAIN EFFECTS OF PLASMA JETTING ACROSS AND ALONG MAGNETIC FIELDS

J. L. Sperling
N. A. Krall
JAYCOR
P. O. Box 85154
San Diego, California 92138

30 April 1981

Final Report for period 1 December 1978—30 April 1981

CONTRACT No. DNA 001-79-C-0050

APPROVED FOR PUBLIC RELEASE;
DISTRIBUTION UNLIMITED.

THIS WORK WAS SPONSORED BY THE DEFENSE NUCLEAR AGENCY
UNDER RDT&E RMSS CODE B322080464 S99QAXHC04124 H2590D.

Prepared for
Director
DEFENSE NUCLEAR AGENCY
Washington, DC 20305

UNCLASSIFIED

SECURITY CLASSIFICATION OF THIS PAGE (When Data Entered)

REPORT DOCUMENTATION PAGE	READ INSTRUCTIONS BEFORE COMPLETING FORM
1. REPORT NUMBER: DNA 5740F	2. GOVT ACCESSION NO.: AD A123645
	3. RECIPIENT'S CATALOG NUMBER:
4. TITLE (and Subtitle): CERTAIN EFFECTS OF PLASMA JETTING ACROSS AND ALONG MAGNETIC FIELDS	5. TYPE OF REPORT & PERIOD COVERED: Final Report for Period 1 Dec 78 — 30 Apr 81
	6. PERFORMING ORG. REPORT NUMBER: J510-81-028
7. AUTHOR(s): J. L. Sperling, N. A. Krall	8. CONTRACT OR GRANT NUMBER(s): DNA 001-79-C-0050
9. PERFORMING ORGANIZATION NAME AND ADDRESS: JAYCOR, P. O. Box 85154, San Diego, CA 92138	10. PROGRAM ELEMENT, PROJECT, TASK AREA & WORK UNIT NUMBERS: Subtask S99QAXHC041-24
11. CONTROLLING OFFICE NAME AND ADDRESS: Director, Defense Nuclear Agency, Washington, D.C. 20305	12. REPORT DATE: 30 April 1981
	13. NUMBER OF PAGES: 100
14. MONITORING AGENCY NAME & ADDRESS (if different from Controlling Office)	15. SECURITY CLASS. (of this report): UNCLASSIFIED
	15a. DECLASSIFICATION DOWNGRADING SCHEDULE: N/A since UNCLASSIFIED

16. DISTRIBUTION STATEMENT (of this Report)

Approved for public release; distribution unlimited.

17. DISTRIBUTION STATEMENT (of the abstract entered in Block 20, if different from Report)

18. SUPPLEMENTARY NOTES

This work was sponsored by the Defense Nuclear Agency under RDT&E RMSS Code B322080464 S99QAXHC04124 H2590D.

19. KEY WORDS (Continue on reverse side if necessary and identify by block number)

Early-time Striations
Striation Seeding
Plasma Jetting
Striations
Ion Resistivity
Electron Resistivity
Alfven Waves

20. ABSTRACT (Continue on reverse side if necessary and identify by block number)

We examine certain plasma effects associated with plasma jetting across and along magnetic field lines during the early-time phase of high-altitude nuclear events. It is shown that plasma jetting across the magnetic field may lead to prompt striations at higher altitudes (well in excess of four hundred kilometers) following a STARFISH type of nuclear burst. Superthermal ions with velocities less than the maximum velocity can participate in the striation formation. It is also demonstrated that ions and electrons

DD FORM 1 JAN 73 1473 EDITION OF 1 NOV 65 IS OBSOLETE

UNCLASSIFIED

SECURITY CLASSIFICATION OF THIS PAGE (When Data Entered)

20. ABSTRACT (Continued)

travelling along magnetic field lines can be pitch angle scattered by waves through a cyclotron resonance process. An example is presented which shows that ion-cyclotron resistivity caused by interaction with Alfven waves can slow the motion of oxygen ions along magnetic field lines following a nuclear burst. The implication of cyclotron resistivity is that high-energy particles deposit their energy closer to their source than would otherwise be predicted.

PREFACE

This report has benefited from discussions with Dr. Ralph Kilb, Dr. Sidney Ossakow, and Major Leon Wittwer. We appreciate the support of Major Wittwer during the course of this work.

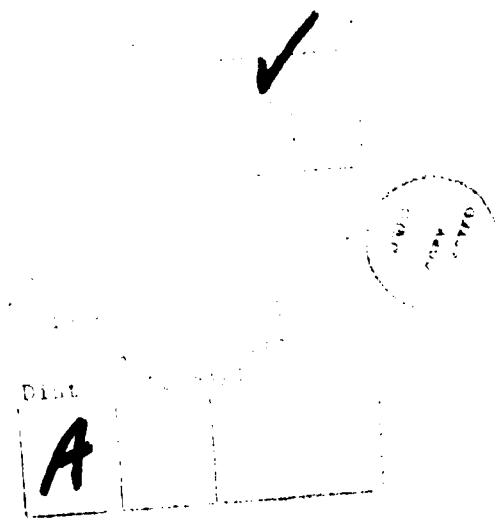

TABLE OF CONTENTS

LIST OF ILLUSTRATIONS

SECTION 1

INTRODUCTION

During the early-time evolution of high-altitude nuclear events, populations of ions form with energies in excess of 10 or even 100 keV.[1,2] Subsequently, a complex series of collisions occur in which the electric charge state of the fast ions changes while the ionization of the thermal plasma background increases. Simultaneously, as their energy degrades, the initial population of high energy ions tends to become part of the thermal plasma background. The spatial and temporal evolution of initial high energy ionized structure must impact later morphology by determining, at least in part, the initial conditions for the later fluid development. However, if chemical releases in the ionosphere are any indication, mechanisms other than collisions may also influence the evolution of high energy ion morphology in the ionosphere. For example, shaped barium injection across the magnetic field in the ionosphere has been observed to cause the formation of magnetic field aligned striations on an ion-gyrotime scale.[3,4] Called "prompt striations" in Reference 3, the structures have been attributed to a purely growing, finite ion-gyroradius, electrostatic flute instability caused by the ion loss cone velocity distribution function inherent to the shaped injection.

The primary purpose of this report is to suggest that the prompt striation phenomena can play a role in the evolution of plasma jets crossing the geomagnetic field after a high altitude nuclear explosion. In particular, for a STARFISH type of nuclear burst, prompt striations could develop at higher altitudes (i.e., well above four hundred kilometers) for superthermal ions with velocity less than the maximum ion velocity possible following a nuclear burst explosion. Another aim of this report is to point out that a cyclotron resonance mechanism can retard the motion of both ions and electrons along magnetic field lines. This cyclotron resistivity process points out a difference between high-altitude nuclear and barium cloud environments. Specifically, shaped barium injection along the ambient magnetic field lines is unaffected by the ion-cyclotron resistivity associated with Alfven waves in predominantly barium plasmas. However, 10 to 100 keV singly ionized monatomic

oxygen particles formed by high-altitude nuclear explosions and travelling along the ambient magnetic field are susceptible to cyclotron resistivity for reasonable oxygen plasma densities and wave magnetic field strength much smaller than the ambient magnetic field. The implication of cyclotron resistivity is that particle energy is deposited closer to their source than would otherwise be predicted.

The remainder of this report is divided in the following way. Section 2 applies prompt striation theory to plasma jetting across the magnetic field under high-altitude nuclear explosion conditions. Section 3 describes the cyclotron resistivity process and a comparative application of the process to high-altitude nuclear explosion and chemical release environments. Section 4 contains concluding remarks and points out areas requiring continued research. Three self-contained appendices, which support the discussion in Section 2, are attached at the end of this report. Specifically, Appendices A, B, and C discuss the effects of electron-ion collisions, background plasma density, and electromagnetic effects on the formation of prompt striations, respectively.

SECTION 2

PROMPT STRIATIONS IN THE HIGH-ALTITUDE NUCLEAR ENVIRONMENT

2.1 INTRODUCTION

Plasma jetting across the magnetic field following barium releases in the ionosphere has been observed to cause the formation of small scale-size field aligned structures on the ion-cyclotron time scale.[3,4] These structures, called prompt striations in Reference 3, could impact the high-altitude nuclear problem in several ways. First, the prompt striations have been attributed to a kinetic instability requiring finite ion-gyroradius. These instabilities are not included in fluid models of the high-altitude nuclear environment. Second, observation of the prompt striations following barium releases indicates that they are not transitory but persist for periods of time which are much longer than the time required for their formation. For example, in Avefria Dos the prompt striations are present for times much longer than one minute although they are formed within several seconds.[4] Third, the saturated state of prompt striations could provide conditions conducive to subsequent fluid growth once the high-velocity ions, which caused the original striation growth, become less energetic. Perhaps this later fluid dynamics is the reason for the prompt striation persistence referred to earlier.

In this section the prompt striation theory is applied to the high-altitude nuclear environment. Electron-ion collisions, cold background plasma and finite ion dynamic pressure all reduce the vigor of linear instability growth and promote stability. These effects are discussed fully in Appendices A, B, and C, and in References 5-7.

2.2 SUMMARY OF THE APPENDICES

In this subsection, salient results found in Appendices A, B, and C are summarized. Particular attention is given to those aspects of the prompt striation theory which have application to the high-altitude nuclear explosion environment.

The linear instability postulated to be the source of prompt striations is a purely growing, finite ion-gyroradius flute mode. The free energy for

this instability is supplied by high velocity ions crossing the ambient magnetic field. In the analysis the ion velocity distribution function is assumed to have the loss cone form:

$$f_i(\vec{v}) = \frac{v_\perp \delta^3}{2\pi\, v_o^3\, A(\delta)} \exp\left(-\frac{\delta^2 (v_\perp/v_o - 1)^2}{2}\right) h(v_{||}) \qquad (2.1)$$

with

$$A(\delta) = \left(\frac{\pi}{2}\right)^{\frac{1}{2}} \left\{(1 + \delta^2)[1 + \mathrm{erf}(\delta/\sqrt{2})] + \left(\frac{2}{\pi}\right)^{\frac{1}{2}} \delta \exp(-\delta^2/2)\right\} ,$$

$$\delta = v_o/v_i \quad . \qquad (2.2)$$

In Eqs. (2.1) and (2.2), $v_\perp$ and $v_{||}$ are the perpendicular and parallel velocities, respectively. The parameters v_o and v_i are constants which together determine mean perpendicular particle velocity and velocity spread about this mean velocity. Because the flute approximation is invoked, the dispersion relation does not depend on the precise functional form for the parallel distribution function, $h(v_{||})$, as long as

$$1 = \int_{-\infty}^{\infty} dv_{||}\, h(v_{||}) \quad . \qquad (2.3)$$

For the physical effects considered in the appendices, the dispersion relation and mode properties depend on six dimensionless parameters:

1) δ, which is a measure of the peakedness of the ion loss cone distribution function,

2) γ/Ω_i, the linear growth rate in units of the loss cone ion-gyrofrequency,

3) kv_o/Ω_i, which gives the wavenumber perpendicular to the ambient field (k) in terms of a typical ion-gyroradius, v_o/Ω_i,

4) $\nu_e/|\Omega_e|$, the electron-ion collision frequency in units of the electron-gyrofrequency,

5) $\bar{\rho}/\rho_i$, the ratio of ambient to loss cone mass density, and

6) $\beta_i \equiv (4\pi\ \rho_i\ v_o^2)/B^2$, the ratio of ion inertial to magnetic field pressure for loss cone ions with speed v_o and mass density ρ_i.

Analysis of the dispersion relation indicates that the instability can occur only in intervals of kv_o/Ω_i such that $J_0(kv_o/\Omega_i)J_1(kv_o/\Omega_i)$ is negative, where J_0 and J_1 are the ordinary Bessel functions of the first kind and order zero and one, respectively. The interval of negative J_0J_1 with smallest kv_o/Ω_i is $2.5 \lesssim kv_o/\Omega_i \lesssim 3.8$. The instability within this interval of kv_o/Ω_i is of greatest interest because it is least susceptible to stabilization by thermal spread in ion loss cone velocity distribution function, electron collisions, and cold plasma background. The separate minimum electron-ion collision, background plasma density, and β_i criterion necessary for stability are shown in Table 2.1 for $\delta = 5$ and $\delta \to \infty$. Values of $\delta = 5$ and $\delta \to \infty$ are specifically considered because the Buaro ion loss cone velocity distribution has been fitted to the $\delta = 5$ form while the most vigorous instability occurs for $\delta \to \infty$.[3,5-7]

Table 2.1. Separate minimum electron-ion collision, background plasma density, and β_i criterion necessary for stability are shown for $\delta = 5$ and $\delta \to \infty$.

	$\nu_e/\lvert\Omega_e\rvert$	$\bar{\rho}/\rho_i$	β_i
$\delta = 5$	4.2×10^{-3}	.023	0.2
$\delta \to \infty$	1.5×10^{-2}	.059	0.56

2.3 APPLICATION OF THE PROMPT STRIATION THEORY TO THE HIGH-ALTITUDE NUCLEAR ENVIRONMENT

In real situations, a variety of stabilization mechanisms can act simultaneously to limit the growth of structure. The purpose of this subsection is to determine the role of electron-ion collision, cold plasma background, and finite ion inertia stabilization in relation to prompt striation formation under high-altitude nuclear explosion conditions. Microfiche data from a Mission Research Corporation simulation of STARFISH is used in the discussion.[1]

First the electron-ion collision and the ion inertia criterion are related to one another and then compared. Reference 8 shows that $\nu_e/|\Omega_e|$ has the following form:

$$\nu_e/|\Omega_e| = \frac{\lambda}{6}\left(\frac{\beta_i\, m_e/m_i}{2\pi^3}\right)^{\frac{1}{2}} \frac{c/v_o}{n_e\, \lambda_D^3} \tag{2.4}$$

with λ the Coulomb logarithm, m_e/m_i electron to ion mass ratio, c the speed of light, n_e the density of loss cone electrons or ions, and λ_D the electron Debye length. In Eq. (2.4) ions have been assumed to be singly charged. For oxygen ions, $\lambda \approx 20$, and $v_o \approx 1 \times 10^8$ cm/sec, Eq. (2.4) becomes

$$\frac{\nu_e}{|\Omega_e|} \approx .74\, \frac{\beta_i^{\frac{1}{2}}}{n_e\, \lambda_D^3} \quad . \tag{2.5}$$

Now in a plasma $n_e\, \lambda_D^3 >> 1$. For example, if $n_e = 1 \times 10^6$ cm^{-3} and $T_e > 1$ eV, $n_e\, \lambda_D^3 > 4.1 \times 10^5$, while if $n_e = 1 \times 10^8$ cm^{-3} and $T_e > 1$ eV, $n_e\, \lambda_D^3 \approx 4.1 \times 10^4$. Moreover, $\beta_i < 0.56$ for instability. It then follows from Eq. (2.5) that electron-ion collisional stabilization is unimportant compared to finite ion inertia stabilization under early-time high altitude nuclear explosion conditions. Even if v_o is 1×10^6 cm/sec rather than 1×10^8 cm/sec, finite ion inertia stabilization would generally take precedence.

Consider singly ionized oxygen ions with $v_o = 1 \times 10^8$ cm/sec. From Table 2.1 it follows that the ion inertia constraint permits instability for oxygen loss cone ion densities satisfying:

$$n_i \lesssim \begin{cases} 6 \times 10^4 \quad B^2 \quad cm^{-3} \quad , \quad \delta = 5 & (2.6a) \\ 1.7 \times 10^5 \quad B^2 \quad cm^{-3} \quad , \quad \delta \to \infty \quad . & (2.6b) \end{cases}$$

In Eqs. (2.6a) and (2.6b), the magnetic field strength is in units of gauss. Also, Eqs. (2.6a) and (2.6b) and Table 2.1 imply that instability requires cold background oxygen ion densities satisfying:

$$\bar{n} \lesssim \begin{cases} 1.4 \times 10^3 \quad B^2 \quad cm^{-3} \quad , \quad \delta = 5 & (2.7a) \\ 1.0 \times 10^4 \quad B^2 \quad cm^{-3} \quad , \quad \delta \to \infty \quad . & (2.7b) \end{cases}$$

Figures 2.1 - 2.8 are taken from microfiche provided by Reference 1 and represent relevant output from the simulation of STARFISH. The combination of these figures and Eqs. (2.6) and (2.7) suggests that high velocity, $v_o \approx 1 \times 10^8$ cm/sec, ions are not likely to be the source of prompt striations in high-altitude nuclear events like STARFISH for three reasons. First, at low altitude both the plasma density and magnetic field strength are largest. However, the maximum magnetic field strength in the blast wave is roughly 1 gauss while the electron number density at these locations is greater than 1×10^5 cm^{-3}. Second, at higher altitudes the magnetic field strength is approximately 0.3 gauss while the electron density exceeds 3×10^3 cm^{-3} where ion velocity is 1×10^8 cm/sec. If cold plasma number density is greater than 1.3×10^2 cm^{-3} for $\delta = 5$ or 9×10^2 for $\delta \to \infty$, instability is impossible. Such cold plasma number densities seem likely. Third, at approximately two seconds mean ion velocity is less than 1×10^8 cm/sec (see Figure 2.8).

To circumvent the finite ion inertia stabilization which is so effective when the magnetic field is weak and the ion velocity is large, it is necessary to consider whether prompt striation formation might be easier if the ion velocity is reduced. For example, if $v_o = 1 \times 10^6$ cm/sec for singly ionized oxygen, then finite ion inertia and cold plasma stabilization imply that

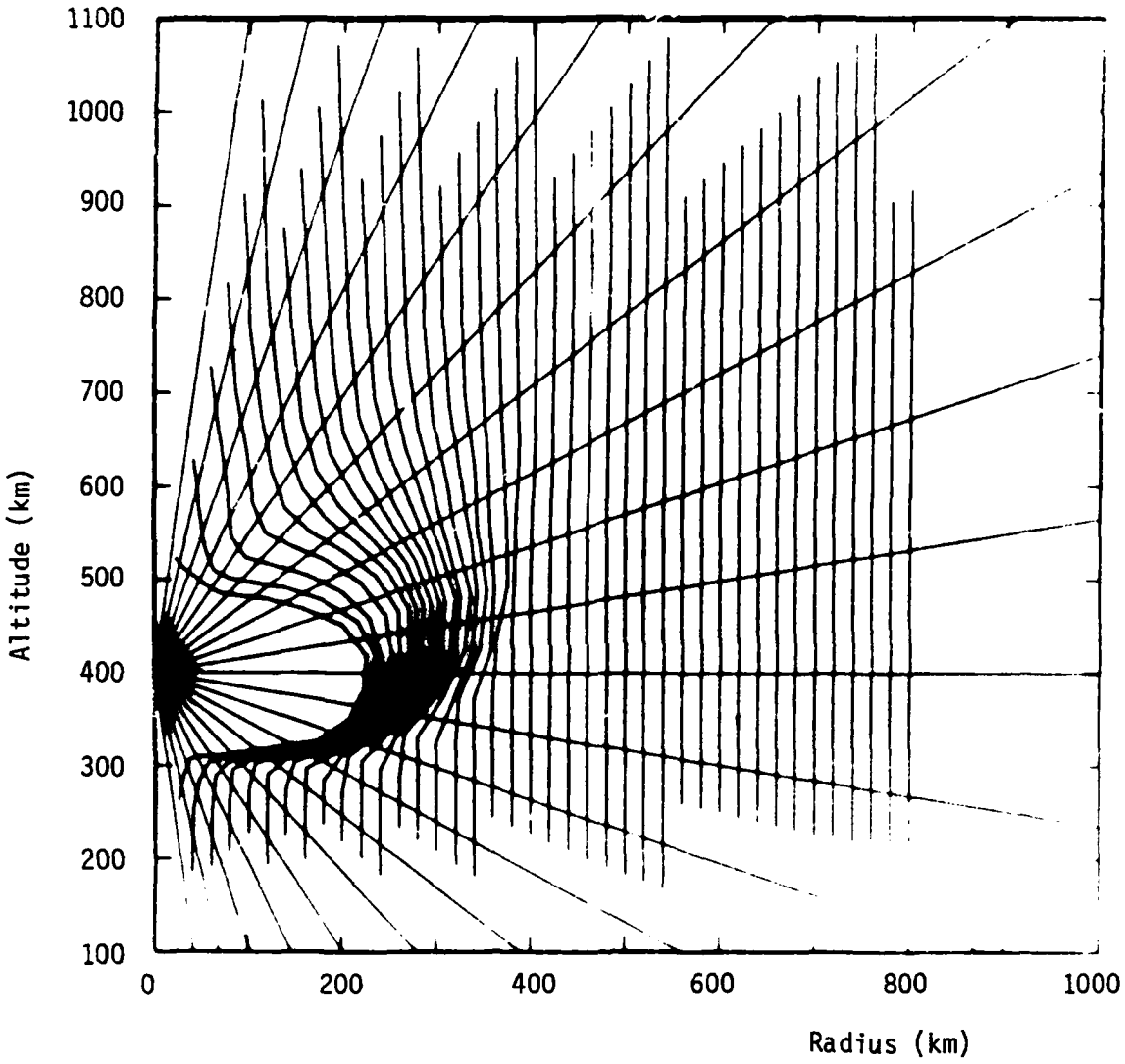

Figure 2.1. Magnetic field line geometry at 150.2 milliseconds for the STARFISH VER238 simulation

A = 1.0E-01	F = 5.0E-01
B = 2.0E-01	G = 6.0E-01
C = 2.5E-01	H = 8.0E-01
D = 3.5E-01	I = 1.0E+00
E = 4.0E-01	J = 1.2E+00

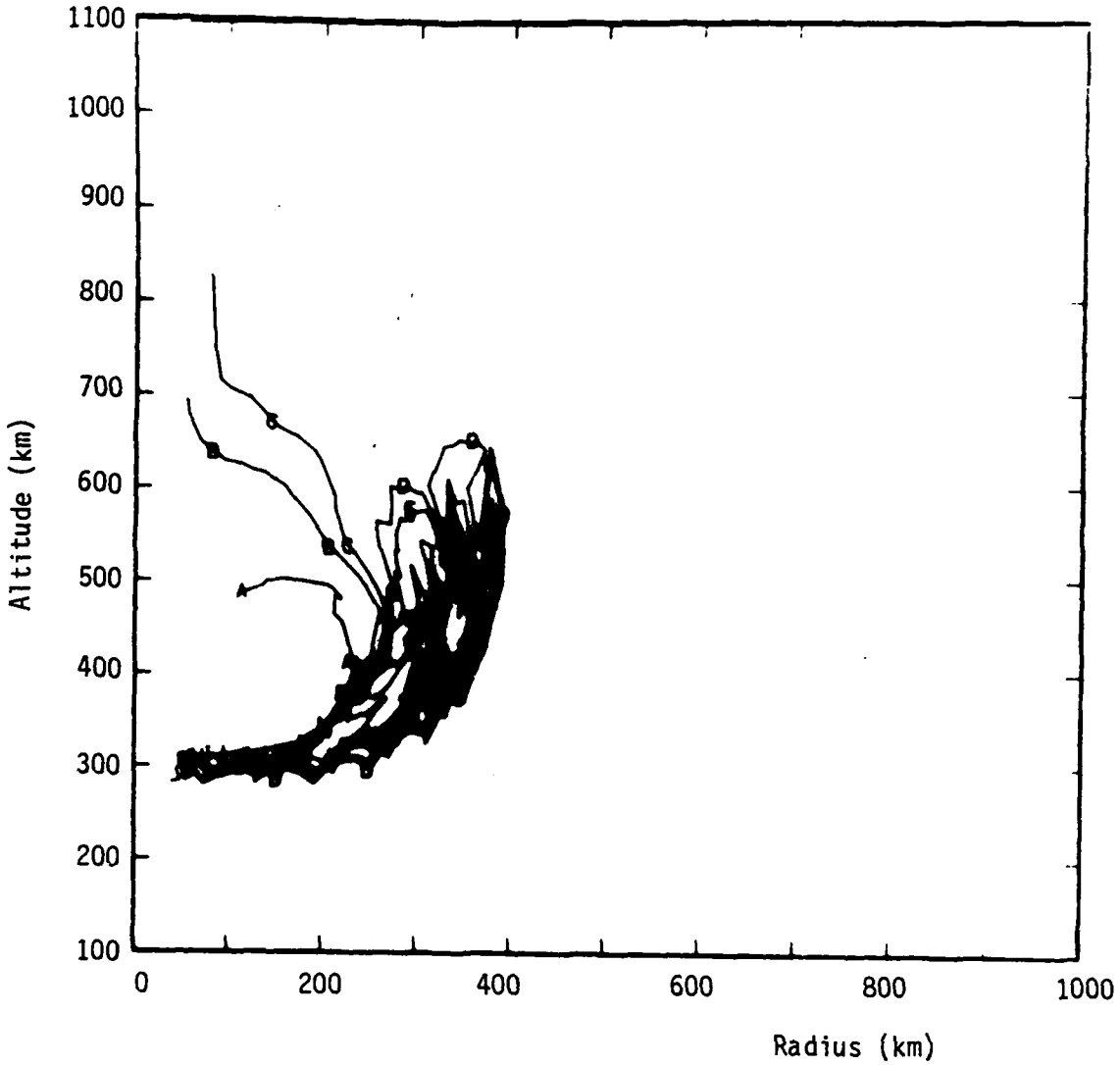

Figure 2.2. Magnetic field strength (gauss) at 150.2 milliseconds for the STARFISH VER238 simulation

A = 1.0E+03
B = 3.0E+03
C = 1.0E+04
D = 3.0E+04
E = 1.0E+05
F = 3.0E+05
G = 1.0E+06
H = 3.0E+06
I = 1.0E+07
J = 3.0E+07
K = 1.0E+08
L = 3.0E+08

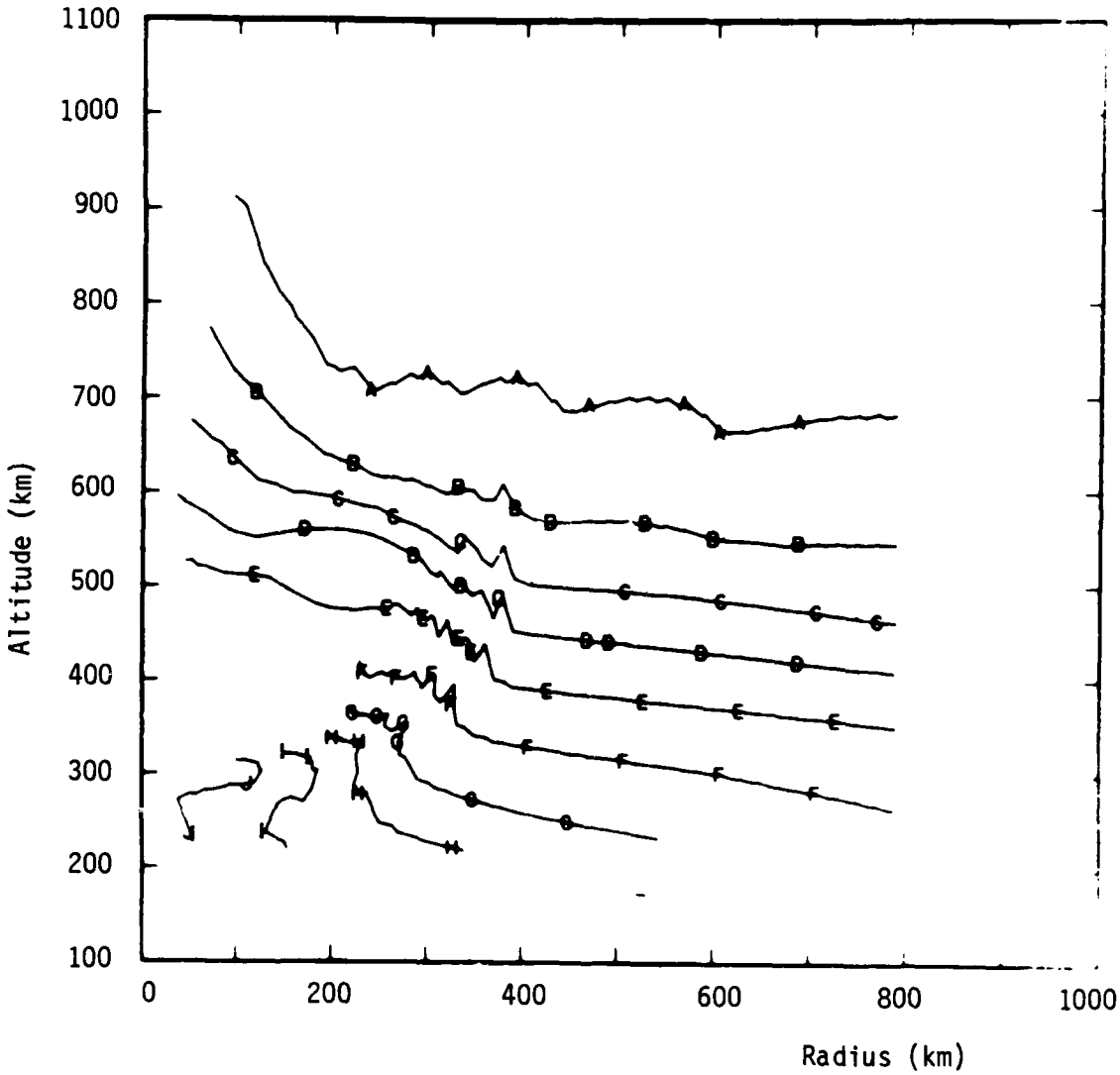

Figure 2.3. Electron number density (cm^{-3}) at 150.2 milliseconds for the STARFISH VER238 simulation

A = 1.0E+06	F = 7.0E+07
B = 3.0E+06	G = 1.0E+08
C = 7.0E+06	H = 2.0E+08
D = 1.0E+07	I = 3.0E+08
E = 3.0E+07	J = 4.0E+08

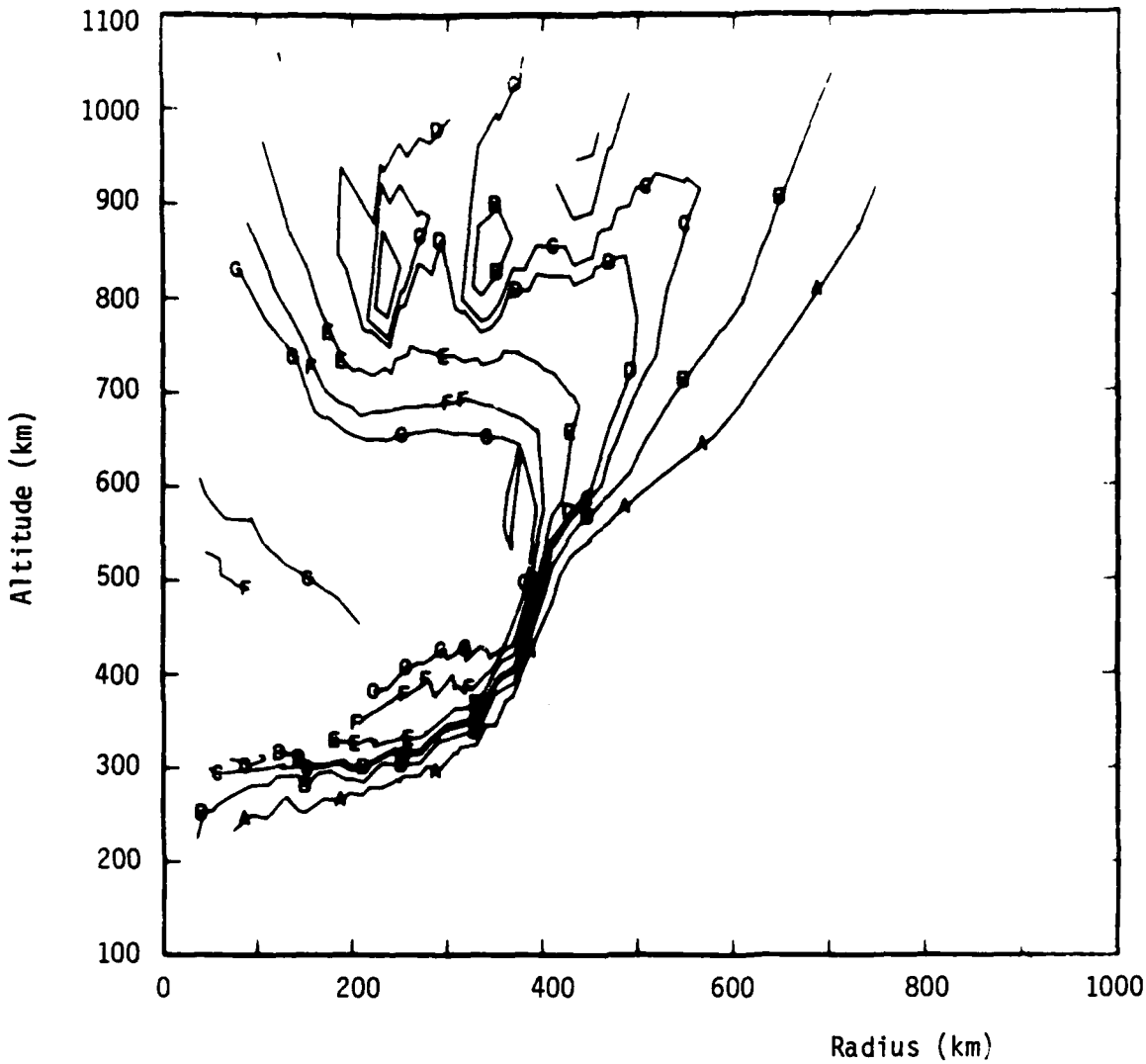

Figure 2.4. Mean ion velocity (cm/sec) at 150.2 milliseconds for the STARFISH VER238 simulation

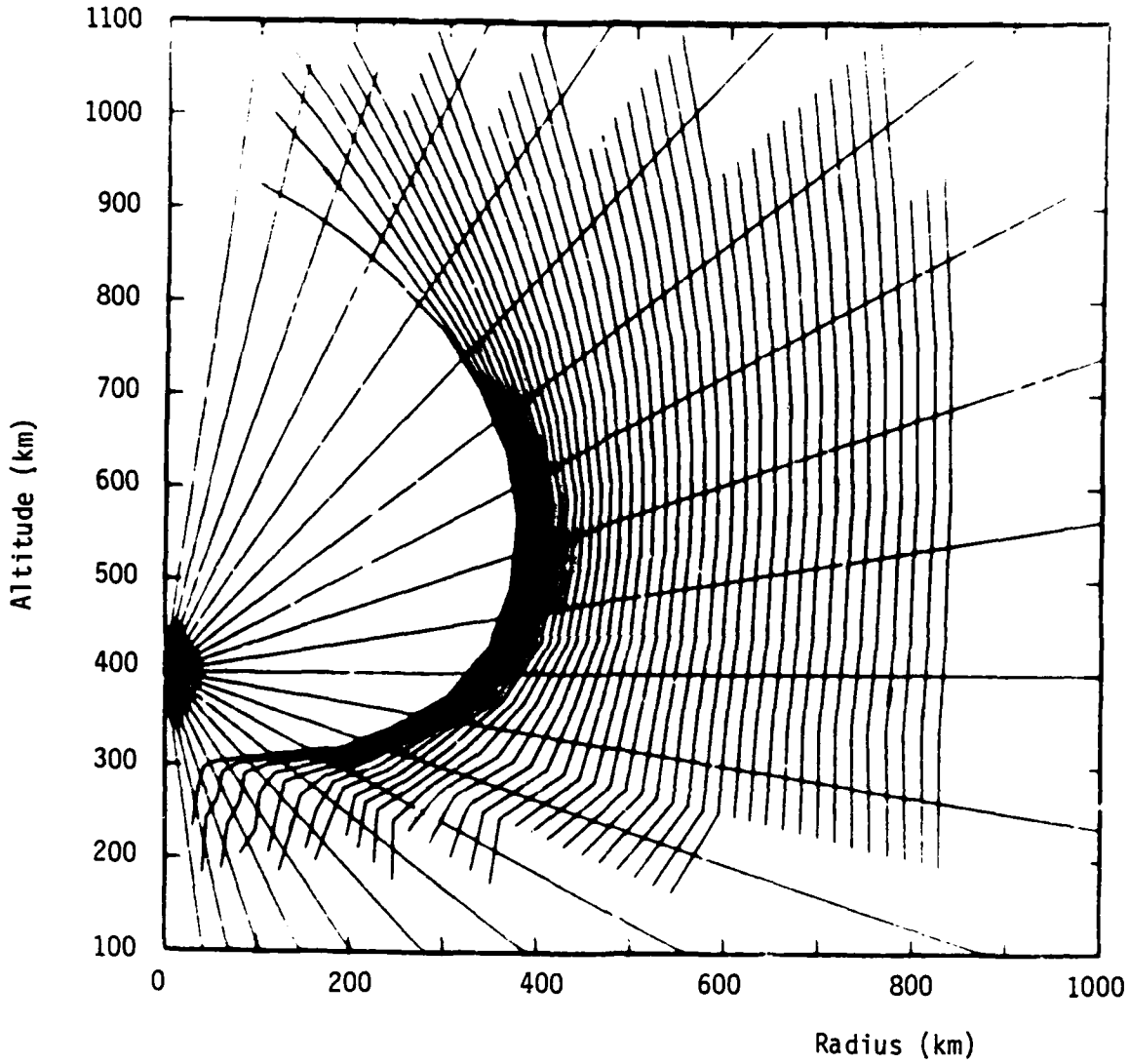

Figure 2.5. Magnetic field line geometry at 2000.7 milliseconds for the STARFISH VER238 simulation

A = 1.0E-01
B = 2.0E-01
C = 2.5E-01
D = 3.5E-01
E = 4.0E-01
F = 5.0E-01
G = 6.0E-01
H = 8.0E-01
I = 1.0E+00
J = 1.2E+00

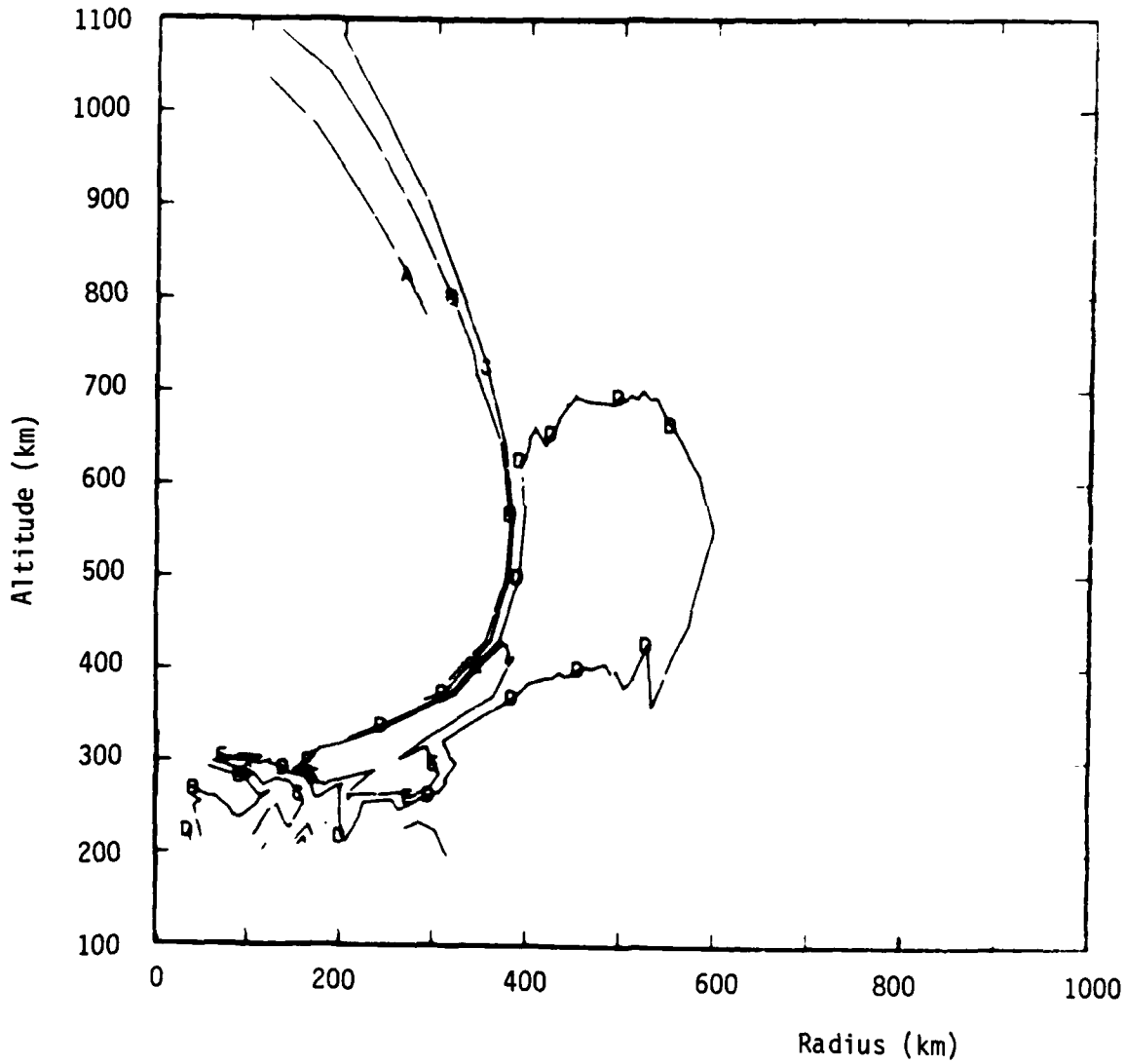

Figure 2.6. Magnetic field strength (gauss) at 2000.7 milliseconds for the STARFISH VER238 simulation

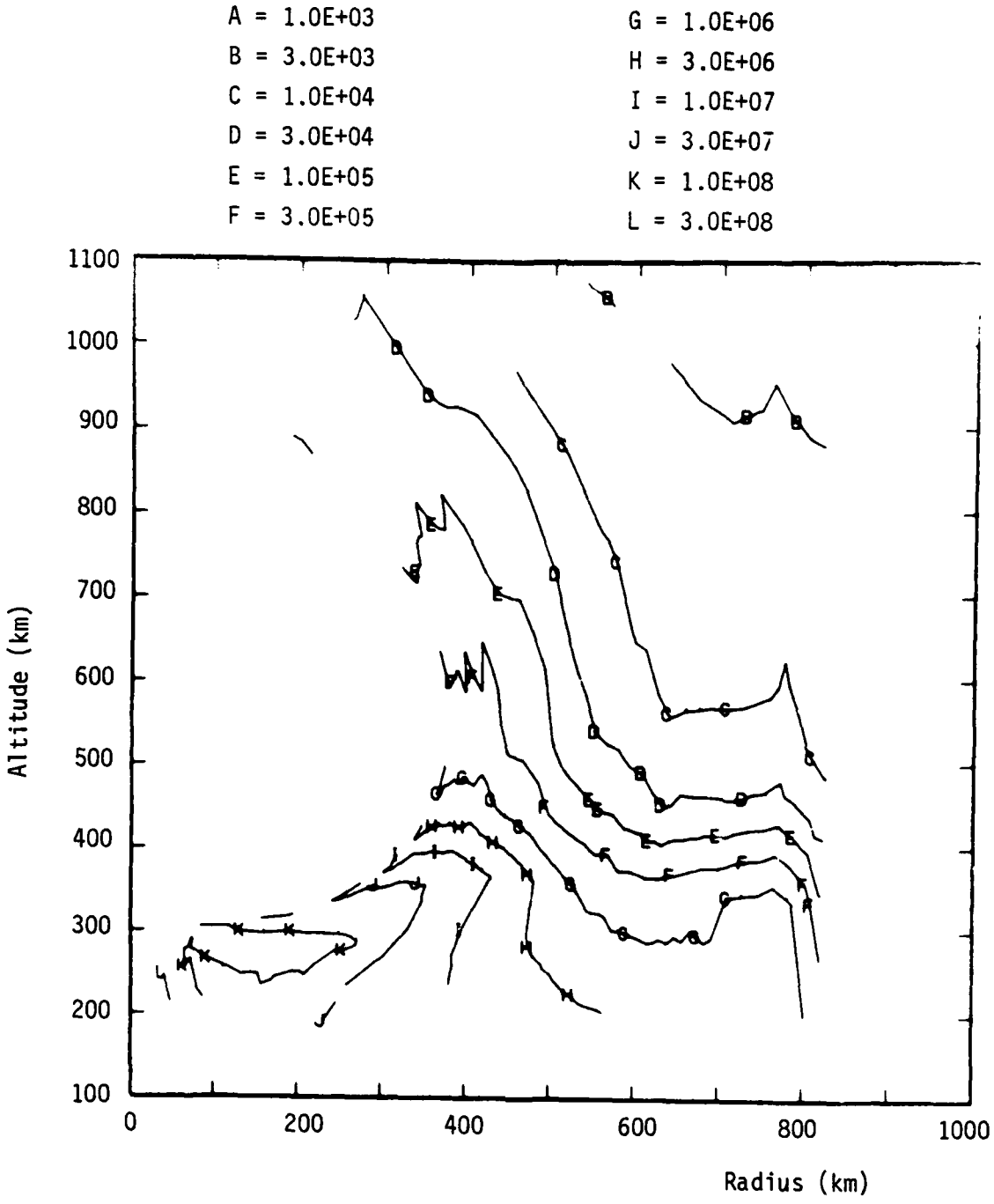

Figure 2.7. Electron number density (cm^{-3}) at 2000.7 milliseconds for the STARFISH VER238 simulation

A = 1.0E+06	F = 7.0E+07
B = 3.0E+06	G = 1.0E+08
C = 7.0E+06	H = 2.0E+08
D = 1.0E+07	I = 3.0E+08
E = 3.0E+07	J = 4.0E+08

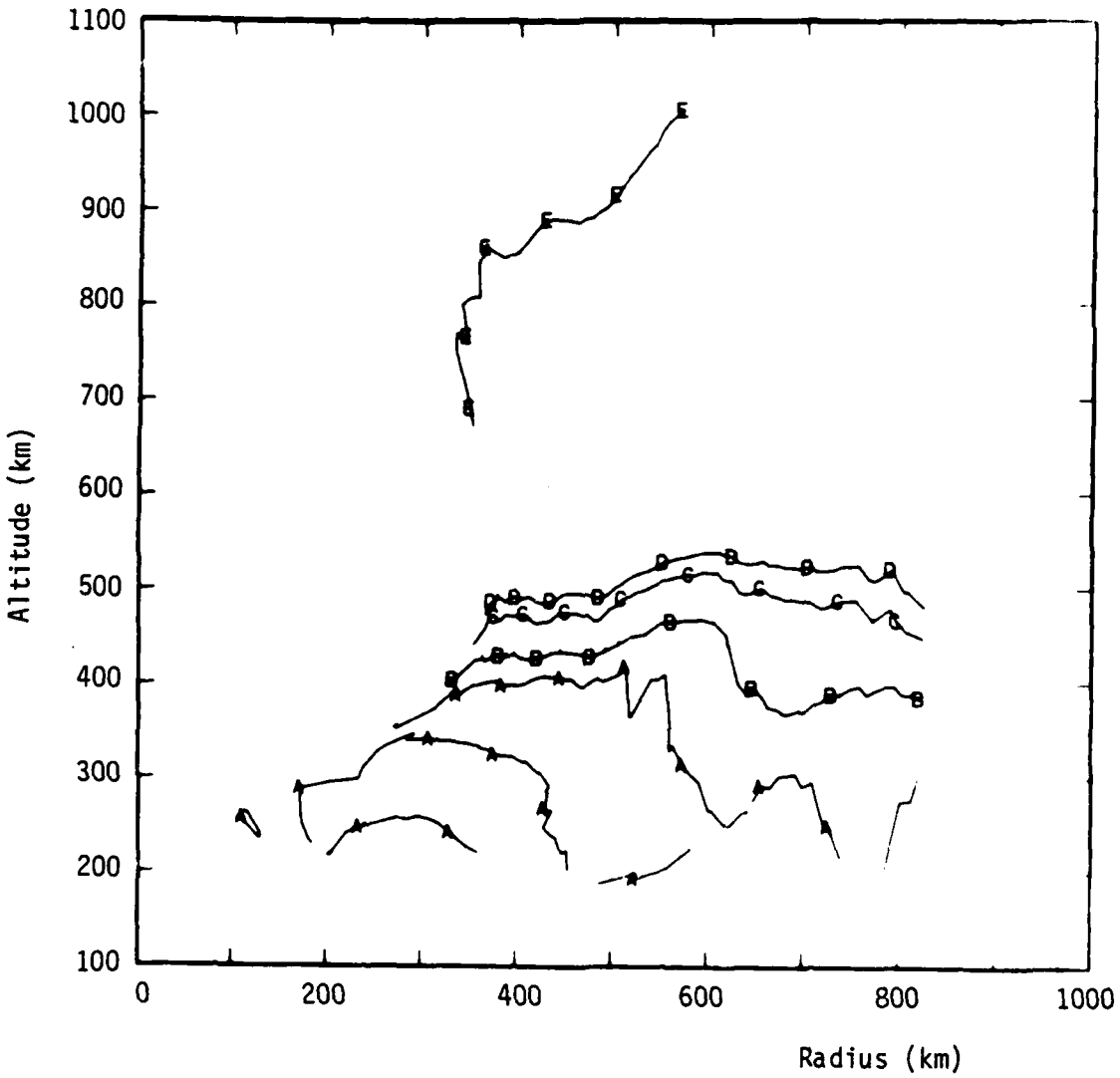

Figure 2.8. Mean ion velocity (cm/sec) at 2000.7 milliseconds for the STARFISH VER238 simulation

$$n_i \lesssim \begin{cases} 6 \times 10^6 \quad B^2 \quad cm^{-3} \quad , & \delta = 5 \qquad (2.8a) \\ 1.7 \times 10^7 \quad B^2 \quad cm^{-3} \quad , & \delta \to \infty \qquad (2.8b) \end{cases}$$

and

$$\bar{n} \lesssim \begin{cases} 1.4 \times 10^5 \quad B^2 \quad cm^{-3} \quad , & \delta = 5 \qquad (2.9a) \\ 1.0 \times 10^6 \quad B^2 \quad cm^{-3} \quad , & \delta \to \infty \quad . \qquad (2.9b) \end{cases}$$

Clearly, Eqs. (2.8) and (2.9) are more easily satisfied than Eqs. (2.6) and (2.7) appropriate to $v_o = 1 \times 10^8$ cm/sec loss cone ions. Furthermore, Figures 2.3 and 2.7 show that plasma density generally decreases with increasing altitudes. Hence, prompt striations are not likely to develop from the highest energy ions at low altitude, below 400 kilometers, but rather from ions with more modest energies at higher altitudes, well above 400 kilometers.

SECTION 3

ION AND ELECTRON CYCLOTRON RESISTIVITY

3.1 INTRODUCTION

In space and laboratory plasmas, electric fields and wave particle processes can cause the formation of a superthermal electron or ion population whose momentum is aligned primarily along the ambient magnetic field lines. Despite the inability of classical resistivity to counter the acceleration of these fast particles under many circumstances, plasma mechanisms exist which tend to impede acceleration along magnetic field lines to infinite energies. Landau damping of bump-in-the-tail instabilities is an example of such an anomalous resistive plasma process.[9] Also, in strongly magnetized plasmas with the electron-cyclotron frequency smaller than the electron plasma frequency, the anomalous electron-cyclotron resonance can markedly inhibit the motion of fast electrons along the ambient magnetic field.[10-12]

The cyclotron resonance process is shown to be an effective anomalous resistivity mechanism for ions as well as electrons in both strongly and weakly magnetized plasmas if two conditions are satisfied. First, it is necessary that the wave frequency be smaller than the relativistically correct gyrofrequency. In fact, strong anomalous resistivity can occur for waves with frequency approaching zero although energy transfer between waves and particles occurs on a much slower time scale. Second, the wave electric and magnetic fields perpendicular to the ambient magnetic field must have an appreciable wavenumber parallel to the ambient field which satisfies the cyclotron resonance condition. An implication of the theory is that cyclotron resistivity requires shorter parallel wavelengths for strongly magnetized plasmas than for weakly magnetized plasmas.

Examples of cyclotron resistivity are presented which emphasize ionospheric applications; however, the theory also has wider application to space and laboratory plasmas. Shaped barium injection along the ambient magnetic field is demonstrated to be unaffected by the ion-cyclotron resistivity process with Alfven waves in predominantly barium plasmas for reasonable barium densities in the ionosphere.[3,13-14] However, 10 to 100 keV singly ionized monatomic

oxygen particles travelling along the ambient magnetic field are shown to be susceptible to cyclotron resistivity for reasonable oxygen plasma densities and wave magnetic field strength much smaller than the ambient magnetic field. Such high energy ions can result from high-altitude nuclear events[1,2] as well as geophysical processes.[15,16]

3.2 THEORETICAL MODEL FOR CYCLOTRON RESISTIVITY

To demonstrate the cyclotron resistivity process, we use an infinite, homogeneous, relativistically correct quasilinear diffusion model. In particular,[17]

$$\frac{\partial f(p_\perp,p_\parallel)}{\partial t} = \sum_k \sum_{n=-\infty}^{\infty} Q_{k,n}(p_\perp,p_\parallel) \tag{3.1}$$

with

$$Q_{k,n}(p_\perp,p_\parallel) = \frac{\pi}{2}\left(\frac{q}{\omega}\right)^2 \left(\frac{1}{p_\perp}\frac{\partial}{\partial p_\perp} n\Omega + \frac{\partial}{\partial p_\parallel}\frac{k_\parallel}{m}\right)(|\theta|/\gamma)^2\, \delta(\omega - n\Omega/\gamma$$

$$- k_\parallel p_\parallel/m\gamma)\left(\frac{n\Omega}{p_\perp}\frac{\partial}{\partial p_\perp} + \frac{k_\parallel}{m}\frac{\partial}{\partial p_\parallel}\right) f(p_\perp,p_\parallel) \quad ,$$

$$|\theta|^2 = \Big| p_\perp J_{n-1}(b)\exp(-i\psi)\, E_+ + p_\perp J_{n+1}(b)$$

$$\exp(i\psi)\, E_- + (2)^{\frac{1}{2}} p_\parallel J_n(b)\, E_\parallel \Big|^2 \quad ,$$

$$\vec{k} = [\hat{e}_x \cos(\psi) + \hat{e}_y \sin(\psi)]\, k_\perp + \hat{e}_\parallel k_\parallel \quad ,$$

$$\vec{p} = m\vec{v}\gamma \quad , \quad b = k_\perp p_\perp/m\Omega \quad , \quad \Omega = qB/mc \quad ,$$

$$\gamma = [1 + (p_\perp^2 + p_{||}^2)/m^2c^2]^{\frac{1}{2}} \quad ,$$

$$E_\pm = (E_x \pm iE_y)/(2)^{\frac{1}{2}} \quad . \tag{3.2}$$

In Eq. (3.1) the particle distribution, f, is a function of the momentum components perpendicular to and parallel to the ambient magnetic field (i.e., $p_\perp$ and $p_{||}$, respectively). In Eqs. (3.1) and (3.2) subscripts x, y, and || denote vector components in the x, y, and magnetic field directions, respectively, and the symbol $\hat{e}$ represents a unit vector. The ambient magnetic field strength, particle charge, particle mass, velocity, and speed of light are given by B, q, m, $\vec{v}$, and c, respectively. For electrons or negative ions, the charge is negative. The wavenumbers, k, and the frequency, ω, are related through the dispersion relation. The summation in the index k is over modes and J_n is the Bessel function of the first kind and order n.

Because this analysis emphasizes cyclotron resonance effects for particles with momentum which is primarily magnetic field aligned, the particle distribution function is assumed to have the following form:

$$f(p_\perp, p_{||}) = \frac{n_o}{2\pi p_\perp} \delta(p_\perp) h(p_{||}) \tag{3.3}$$

for real space density n_o. In Eq. (3.3), $\delta(p_\perp)$ and $h(p_{||})$ are the Dirac delta function in $p_\perp$ and a general function of $p_{||}$, respectively.

With the choice of particle distribution function given by Eq. (3.3), it follows that only the n = -1, 0 and +1 cyclotron resonances can be effective in altering particle trajectories because they do not require finite gyroradius. The subsequent discussion will emphasize the n = -1 and +1 resonances which, unlike the n = 0 Landau resonance, can be very weakly dependent on wave frequency.

To demonstrate that the n = -1 and +1 resonances can be effective anomalous resistivity mechanisms, it is sufficient to take appropriate moments of Eq. (3.1). For an arbitrary function of $p_\perp$ and $p_{||}$, $g(p_\perp, p_{||})$, the rate at which the $g(p_\perp, p_{||})$ moment changes for mode k and cyclotron harmonic n is:

$$\left\langle \frac{\partial}{\partial t} \left[n_o \, g(p_\perp, p_\parallel) \right] \right\rangle_{k,n} = 2\pi \int_0^\infty dp_\perp \, p_\perp \int_{-\infty}^\infty dp_\parallel$$

$$g(p_\perp, p_\parallel) \, Q_{k,n}(p_\perp, p_\parallel) \quad . \tag{3.4}$$

Hence,

$$\left\langle \frac{\partial}{\partial t} \left(n_o p_\parallel \right) \right\rangle_{k,n} = \frac{k_\parallel}{\omega} \, \frac{dW_{k,n}}{dt} \quad , \tag{3.5a}$$

$$\left\langle \frac{\partial}{\partial t} \left(n_o p_\parallel^2 \right) \right\rangle_{k,n} = 2m \int_{-\infty}^\infty dp_\parallel \, (\gamma\omega - n\Omega) \, B_{k,n}(p_\perp, p_\parallel) \quad , \tag{3.5b}$$

$$\left\langle \frac{\partial}{\partial t} \left(n_o p_\perp^2 \right) \right\rangle_{k,n} = 2m \, \frac{n\Omega}{\omega} \, \frac{dW_{k,n}}{dt} \quad , \tag{3.5c}$$

$$\frac{dW_{k,n}}{dt} \equiv \left\langle \frac{\partial}{\partial t} \left(\gamma mc^2 \right) \right\rangle_{k,n} = \omega \int_{-\infty}^\infty dp_\parallel B_{k,n}(p_\perp, p_\parallel) \quad , \tag{3.5d}$$

In Eqs. (3.5b) and (3.5d),

$$B_{k,n}(p_\perp, p_\parallel) = \frac{\pi n_o n\Omega}{2m} \left(\frac{q}{k_\parallel c} \right)^2 \gamma^{-2} \left| \left[B_y - iB_x + \frac{k_\perp c}{\Omega} \gamma \, E_\parallel \right. \right.$$

$$\exp(i\psi)] \, \delta_{n,1} + \left[B_y + iB_x - \frac{k_\perp c}{\Omega} \gamma \, E_\parallel \right.$$

$$\left. \left. \exp(-i\psi)] \delta_{n,-1} \right|^2 \delta(\omega - n\Omega/\gamma - k_\parallel p_\parallel / m\gamma) h(p_\parallel) \right. \quad , \tag{3.6}$$

which is derivable from Eq. (3.1) and Faraday's law. In Eq. (3.6), wave magnetic fields are denoted by B_y and B_x.

Equation (3.5d) shows that wave fields must vary with time if energy is to be transferred between fields and charged particles. For nonzero frequencies, Eqs. (3.5) and (3.6) also indicate that the n = +1 resonance causes energy to be removed from negatively charged particles and to be added to positively charged particles. Similarly, the n = -1 resonance adds and subtracts energy from negatively and positively charged particles, respectively.

Irrespective of how or whether energy is exchanged between electromagnetic or electrostatic fields and particles, Eqs. (3.5) and (3.6) demonstrate that the parallel momentum is always reduced while the perpendicular momentum becomes greater for both the n = -1 and +1 resonances as long as $\omega < |\Omega/\gamma|$. The key requirement for pitch angle scattering is the presence of particles satisfying the resonance condition,

$$k_{||} p_{||}/m = \gamma\omega - n\Omega \tag{3.7}$$

or for $\gamma\omega << |n\Omega|$,

$$k_{||} p_{||}/m \approx - n\Omega \quad . \tag{3.8}$$

Equation (3.8) shows that as particle parallel momentum increases, the parallel wavelength required for cyclotron resistivity becomes longer.

3.3 COMPARATIVE APPLICATION BETWEEN NUCLEAR AND BARIUM CLOUD ENVIRONMENTS

The purpose of this subsection is to illustrate a difference between high-altitude nuclear and barium cloud environments in the ionosphere. Specifically, in the example presented here, it is demonstrated that 10 to 100 keV oxygen ions injected parallel to the magnetic field lines by nuclear explosion can be retarded by ion-cyclotron resistivity with Alfven waves for reasonable densities, e.g., 1×10^6 cm^{-3}; however, barium ions injected parallel to the magnetic field by shaped injection are not retarded by the ion-cyclotron resistivity with Alfven waves in a predominantly barium plasma unless the density is relatively high (i.e., much greater than 1.4×10^7 cm^{-3}). Such high barium densities may be difficult to achieve for the shaped injection.

For the cyclotron resistivity process to be effective for waves with frequencies well below the ion-cyclotron frequency, Eq. (3.8) must be satisfied. Figure 3.1 shows, for B = 0.3 gauss, the necessary wavelengths for resonance as a function of barium and monatomic oxygen energy. The figure has three significant features. First, parallel wavelength increases with ion energy. Second, for equal energies barium requires longer parallel wavelengths to satisfy Eq. (3.8) than oxygen. Third, the parallel wavelengths necessary for cyclotron resistivity are in excess of 1 kilometer for ion energies greater than 100 eV. For 1×10^5 eV ions, the required parallel wavelengths are approximately 1×10^2 kilometers for barium and 40 kilometers for oxygen.

As a specific quantitative example we consider the case of Alfven waves propagating along the ambient magnetic field and interacting with the superthermal ions travelling along the ambient magnetic field. The origin of the Alfven waves is not important for the present example but could be associated with a nuclear explosion, barium release, or other abrupt change in the ionosphere.[13,15] Besides having a frequency below the ion-cyclotron frequency, the significant feature of the waves is that for propagation parallel to the ambient magnetic field, the wave has no parallel electric field associated with it. Hence, only the wave magnetic field contributes to cyclotron resistivity in Eq. (3.5).

Consider a barium ion with a kinetic energy of 160 eV and speed of 1.5×10^6 cm/sec. For B = 0.3 gauss, Eq. (3.8) and Figure 3.1 indicate that a parallel wavelength of 4.5 kilometers is required for cyclotron resistivity to alter the ion pitch angle. For the wave frequency to be much smaller than the barium-cyclotron frequency it is necessary that

$$k_{\parallel} v_A \ll \Omega_i \tag{3.9}$$

with v_A the Alfven speed and Ω_i the ion-cyclotron frequency. With B = 0.3 gauss, Eq. (3.9) implies that the resonance condition cannot be satisfied unless the barium ion density is much greater than 1.4×10^7 cm^{-3}. Hence, unless such high barium densities can be made to exist for shaped barium injection along the magnetic field in the ionosphere, cyclotron resonance

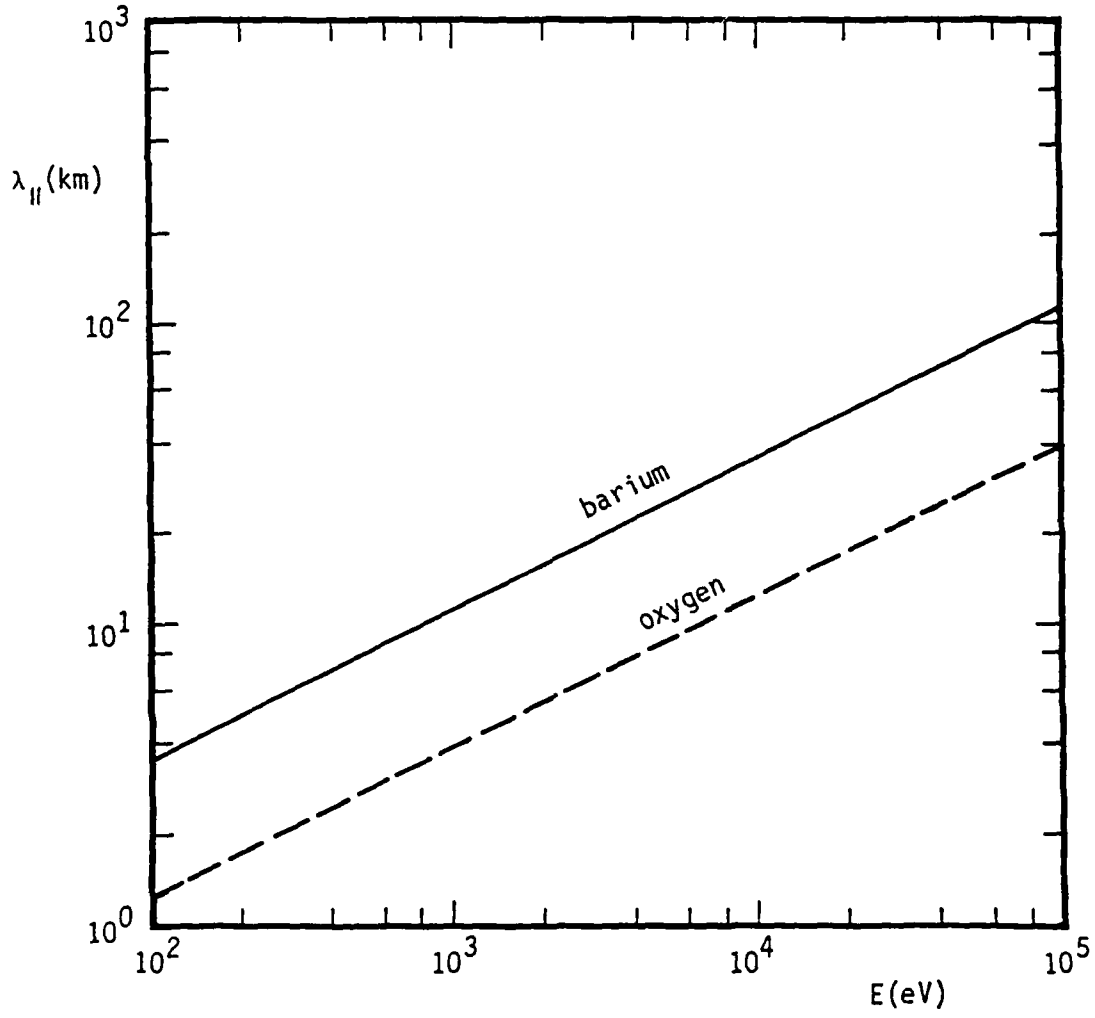

Figure 3.1. The solution of Eq. (3.8), parallel wavelength in kilometers versus ion energy in electron volts, for barium (——) and monatomic oxygen (– –). The magnetic field strength is 0.3 gauss.

between Alfven waves and superthermal barium ions in a predominantly barium plasma is highly improbable.

Monatomic oxygen ions with kinetic energy of 1×10^4 and 1×10^5 eV can undergo cyclotron resistivity with B = 0.3 eV only if $2\pi/k_{\parallel}$ = 12 and 38 kilometers, respectively. The monatomic oxygen densities required to satisfy Eq. (3.9) for the aforementioned parallel wavelengths are in excess of 2.3×10^5 and 2.3×10^4 cm^{-3}, respectively. Hence, in contrast to the barium example presented before, oxygen cyclotron resistivity due Alfven waves is possible in the ionosphere if the wave magnetic field strength is large enough.

When it is active, cyclotron resistivity is significant only if the momentum drag caused by it is larger than classical collisional drag. For monatomic oxygen energies greater than 3 keV and an electron temperature of 0.1 eV, Coulomb drag on electrons is much larger than Coulomb drag on ions.[18] Consequently, for cyclotron resistivity due to mode k and cyclotron harmonic n to dominate over classical resistivity it is necessary that[18]

$$\left\langle \frac{\partial}{\partial t} (n_o p_{\parallel}) \right\rangle_{k,n} > 5.4 \times 10^{-55} \, n_e n_o \int_{-\infty}^{\infty} dp_{\parallel} \, p_{\parallel}^{-2} \, h(p_{\parallel}) \ln(\Lambda_{ie}) \quad , \tag{3.10}$$

where n_e is the electron density (cm^{-3}) and the Coulomb integral, $\ln(\Lambda_{ie})$, is specified later. The right-hand side of Eq. (3.10) is valid so long as the distribution function, $h(p_{\parallel})$, corresponds to most oxygen particles having energies greater than 3 keV.

To permit quantitative evaluation of the left-hand side of Eq. (3.10), we assume the following form for $h(p_{\parallel})$:

$$h(p_{\parallel}) = (2\pi \, m_i^2 v_i^2)^{-\frac{1}{2}} \exp[-(p_{\parallel} - p_o)^2 / 2 m_i^2 v_i^2] \tag{3.11}$$

with p_o and v_i constants and m_i the ion mass.

Conventional plasma instability theory might suggest that the specified form of $h(p_{\parallel})$ could be susceptible to waves which grow via the inverse Landau damping mechanism, especially if the parallel phase velocities of the waves is less than p_o/m_i. We circumvent this possibility by noting that for the chosen distribution function inverse Landau damping will not promote instability for parallel phase velocities in excess of p_o/m_i. In any case, cyclotron resistivity can act whether or not another source of anomalous resistivity is active.

The right-hand side of Eq. (3.11) can be integrated approximately by the saddle point methods if the distribution function is strongly peaked with $p_o >> m_i v_i$ and the weak dependence of the Coulomb logarithm on momentum is neglected.[19] Equation (3.10) becomes:

$$\left\langle \frac{\partial}{\partial t} (n_o p_{\parallel}) \right\rangle_{k,n} > 5.4 \times 10^{-55} \, n_e n_o \, \delta p_o^{-2} \, (f_o'')^{-\frac{1}{2}}$$

$$\exp(-f_o) \, \ln(\Lambda_{ie}) \qquad (3.12)$$

with

$$f_o = 0.5 \, \delta^2 \, (y_1 - 1)^2 + 2 \ln(y_1) \quad , \quad f_o'' = \delta^2 - 2/y_1^2 \quad ,$$

$$y_1 = 0.5 \, [1 + (1 - 8/\delta^2)^{\frac{1}{2}}] \quad , \quad \delta = p_o/m_i v_i \quad . \qquad (3.13)$$

Writing the argument of the Coulomb logarithm as:[20]

$$\Lambda_{ie} = \left(\frac{\kappa T_e}{4\pi n_e e^2} \right)^{\frac{1}{2}} \frac{m_e p_o^2}{e^2 m_i^2} \qquad (3.14)$$

permits the complete specification of the right-hand side of Eq. (3.13). In Eq. (3.14), the parameters e, κ, T_e, m_i, and m_e denote the magnitude of the electron charge, Boltzmann's constant electron temperature, ion mass, and electron mass, respectively.

Figure 3.2 is a plot of wave magnetic field strength in gauss versus monatomic oxygen energy ($0.5\ p_o^2/m_i$) in eV necessary to satisfy Eq. (3.12) for $n_e = 1 \times 10^6\ cm^{-3}$, $B_o = 0.3$ gauss, $T_e = 0.1$ eV, $\delta = 5$, and $m_i\Omega_i/k_{||}p_o = 1.5$. The figure shows that wave magnetic field strengths much smaller than the ambient magnetic field are sufficient to permit cyclotron resistivity to dominate over classical resistivity especially for high energy oxygen ions. In particular, for $p_o^2/2m_i$ values of 10 keV and 100 keV, wave magnetic field strengths for comparable cyclotron and classical resistivity are 5×10^{-3} and 9×10^{-4} gauss, respectively. Larger values of the wave fields result in the dominance of cyclotron resistivity.

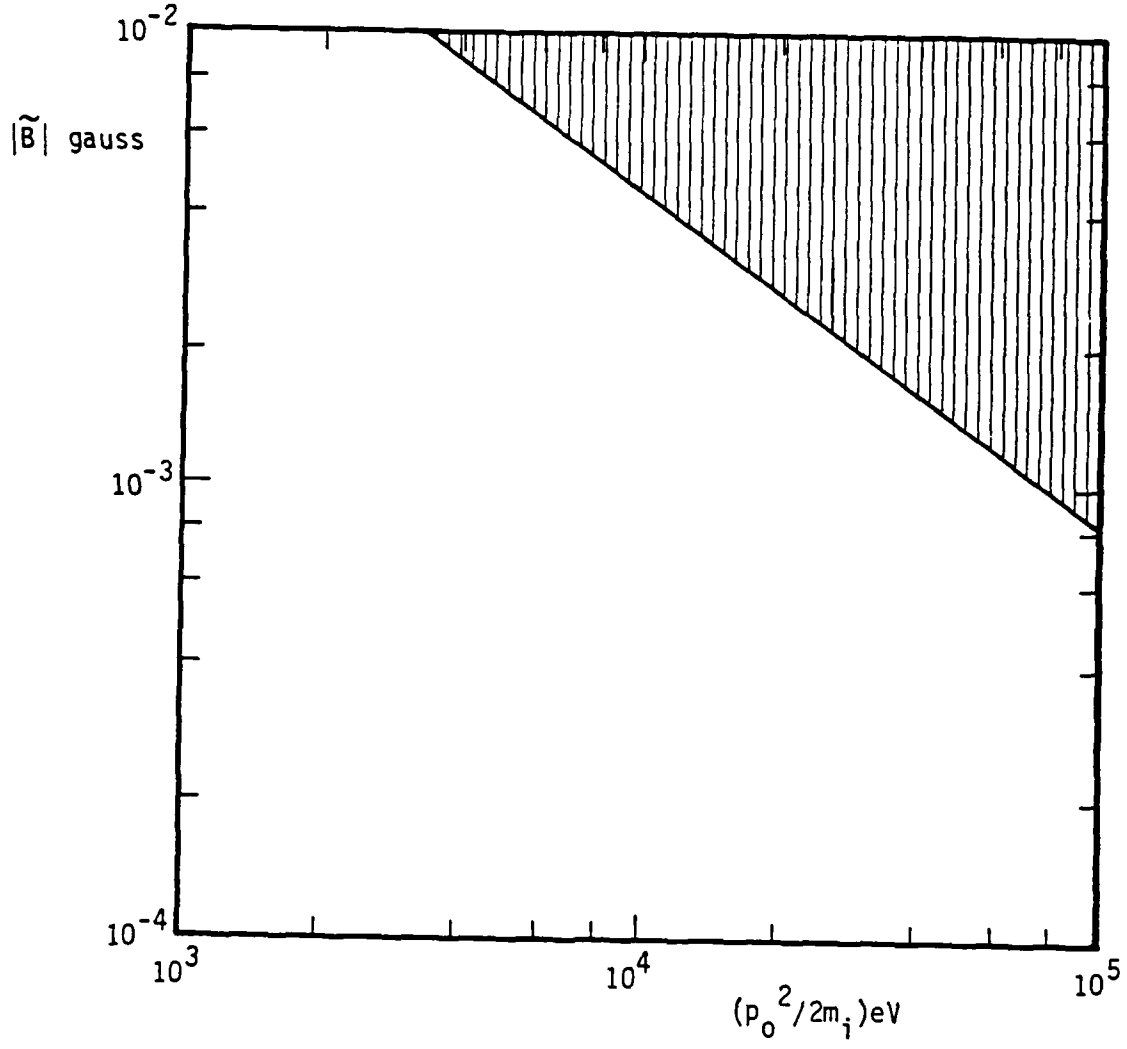

Figure 3.2. Plot of fluctuation magnetic field strength $|B_y \pm iB_x| \approx \tilde{B}$ (gauss) versus oxygen kinetic energy for B = 0.3 gauss, $n_e = 1 \times 10^5$ cm^{-3}, and $T_e = 0.1$ eV. Shaded region above the curve indicates the parameter space for which cyclotron resistivity dominates over classical resistivity.

SECTION 4

CONCLUDING REMARKS

Prompt striations have been observed in some barium release experiments as plasma tries to jet across the ambient magnetic field.[3,4] They have been postulated to be the result of a collective process driven by free energy available from an ion loss cone distribution function associated with the jetting.[3,5-7] It has been shown in the appendices that electron-ion collisions, background plasma density, and finite ion inertial pressure all tend to reduce the linear growth rate of the instability. However, for application of the theory to the high-altitude nuclear environment electron-ion collisional stabilization is unimportant. Finite ion inertial pressure seems to virtually eliminate the possibility that the most energetic ions formed after a high-altitude explosion can be the source of prompt striations in the weak magnetic field environment of the ionosphere. However, in a burst like STARFISH, prompt striations could develop from a class of ions with lower velocities perpendicular to the ambient magnetic field, e.g., between 1×10^6 and 1×10^7 cm/sec. The development of prompt striations would benefit from the lower background plasma density environment available at higher altitudes, especially well above 400 kilometers for a STARFISH type burst.

Ion and electrons moving along magnetic field lines have been shown to be susceptible to a pitch angle scattering process associated with a cyclotron resonance phenomena. An implication of this cyclotron resistivity is that high energy ions and electrons travel less rapidly along magnetic field lines than would otherwise be predicted and so must deposit their energy closer to their source. It has been shown that the particular process of ions interacting with Alfven waves can more easily occur in the high-altitude nuclear rather than in the barium cloud environment. Hence, ion-cyclotron resistivity with Alfven waves represents a way that barium releases can differ from nuclear explosions in the ionosphere.

Questions still remain concerning the applicability of prompt striation and cyclotron resistivity processes to the high-altitude nuclear environment. Regarding prompt striations, the kinetic nonlinear saturated state is not obvious

in the ionosphere. An interesting possibility is that the linear instability postulated to be the source of prompt striations readily couples to longer wavelengths in guiding center fashion. In Reference 21 it is suggested that the energy spectrum of the system might go as k^0 for long wavelengths and $k^{-8/3}$ for short wavelengths. This guiding center saturation mechanism should be compared to other possible saturation processes for the instability. It is also important to know whether the correct kinetic saturated state could form the basis for later fluid evolution as ion energies decrease and fluid assumptions become more reasonable. Regarding cyclotron resistivity, the ultimate momentum distribution function which results from interaction between waves and particles has not been determined. This distribution function is necessary for determining the spatial and temporal energy deposition by super-thermal particles by other processes, say charge exchange.[2] The possibility that field aligned structuring could develop as pitch angle scattering occurs should also be studied.

REFERENCES

1. Kilb, R. W., private communication.
2. Goldman, S. R. and Sperling, J. L., "Some Physical and Chemical Aspects of Striation Structure," JAYCOR Report J510-80-023/2128-02, August 1980.
3. Simons, D. J., Pongratz, M. B., and Gary, S. P., "Prompt Striations in Ionospheric Barium Clouds Due to a Velocity Space Instability," J. Geophys. Res., 85, p. 671, 1980.
4. McDonald, B. E., Keskinen, M. J., Ossakow, S. L., and Zalesak, S. T., "Computer Simulation of Gradient Drift Instability Processes in Operation Avefria," J. Geophys. Res., 85, p. 2143, 1980.
5. Sperling, J. L. and Krall, N. A., "Electron-Ion Collision Effects on the Formation of Prompt Striations," J. Geophys. Res., 86, p. 5726, 1981.
6. Sperling, J. L. and Krall, N. A., "Stabilization of Electrostatic, Purely Growing, Finite Ion-Gyroradius Flute Instabilities in the Ionosphere," J. Geophys. Res., 86, p. 7513, 1981.
7. Sperling, J. L., "Electromagnetic Effects in the Analysis of Prompt Striations," JAYCOR Report J510-81-017/2128-02, March 1981.
8. Braginskii, S. I., "Reviews of Plasma Physics I," edited by M. A. Leontovich, Consultants Bureau, New York, 1965, p.205.
9. Simon, A. and Rosenbluth, M. N., "Single-Mode Saturation of the Bump-on-Tail Instability, Immobile Ions," Phys. Fluids, 19, p. 1576, 1976.
10. Liu, C. S. and Mok, Y., "Nonlinear Evolution of Runaway-Electron Distribution and Time-Dependent Synchrotron Emission from Tokamaks," Phys. Rev. Lett., 38, p. 162, 1977.
11. Molvig, K., Tekula, M. S., and Bers, A., "Theory of the Runaway Electron Tail," Phys. Rev. Lett., 38, p. 1404, 1977.
12. Palmadesso, P. J., "Strong D.C. Anomalous Resistivity in a Magnetized Plasma," Bull. Am. Phys. Soc., 25, p. 874, 1980.

13. Kelley, M. C., Pedersen, A., Fahleson, U. V., Jones, D., and Kohn, D., "Active Experiments Stimulating Waves and Particle Precipitation with Small Ionospheric Barium Releases," J. Geophys. Res., 79, p. 2859, 1974.

14. Koons, H. C. and Pongratz, M. B., "Ion Cyclotron Waves Generated by an Ionospheric Barium Injection," J. Geophys. Res., 84, p. 533, 1979.

15. Banks, P. M., "Space Plasma Physics: The Study of Solar-System Plasmas, Volume I Working Papers," National Academy of Sciences, Washington, D.C., 1979, p. 688.

16. Sharp, R. D., Johnson, R. G., and Shelley, E. G., "The Morphology of Energetic O^+ Ions During Two Magnetic Storms: Latitudinal Variations," J. Geophys. Res., 81, p. 3292, 1976.

17. Hamasaki, S., Klein, H. H., Krall, N. A., McBride, J. B., and Sperling, J. L., "Microwave Heating of the ELMO Bumpy Torus Relativistic Ring," Phys. Fluids, 24, p. 1706, 1981.

18. Book, D. L., "1978 Revised Plasma Formulary," Naval Research Laboratory, Washington, D.C., p. 25.

19. Erdelyi, A., "Asymptotic Expansions," Dover, New York, 1956, Ch. 2.

20. Spitzer, L., "Physics of Fully Ionized Plasmas," John Wiley and Sons, New York, 1962, Ch. 5.

21. Swift, D. W., "Turbulent Generation of Electrostatic Fields in the Magnetosphere," J. Geophys. Res., 82, p. 5143, 1977.

APPENDIX A

ELECTRON-ION COLLISION EFFECTS ON PROMPT STRIATION FORMATION

ABSTRACT

Electron-ion collisions have been included in the analysis of electrostatic, purely growing, finite ion-gyroradius, flute instabilities generated by a loss cone distribution of energetic ions in the ionosphere. It is shown that the collisions not only reduce the growth rate below the value predicted by collisionless theory, but also result in a second lower growth rate mode not found in collisionless theory. Although the electron-ion collision frequency is larger than the ion-gyrofrequency for the parameters of the Buaro barium release experiment, the growth rate of the linearly most unstable mode is not appreciably modified by the collisions from the value predicted from collisionless theory. Electron-ion collisions have a greater impact on the instability as the electron density is increased. Complete stabilization through electron-ion collisions requires densities in excess of 8.7×10^7 cm^{-3}.

A-1. INTRODUCTION

The formation of magnetic field aligned structures, striations, is an ionospheric physics problem of considerable interest because of their adverse impact on communication.[A1,A2] At low altitudes a generally agreed upon process for striation growth is the $\vec{E}\times\vec{B}$ gradient drift instability (e.g., see Reference A3 for a detailed analysis). However, at higher altitudes striations are not readily attributed to the gradient drift mechanism but are nevertheless observed in shaped barium releases such as Buaro.[A4] The authors of Reference A4 call the structures observed in Buaro prompt striations because of their rapid appearance and attribute these striations to an electrostatic finite ion-gyroradius, purely growing, flute instability generated by an ion loss cone distribution function appropriate for the plasma following the barium release. Corroboration for the theory of Reference A4 is the experimental observation in Buaro of various ion-cyclotron harmonic modes.

The purpose of this paper is to include electron-ion collisions into the analysis of the finite ion-gyroradius flute instability. Motivation for considering electron-ion collision effects is that even for the electron densities in the Buaro experiment[A4] (i.e., 4×10^5 cm^{-3}), the electron-ion collision frequency is much larger than the ion-gyrofrequency which is the characteristic growth rate for the finite ion-gyroradius, purely growing, modes. It is shown that electron-ion collisions do not markedly alter the instability dispersion relation for Buaro parameters but could have a significant effect for higher density experiments.

This appendix is divided into four sections. In Section A-2 the theoretical model and some qualitative implications of the model are described. In Section A-3 quantitative solutions of the dispersion relation are presented and discussed. Section A-4 is a discussion of the significant features of the analysis and results.

A-2. THEORETICAL MODEL

The theoretical model assumes an infinite homogeneous plasma, with a loss cone distribution of ions superposed on a Maxwellian distribution of electrons. Reference A4 indicates that this is the appropriate distribution function after the barium release. For the purely growing modes being considered the inverse wavenumber is smaller than the ion-cyclotron radius but larger than the electron-cyclotron radius. Consequently, the ion response to the modes requires a fully kinetic treatment while the electron response can be recovered from the fluid equations. Electrostatic flute modes with the plane wave variation, $\exp[i(k_\perp y - \omega t)]$, are also assumed with $k_\perp$, y, ω, and t being the wavenumber component perpendicular to the ambient magnetic field, y-directed coordinate, wave frequency in radians per second, and time, respectively. With the assumed plasma and wave model, the ion response is identical to that found in Reference A4. Specifically:

$$\kappa_i = \frac{k_\perp \omega_{pi}^2}{b_i} \sum_{p=1}^{\infty} \frac{2\omega^2}{\omega^2 - p^2\Omega_i^2} \frac{(2p-1)\, I_{p,p-1}}{\omega^2 - (p-1)^2\Omega_i^2} \qquad (A.1)$$

where

$$\omega_{pi}^2 = 4\pi\, n_i e^2/m_i \quad , \quad \Omega_i = eB_o/m_i c \quad , \quad b_i = v_o/\Omega_i \quad ,$$

$$I_{p,p-1} = \frac{\delta^3}{A(\delta)} \int_0^\infty dx\; x\; J_p(k_\perp b_i x)\; J_{p-1}(k_\perp b_i x)\; \exp[-0.5\delta^2(x-1)^2]$$

$$A(\delta) = \left(\frac{\pi}{2}\right)^{\frac{1}{2}} \left\{(1+\delta^2)[1 + \mathrm{erf}(\delta/\sqrt{2})] + \left(\frac{2}{\pi}\right)^{\frac{1}{2}} \delta \exp(-0.5\delta^2)\right\} \qquad (A.2)$$

In Eq. (A.2), the parameters n_i, e, m_i, B_o, and c denote the ion density, magnitude of the elementary electron charge, ion mass, magnetic field strength, and speed of light, respectively. The ordinary Bessel function of the first

kind and order p is represented by J_p. For the singly ionized quasineutral plasma assumed in the present calculation,

$$n_i = n_e \quad . \tag{A.3}$$

The parameters v_o, v_i, and $\delta = v_o/v_i$ are associated with the form for the loss cone ion distribution function,

$$f_i(\vec{v}) = \frac{\delta^3 \, v_\perp}{(2\pi)^{3/2} \, v_i \, v_o^{\,3} \, A(\delta)} \exp\left(- \frac{(v_\perp - v_o)^2}{2v_i^{\,2}} - \frac{v_{||}^{\,2}}{2v_i^{\,2}} \right) \tag{A.4}$$

where $v_\perp$ and $v_{||}$ are the perpendicular and parallel velocity components, respectively.

The electron response to the electrostatic flute mode is:

$$\kappa_e = - k_\perp^{\,2} \, \frac{\omega_{pe}^{\,2}}{\Omega_e^{\,2}} \, (1 + i\nu_e/\omega) \tag{A.5}$$

where

$$\omega_{pe}^{\,2} = 4\pi \, n_e e^2/m_e \quad , \qquad \Omega_e = -eB_o/m_e c \quad ,$$

$$\nu_e = \frac{n_e}{3.5 \times 10^5 \, T_e^{\,3/2}} \left[23.4 - 1.15 \log_{10}(n_e) + 3.45 \log_{10}(T_e) \right] . \tag{A.6}$$

In the expression for the electron collision frequency, which is an approximation valid near thermal equilibrium, the density and temperature are in units of cm^{-3} and eV, respectively.[A5] Equation (A.6) includes both the electron polarization and Pederson current responses to the wave electric field and can be derived either from kinetic equations (e.g., Eq. 11 of Reference A6 in the limit of $k_\perp^{\,2} v_e^{\,2}/\Omega_e^{\,2} \to 0$ where v_e is the electron thermal speed) or from

fluid equations. An assumption made in the present analysis and justified in Subappendix AA is that the ion response to waves is unaffected by electron-ion collisions while the electron dynamics in the wave are not modified by the ion response.

The dispersion relation can now be written as:

$$k_\perp^2 = \kappa_i + \kappa_e \quad . \tag{A.7}$$

For purely growing modes, $i\gamma = \omega$ with γ real. With the definitions,

$$y = \gamma/\Omega_i \quad , \qquad a = \nu_e/\Omega_i \quad , \tag{A.8}$$

and the general ionospheric relation,

$$\omega_{pe}^2/\Omega_e^2 \gg 1 \quad , \tag{A.9}$$

the dispersion relation can be rewritten in the following way:

$$a = -y\left[1 + 2\,\frac{m_i/m_e}{k_\perp b_i}\sum_{p=1}^{\infty}\frac{y^2}{y^2+p^2}\,\frac{(2p-1)\,I_{p,p-1}}{y^2+(p-1)^2}\right] \quad . \tag{A.10}$$

For $a \to 0$, this expression is equivalent to the homogeneous plasma dispersion relation found in Reference A4.

For $m_i/m_e \gg 1$, a good approximation to Eq. (A.10) is:

$$\nu_e \approx -2\,\frac{|\Omega_e|}{k_\perp b_i}\sum_{p=1}^{\infty}\frac{2y^3}{y^2+p^2}\,\frac{(2p-1)\,I_{p,p-1}}{y^2+(p-1)^2} \tag{A.11}$$

where $|\Omega_e|$ is the magnitude of the electron-cyclotron frequency. The significant feature of Eq. (A.11) is that for specified values of ν_e, $k_\perp b_i$, and δ,

all ion species have the same eigenvalue, y. However, the absolute growth rate is larger for less massive, higher gyrofrequency ion species. For example, the growth rate for monatomic oxygen is greater than for barium by the ratio of the barium to oxygen particle masses.

A-3. RESULTS

In the absence of electron-ion collisions and a very peaked distribution function with $v_o >> v_i$, there are a very large, but finite denumerable, number of zones in $k_\perp b_i$ space which permit positive growth rate solutions of the dispersion relation. The mathematical reason for these different zones, which correspond to negative values of $J_0(k_\perp b_i)\, J_1(k_\perp b_i)$, is the sinusoidal nature of Bessel functions and the slow decrease in maximum amplitude of the Bessel function oscillations as $k_\perp b_i$ increases. The maximum possible normalized growth rate $[(\gamma/\Omega_i)_{max}]$ versus $k_\perp b_i$ is shown for the first three unstable zones in Figure A.1 (zone I, $2.5 \lesssim k_\perp b_i \lesssim 3.8$; zone II, $5.6 \lesssim k_\perp b_i \lesssim 7.0$; zone III, $8.7 \lesssim k_\perp b_i \lesssim 10.1$). A characteristic feature of each of the solutions is the sharp increase in growth rate near the marginal values of $k_\perp b_i$ which permit growth. The change in growth rate is not as noticeable for values of $k_\perp b_i$ away from the marginal values. The figure also shows that the maximum growth rate of each zone increases with zone number, at least for the first three zones illustrated.

In the subsequent discussion detailed quantitative results will be confined to the first two unstable zones. Additional qualitative comments will be made concerning the higher number unstable zones.

Equation (A.10) has been evaluated numerically to determine the electron-ion collision frequency consistent with linear wave growth rate and perpendicular wavenumber. Figures A.2a to A.2f are plots of normalized collision frequency versus normalized linear wave growth rate for various values of $k_\perp b_i$ and δ.

A general characteristic feature of each curve in the figures is the two nonzero values for the growth rate which can occur when the electron-ion collision frequency is not equal to zero. In particular, for zero collision frequency the only solution of Eq. (A.10) which yields a positive growth rate is the one determined by the dispersion relation of Reference A4. As the electron-ion collision frequency increases, the maximum growth rate of the instability decreases below the value calculated neglecting collisions. In addition, a second purely growing solution of lower growth rate exists. This solution is not found in a theoretical model which neglects collisions. As the electron-

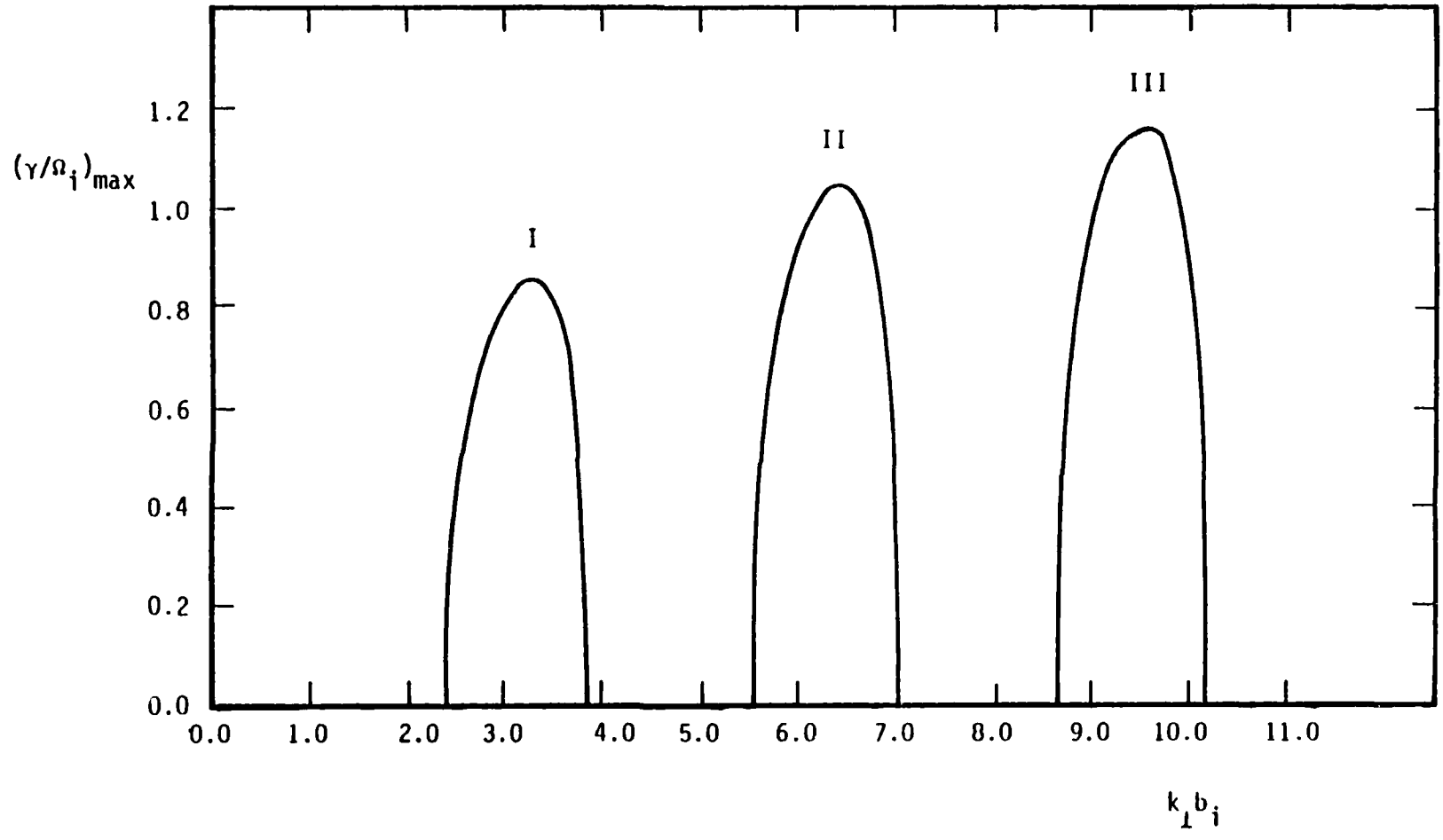

Figure A.1. Maximum possible normalized growth rate, $(\gamma/\Omega_i)_{max}$, versus $k_\perp b_i$ for $\delta \to \infty$ and the first three unstable zones

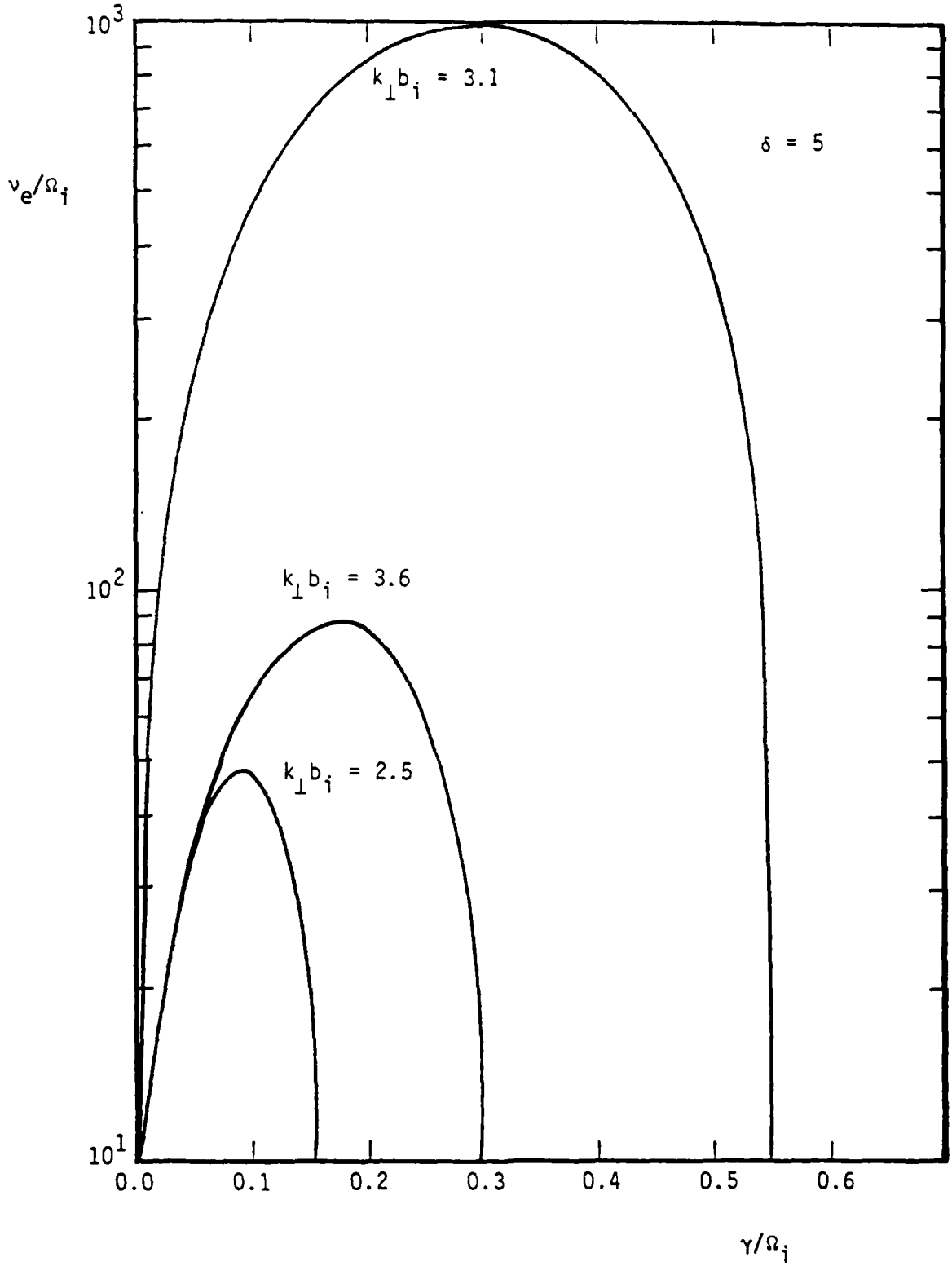

Figure A.2a. ν_e/Ω_i versus γ/Ω_i for different values of $k_\perp b_i$ and $\delta = 5$

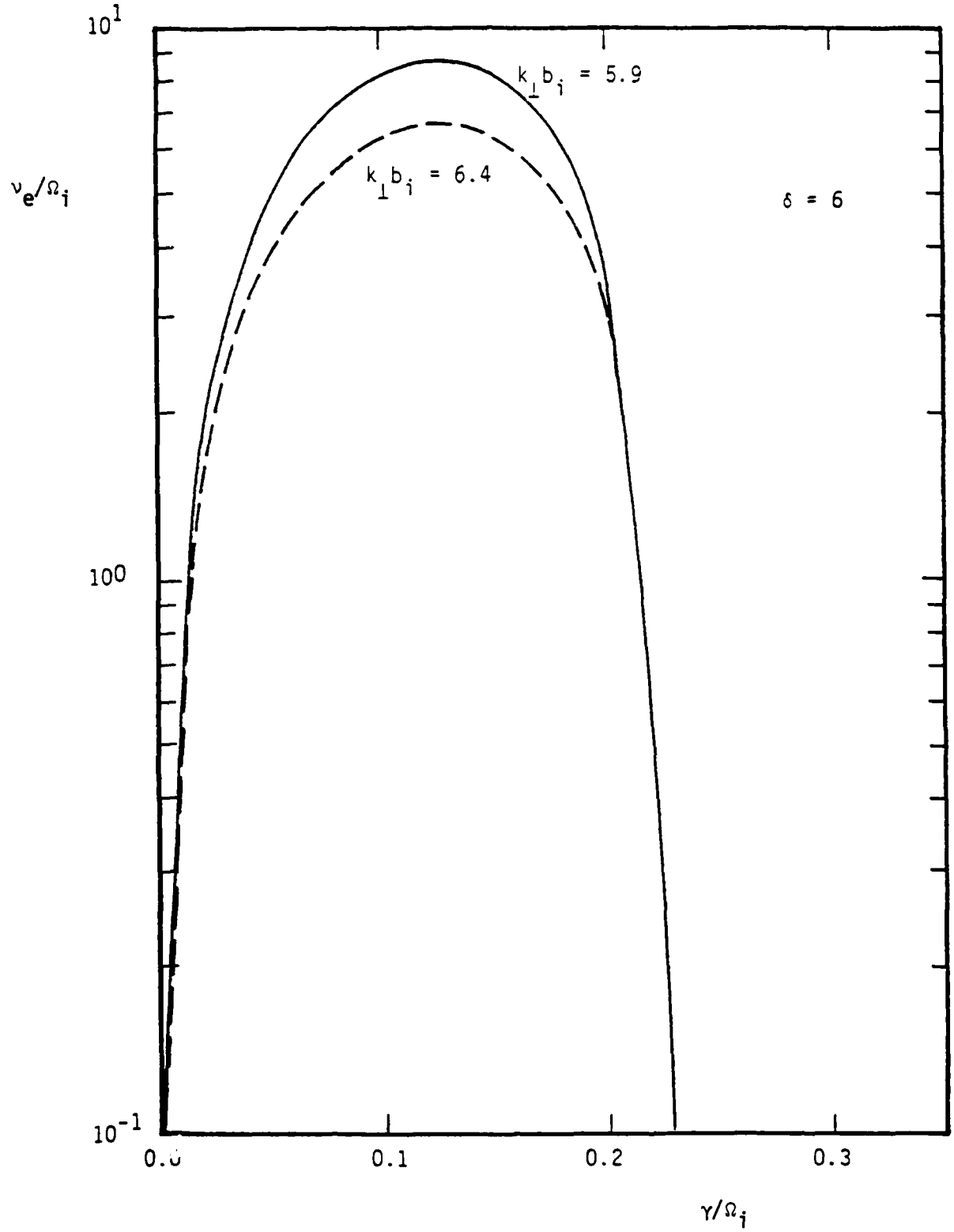

Figure A.2b. ν_e/Ω_i versus γ/Ω_i for different values of $k_\perp b_i$ and $\delta = 10$

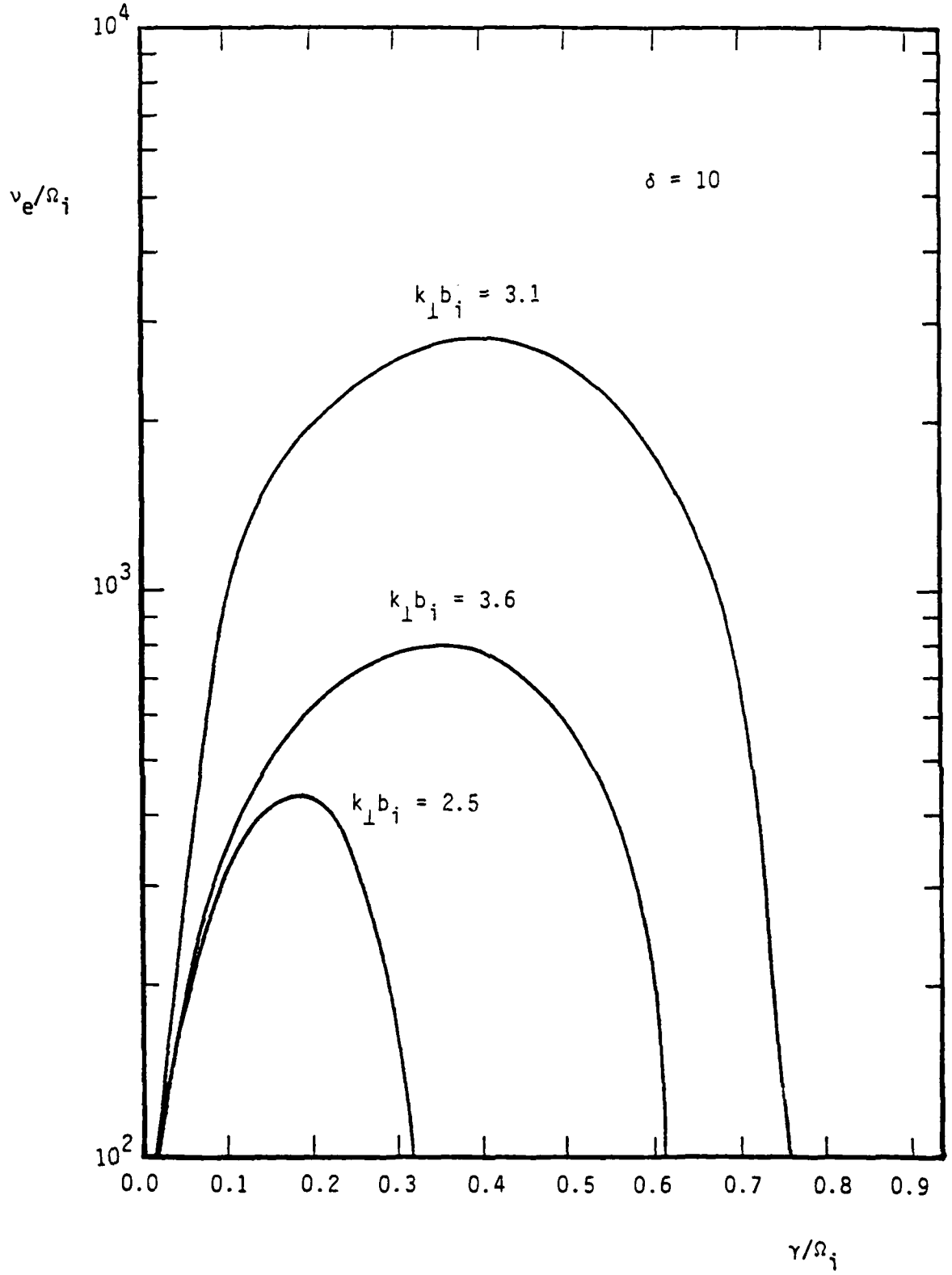

Figure A.2c. ν_e/Ω_i versus γ/Ω_i for different values of $k_\perp b_i$ and δ = 10

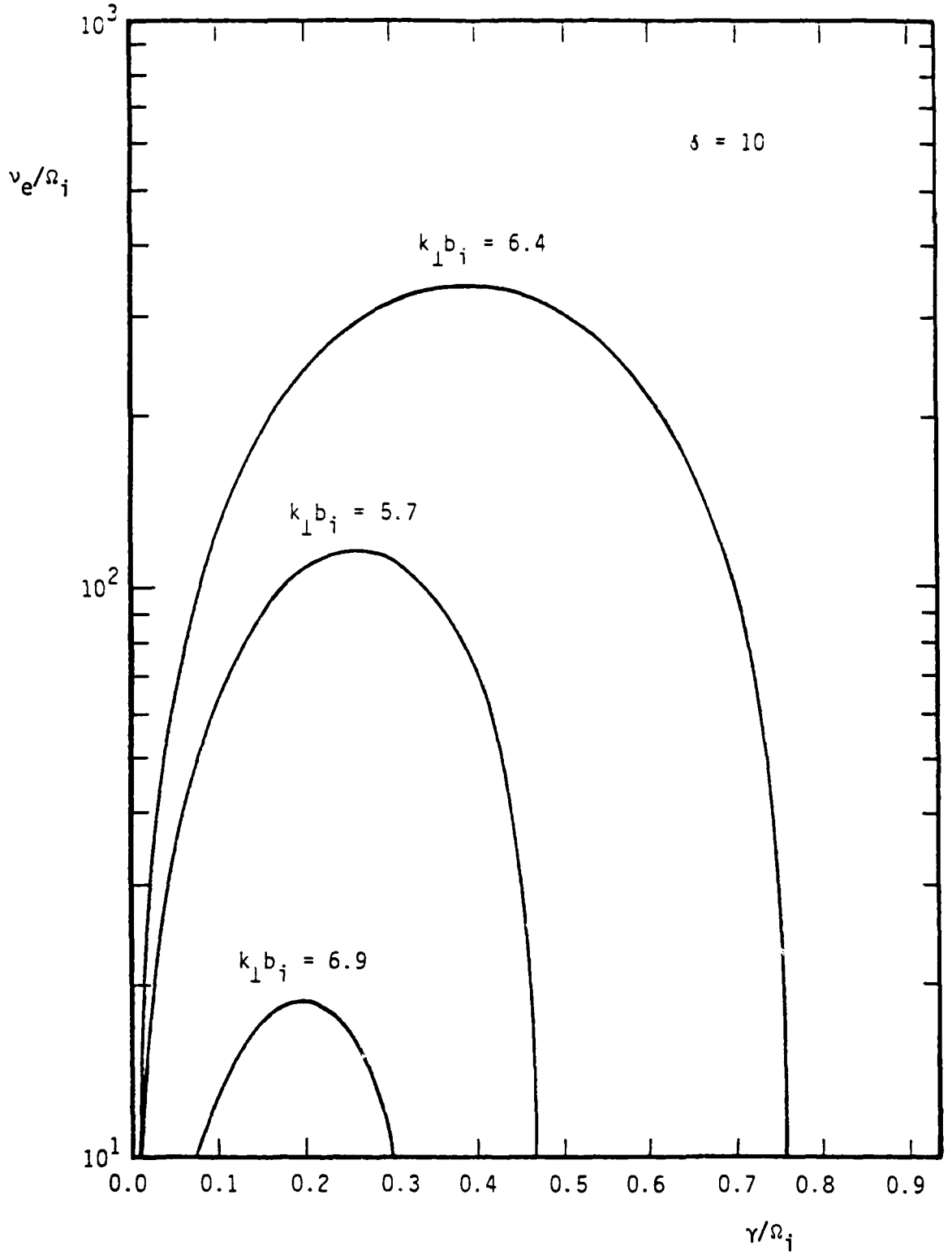

Figure A.2d. ν_e/Ω_i versus γ/Ω_i for different values of $k_\perp b_i$ and δ = 10

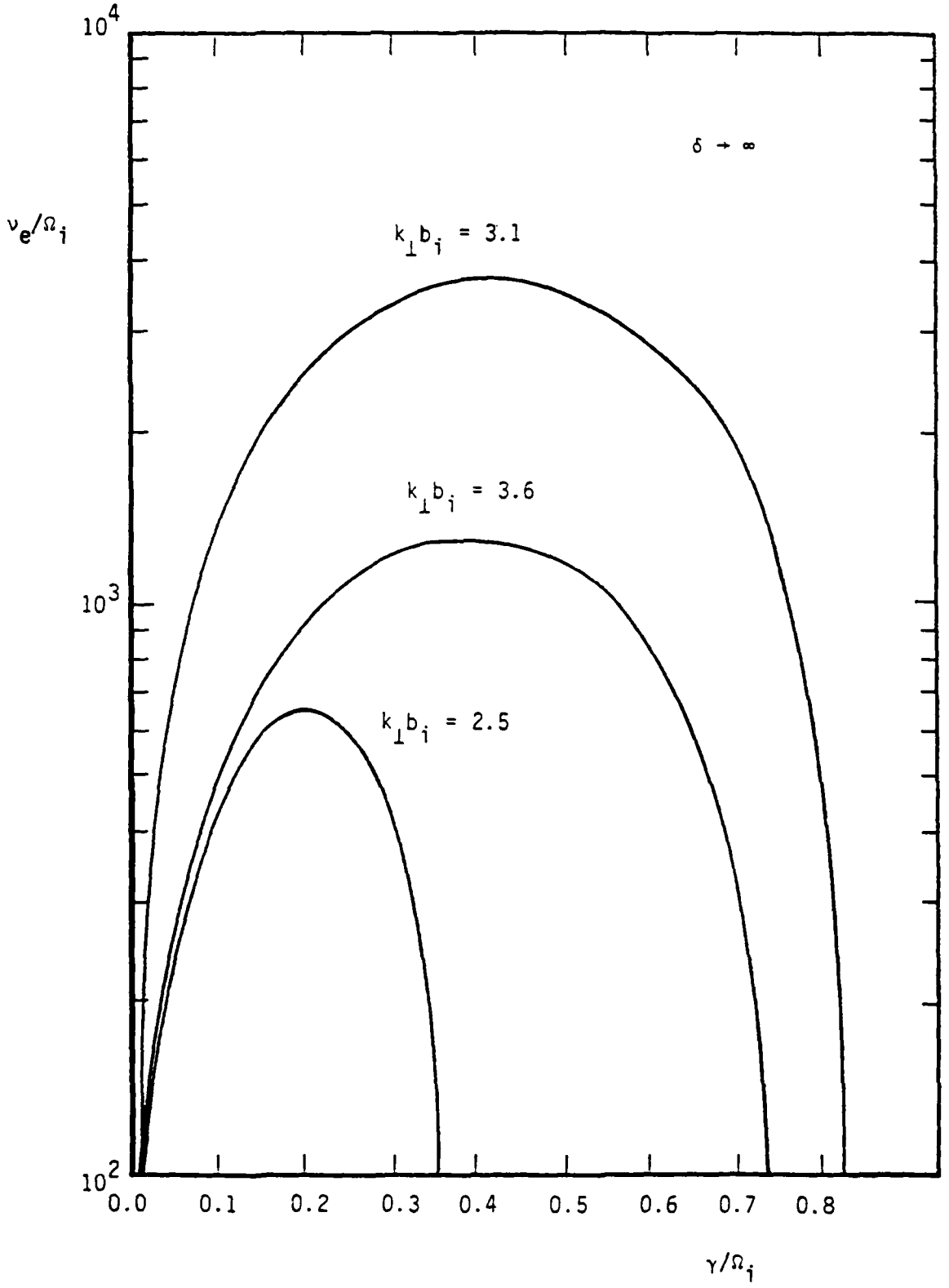

Figure A.2e. ν_e/Ω_i versus γ/Ω_i for different values of $k_\perp b_i$ and $\delta \to \infty$

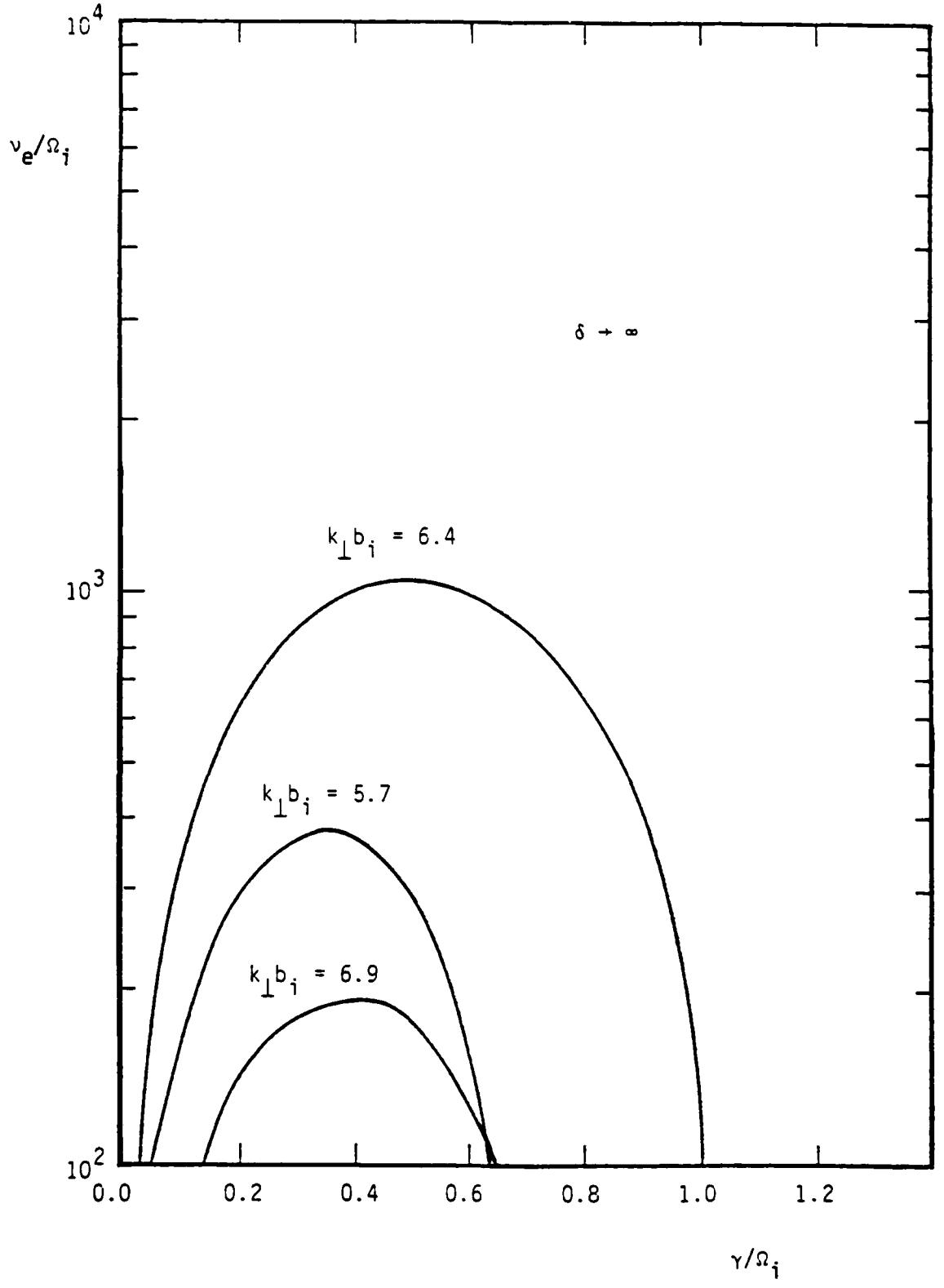

Figure A.2f. ν_e/Ω_i versus γ/Ω_i for different values of $k_\perp b_i$ and $\delta \to \infty$

ion collision frequency is increased further, the growth rates of the two solutions to Eq. (A.10) become more comparable. Eventually, for the maximum collision frequency which permits solution to Eq. (A.10) for a specific $k_\perp b_i$, the two solutions have the same growth rate. This growth rate is lower than the maximum growth rate calculated in the absence of collisions, but nevertheless can be a substantial fraction of the ion-cyclotron frequency (i.e., $\gamma/\Omega_i \gtrsim 0.1$).

Comparing the plots in Figures A.2a to A.2f, it is clear that as the parameter δ gets larger the maximum collision frequency which permits solution to Eq. (A.10) increases and the instability gets more vigorous. The physical mechanism behind this increased instability strength is the greater availability of velocity space free energy as the velocity space distribution function becomes more singular. Mathematically, the magnitude and sign of the Bessel functions for a specific value of $k_\perp b_i$ is not washed out by integration over the distribution function.

Figures A.2a to A.2f demonstrate that the linear instability growth and the variation of growth rate with the electron-ion collision frequency both depend in a sensitive way on the magnitude of $k_\perp b_i$. For example, in Figure A.2a the maximum growth rates for $k_\perp b_i = 3.1$ and 3.6 are approximately 0.55 Ω_i and 0.3 Ω_i, respectively. The $k_\perp b_i = 3.1$ mode is stabilized by $\nu_e/\Omega_i \gtrsim 980$, while the $k_\perp b_i = 3.6$ mode is stabilized by much lower values of the collision frequency, $\nu_e/\Omega_i \gtrsim 87$.

Figures A.3a and A.3b show the maximum value of ν_e/Ω_i [i.e., $(\nu_e/\Omega_i)_{max}$] which permits a solution of Eq. (A.10) for the first two unstable zones and specified value for δ. Values of ν_e/Ω_i which exceed the magnitude indicated by the curves cannot satisfy Eq. (A.10), while those values below the curve can satisfy the equation. Unstable zone I solutions have been found for $\delta \geq 4$ but not for $\delta \leq 3$; however, for zone II, $\delta \geq 6$ provides a solution while $\delta \leq 5$ does not. Since Reference A4 primarily considered $\delta = 5$, that paper does not include the second unstable zone.

Comparison of Figures A.3a and A.3b indicates that, although Figure A.1 shows that the zone II instability can, in principle, have a greater growth rate than the zone I instability, electron-ion collisions stabilize the zone II instability more easily than the zone I instability. For $\delta \to \infty$, $(\nu_e/\Omega_i)_{max}$ is approximately equal to 3750 in zone I and 1100 in zone II. Qualitative

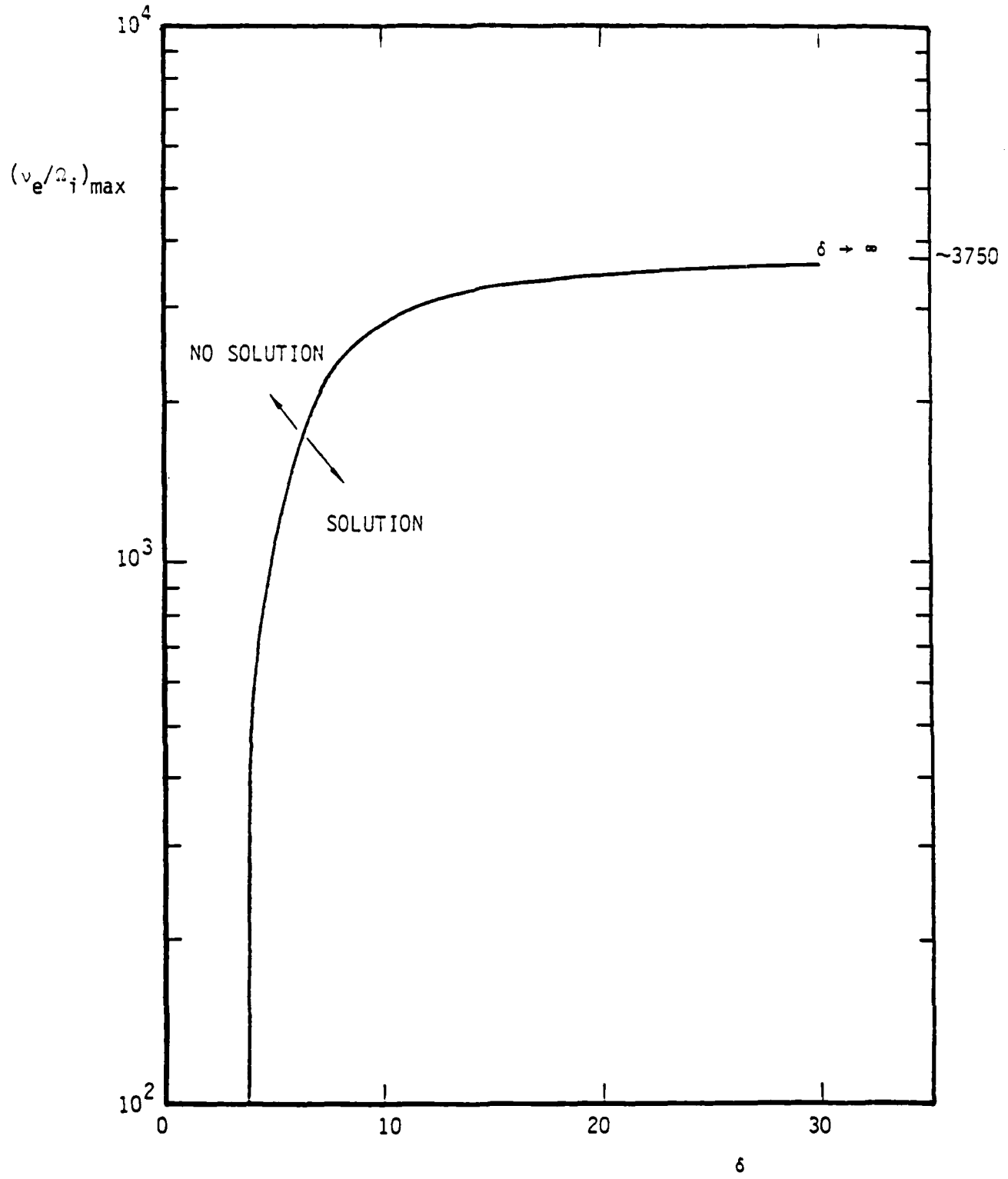

Figure A.3a. The maximum value of ν_e/Ω_i, $(\nu_e/\Omega_i)_{max}$, which permits solution of Eq. (A.9) versus δ for zone I. $(\nu_e/\Omega_i)_{max}$ for $\delta \to \infty$ is indicated on the right-hand side of the plot. Values of ν_e/Ω_i which exceed the magnitude indicated by the curves cannot satisfy Eq. (A.10), while those values below the curve can satisfy the equation.

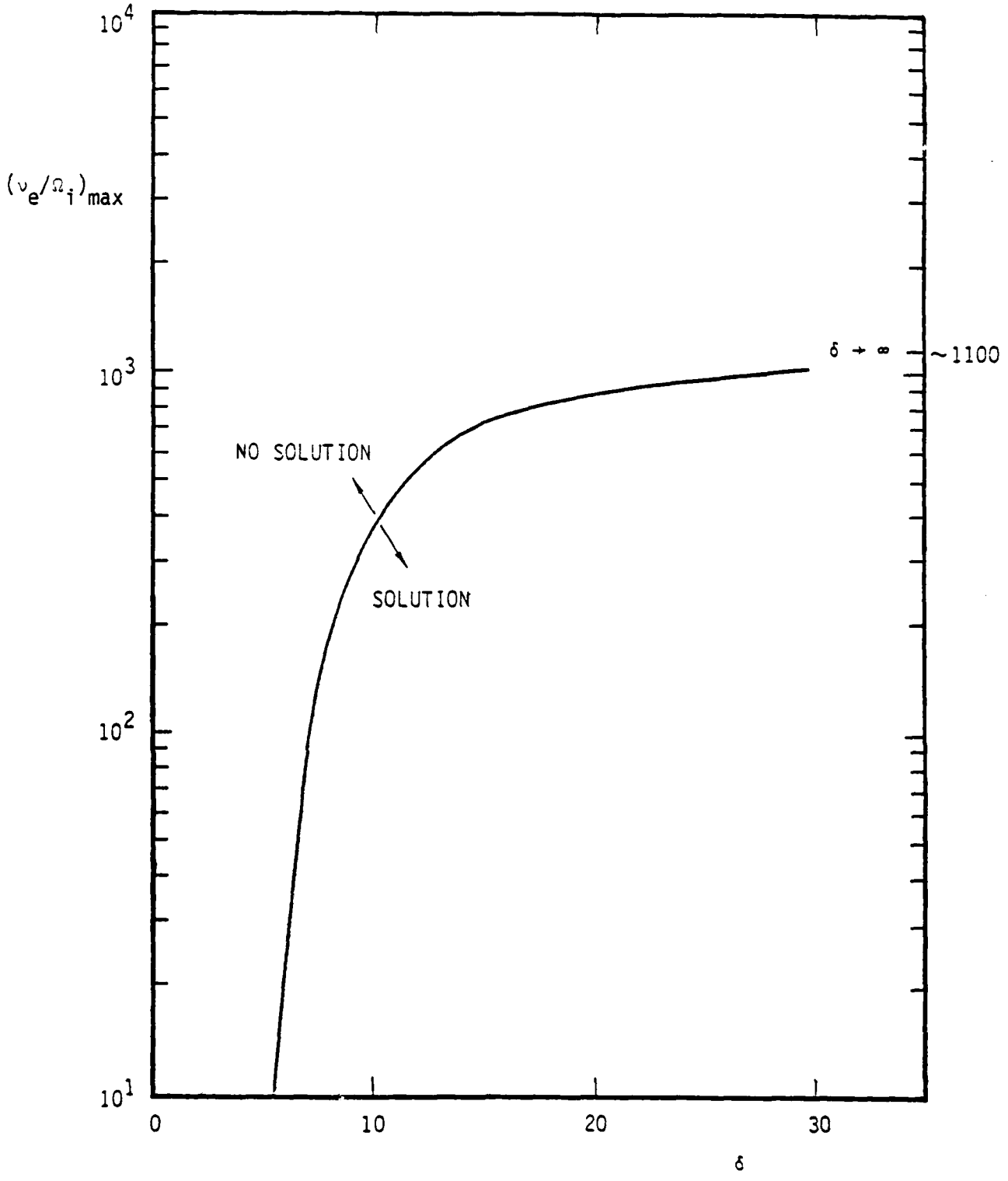

Figure A.3b. The maximum value of ν_e/Ω_i, $(\nu_e/\Omega_i)_{max}$, which permits solution of Eq. (A.9) versus δ for zone II. $(\nu_e/\Omega_i)_{max}$ for $\delta \to \infty$ is indicated on the right-hand side of the plot. Values of ν_e/Ω_i which exceed the magnitude indicated by the curves cannot satisfy Eq. (A.10), while those values below the curve can satisfy the equation.

examination of the third and higher unstable zones shows the general trend that stability through electron-ion collisions is more easily achieved as $k_\perp b_i$ increases. The physical reasoning behind this stabilization behavior is that waves which require higher harmonics of the wavelength to fit within the circumference of an ion-cyclotron orbit are more easily disrupted by phenomena which prevent ion-cyclotron orbits from being perfect circles. Mathematically, the stabilization for large $k_\perp b_i$ is easier because characteristically Bessel function oscillations about zero decrease in magnitude with argument.

A-4. DISCUSSION

By including electron-ion collisions in the analysis of electrostatic, finite ion-gyroradius, purely growing, flute modes, it has been demonstrated that, when unstable solutions to the dispersion relation exist, there are generally two solutions which satisfy the dispersion relation. Both solutions have growth rates which lie below the values predicted by collisionless theory. Above the value of the collision frequency for which both solutions merge, no purely unstable mode can exist for the specified values of $k_\perp b_i$ and δ.

The paper by Simons, et al.,[A4] proposes that the finite gyroradius, purely growing mode is the source of prompt striations in the Buaro barium release and so it is useful to determine the role of electron-ion collisions with the assumed and measured parameters of the Buaro plasma (i.e., $n_i \approx 4 \times 10^5$ cm^{-3}, $B_o \approx 0.32$ gauss, and $\delta = 5$). For an electron temperature of $T_e \approx 0.1$, the ratio of ν_e/Ω_i is equal to 21.7. Examining Figure A.2a, it is evident that the electron-ion collisions in the Buaro plasma do not significantly alter the growth rate of the most unstable mode predicted by collisionless theory (i.e., $k_\perp b_i \approx 3.1$ and $\gamma/\Omega_i \approx 0.55$).

For plasma densities which are higher than appropriate to the Buaro experiment, the electron-ion collision frequency has a corresponding greater stabilizing impact on the finite gyroradius purely growing flute modes. For example, if $n_i \approx 1 \times 10^7$ cm^{-3} and $T_e \approx 0.1$ eV, then $\nu_e/\Omega_i \approx 480$ and the maximum growth rate for $k_\perp b_i \approx 3.1$ in Figure A.2a is reduced to $0.48\ \Omega_i$ from the collisionless value of $0.55\ \Omega_i$. Figures A.3a and A.3b show that with $\nu_e/\Omega_i \approx 480$, no solution is possible for $\delta \lesssim 4$ in zone I and $\delta \lesssim 11$ in zone II. For even higher densities, $n_i \gtrsim 8.7 \times 10^7$ cm^{-3}, Figures A.3a and A.3b show that self electron-ion collisions are sufficient to completely stabilize the finite gyroradius, purely growing, modes. Such relatively high electron densities are required to stabilize the instability because of the weak electron polarization and Pederson response to the modes.

REFERENCES

A1. Booker, H. G., "Radio Scattering in the Lower Ionosphere," J. Geophys. Res., 64, p. 2164, 1959.

A2. Glasstone, S., "The Effects of Nuclear Weapons," U. S. Government Printing Office, Washington, D.C., 1962.

A3. Goldman, S. R., Baker, L., Ossakow, S. R., and Scannapiece, A. J., "Striation Formation Associated with Barium Clouds in an Inhomogeneous Ionosphere," J. Geophys. Res., 81, p. 5097, 1976.

A4. Simons, D. J., Pongratz, M. B., and Gary, S. P., "Prompt Striations in Barium Clouds," J. Geophys. Res., 85, p. 671, 1980.

A5. Braginskii, S. I., "Transport Processes in Plasmas," in Reviews of Plasma Physics, Vol. 1, edited by M. A. Leontovich, Consultants Bureau, New York, 1965.

A6. Sperling, J. L. and Goldman, S. R., "Electron Collisional Effects on Lower Hybrid Drift Instabilities in the Ionosphere," J. Geophys. Res., 85, p. 3494, 1980.

SUBAPPENDIX AA

In this subappendix it is shown that the lowest order ion response to the waves is unaffected by electron-ion collisions, while the electron dynamics in the wave are not modified by the ion response.

The demonstration that the lowest order ion response is not affected by electron-ion collision consists of two parts. First, the characteristic frequency for ions to change their momentum by a substantial amount due to collisions with electrons is:

$$\nu_i \approx (m_e/m_i)\, \nu_e \quad . \tag{AA.1}$$

For typical plasma densities and temperatures in the ionosphere (i.e., $n_e \lesssim 10^7$ cm^{-3} and $T_e \approx 0.1$ eV), the quantitative value of ν_i is very much smaller than the characteristic linear growth rate of the instability (i.e., $\gamma \lesssim \Omega_i$). Second, the electron response to the waves [see Eq. (A.5)] is in magnitude very much smaller than the individual terms in the ion response [see Eq. (A.1)]. Hence, the electron currents in the waves cannot significantly alter the ion dynamics through electron-ion collisions.

To show that the ion coupling through electron-ion collisions does not significantly modify the electron response to the waves under consideration, it is convenient to examine the electron momentum equation,

$$-i\omega m_e n_e \vec{v}_{e1} = -e\vec{E}_1 n_e \frac{\vec{v}_{e1}\times\vec{B}_o}{c} - m_e n_e \nu_e (\vec{v}_{e1} - \vec{v}_{i1}) \quad , \tag{AA.2}$$

where subscript "1" denotes wave quantities. To lowest order in inverse magnetic field strength,

$$v_{e1}^{(0)} = c\,\frac{\vec{E}_1\times\vec{B}_o}{B_o^2} \quad . \tag{AA.3}$$

To next order,

$$i\omega m_e n_e \vec{v}_{e1}^{(0)} = e n_e \frac{\vec{v}_{e1}^{(1)} \times \vec{B}_0}{c} + m_e n_e \nu_e \left(\vec{v}_{e1}^{(0)} - \vec{v}_{i1}\right) \quad . \quad \text{(AA.4)}$$

From Eq. (AA.4) it is evident that the ion velocity in the waves does not significantly affect the electron velocity if:

$$|\vec{v}_{i1}/\vec{v}_{e1}^{(0)}| \ll 1 \quad . \quad \text{(AA.5)}$$

Now the dielectric elements which reflect the $\vec{E}\times\vec{B}$ velocity, in the limit of low frequency and infinitesimal wave number, are $\kappa_{x,y}$ and $\kappa_{y,x}$, where x and y are the two coordinates orthogonal to the magnetic field. In particular, for electrons:

$$|\kappa_{x,y}^{(e)}| = |\kappa_{y,x}^{(e)}| = |\omega_{pe}^2/\Omega_e\omega| \quad , \quad \text{(AA.6)}$$

while for the ions:

$$|\kappa_{x,y}^{(i)}| = |\kappa_{y,x}^{(i)}|$$

$$= 2\pi \left| \frac{\omega_{pi}^2}{\omega} \sum_{p=1}^{\infty} \frac{p^2\Omega_i^3}{k_\perp^2(p^2\Omega_i^2-\omega^2)} \int_{-\infty}^{\infty} dv_\parallel \int_0^{\infty} dv_\perp v_\perp \right.$$

$$\left. \frac{\partial f_i(\vec{v})}{\partial v_\perp} \frac{\partial}{\partial v_\perp} [J_p^2(k_\perp v_\perp/\Omega_i)] \right|$$

$$= 2\pi \left| \frac{\omega_{pi}^2}{\omega} \sum_{p=1}^{\infty} \frac{p^2\Omega_i}{k_\perp^2 (p^2\Omega_i^2 - \omega^2)} \int_{-\infty}^{\infty} dv_\parallel \int_0^{\infty} dv_\perp \frac{\partial}{\partial v_\perp} \right.$$

$$\left. \left[v_\perp \frac{\partial f_i}{\partial v_\perp} \right] J_p^2(k_\perp v_\perp/\Omega_i) \right| \quad . \qquad \text{(AA.7)}$$

For purely growing modes $i\gamma = \omega$ and it follows that:

$$|\kappa_{x,y}^{(i)}| \leq 2\pi \left| \frac{\omega_{pi}^2 \Omega_i}{\gamma k_\perp^2} \sum_{p=1}^{\infty} \int_{-\infty}^{\infty} dv_\parallel \int_0^{\infty} dv_\perp \frac{\partial}{\partial v_\perp} \right.$$

$$\left. \left[v_\perp \frac{\partial f_i(v_\perp)}{\partial v_\perp} \right] J_p^2(k_\perp v_\perp/\Omega_i) \right|$$

$$= \pi \left| \frac{\omega_{pi}^2 \Omega_i}{\gamma k_\perp^2} \int_{-\infty}^{\infty} dv_\parallel \int_0^{\infty} dv_\perp \frac{\partial}{\partial v_\perp} \right.$$

$$\left. \left[v_\perp \frac{\partial f_i(\vec{v})}{\partial v_\perp} \right] [1 - J_o^2(k_\perp v_\perp/\Omega_i)] \right|$$

$$= \pi \left| \frac{\omega_{pi}^2}{\gamma \Omega_i} \int_{-\infty}^{\infty} dv_\parallel \int_0^{\infty} dv_\perp v_\perp^2 \frac{\partial}{\partial v_\perp} \right.$$

$$\left. \left[v_\perp \frac{\partial f_i(\vec{v})}{\partial v_\perp} \right] (k_\perp v_\perp/\Omega_i)^{-2} [1 - J_o^2(k_\perp v_\perp/\Omega_i)] \right| \quad , \text{(AA.8)}$$

with the equality being valid in the limit of $\gamma \to 0$. In deriving Eq. (AA.8), the standard Bessel function addition theorem,

$$1 = J_o^2(z) + 2 \sum_{p=1}^{\infty} J_p^2(z) \qquad \text{(AA.9)}$$

has been used. In the limit of $k_\perp \to 0$, Eq. (AA.8) becomes:

$$|\kappa_{x,y}^{(i)}| < 2\pi \left| \frac{\omega_{pi}^2}{\omega\Omega_i} \int_{-\infty}^{\infty} dv_\parallel \int_0^{\infty} dv_\perp v_\perp f_i(\vec{v}) \right| = \left| \frac{\omega_{pi}^2}{\omega\Omega_i} \right| \qquad \text{(AA.10)}$$

Examining Eqs. (AA.6) and (AA.9), it is evident that:

$$|\kappa_{x,y}^{(i)}| \leq |\kappa_{x,y}^{(e)}| \qquad \text{(AA.11)}$$

with the equality holding if $\gamma, k_\perp \to 0$.

For the values of frequency and wavenumber considered in this paper (i.e., growth rates a sizeable fraction of the ion-cyclotron frequency and $k_\perp v_\perp/\Omega_i > 2.5$), the inequality holds and Eq. (AA.5) is satisfied to lowest order.

APPENDIX B

STABILIZATION OF PROMPT STRIATIONS BY BACKGROUND PLASMA

ABSTRACT

The ambient background plasma is shown to have an important stabilizing influence on the generation of electrostatic, purely growing, finite ion-gyroradius, flute instabilities driven by ion loss cone distribution functions associated with shaped barium injection across the ambient magnetic field in the ionosphere. This stabilization implies that such short scale size instabilities and the striations they produce will only be present if the background plasma density is low enough. Consistent with the experimental observations of the striations, it is shown that for the parameters of the Buaro barium release experiment the background plasma density is insufficient to completely stabilize the finite ion-gyroradius modes; however, background ion density does reduce the growth rate from the level predicted with a theory which does not include the background plasma dynamics.

B-1. INTRODUCTION

Plasmas containing a population of ions with a loss cone velocity distribution function are susceptible to instabilities which drive ions into the loss cone at a much faster rate than classical collisional processes.[B1,B2] In fact, these instabilities are thought to be the limiting factor for modern mirror machines.[B3-B5] However, loss cone instabilities are not isolated to the laboratory.

Recently it has been suggested that electrostatic, purely growing, finite ion-gyroradius, flute instabilities caused by an ion loss cone distribution function are responsible for the prompt striations observed in the Buaro shaped barium release.[B6] The purpose of this paper is to show that these finite ion-gyroradius instabilities are not a general feature of ionospheric plasma expansion across a magnetic field. In fact, they can be stabilized for realizable values of the background plasma density even though complete stabilization does not occur for the parameters of the Buaro experiment. Quantitative results presented here are not only consistent with those of Swift for the special case of monoenergetic loss cone ions[B7] but also include the effects of background plasma for more distributed loss cone ion distribution functions. Moreover, they are in agreement with research in the mirror fusion program which indicates enhanced stability of loss cone modes when less energetic plasma is present.[B3,B4] When stabilization does occur, instabilities characterized by slower growth times and larger scale lengths such as the EXB gradient drift instability [e.g., see Reference B8 for a detailed analysis] must determine striation structure rather than the characteristically more vigorous and smaller scale size finite ion-gyroradius modes.

This appendix is divided into four sections. Section B-2 describes the theoretical model for the calculation and qualitative implications of the dispersion relation. Section B-3 contains quantitative results of the solution to the dispersion relation, while Section B-4 summarizes the theory and results. Suggested experiments for testing the theory are presented.

B-2. THEORETICAL MODEL

An infinite homogeneous plasma model consisting of two components is assumed. The first component is the thermal plasma background which corresponds to the ambient ionosphere. The second component is the high velocity ion component (with associated electrons) which arises from the shaped barium release or possibly some other natural or artificial phenomena,[B6,B7] and is assumed to have a loss cone velocity distribution shown to be the appropriate distribution function after a shaped barium release.[B6]

The thermal background plasma consists of electrons with density n_{eo} and several singly ionized ion species (designated by subscript j) of density, n_{jo}. Quasineutrality requires,

$$n_{eo} = \sum_j n_{jo} \quad . \tag{B.1}$$

The background magnetic field has strength B_o. The modes considered in this appendix are plane waves corresponding to the electrostatic limit of extraordinary mode propagation. They are assumed to be purely growing with growth rate γ, and to be flute-like with the only spatial variation perpendicular to the magnetic field ($k_\perp$). The electric potential associated with the wave satisfies Laplace's equation, $k_\perp^2 [1 + 4\pi (\kappa_1 + \kappa_2)]\phi = 0$, where κ_1 and κ_2 are the ambient and loss cone plasma susceptibilities, respectively.

With the chosen plasma model the contribution of the ambient plasma to the electrostatic dielectric is:[B9]

$$\kappa_1 = (4\pi)^{-1} \left[\frac{\omega_{eo}^2}{\Omega_e^2} + 2 \sum_j \frac{\omega_{jo}^2}{k_\perp^2 v_j^2} \sum_{p=1}^{\infty} \frac{p^2 \Omega_j^2}{\gamma^2 + p^2 \Omega_j^2} \right.$$

$$\left. \cdot I_p (k_\perp^2 b_j^2) \exp (-k_\perp^2 b_j^2) \right] \tag{B.2}$$

where

$$\omega_{eo}^2 = 4\pi\, n_{eo}\, e^2/m_e \quad , \quad \omega_{jo}^2 = 4\pi\, n_{jo}\, e^2/m_j \quad , \quad b_j = v_j/\Omega_j \quad ,$$

$$v_j = (T_j/m_j)^{\frac{1}{2}} \quad , \quad \Omega_e = -eB_o/m_e c \quad , \quad \Omega_j = eB_o/m_j c \quad . \tag{B.3}$$

In Eqs. (B.2)-(B.3), the symbol I_p represents the modified Bessel function of the first kind and order p. Also, e, m_e, m_j, T_j, and c represent the magnitude of the electron charge, the electron mass, mass of a single particle of background ion species j, temperature of background ion species j, and the speed of light, respectively. Two assumptions made in writing Eq. (B.2) are that the electron-gyroradius is much smaller than the inverse perpendicular wavenumber and that the wave frequency is much smaller than the electron-gyrofrequency. Also, collision effects are neglected.

The high velocity ion plasma contribution to the dielectric is given by:[B6,B10]

$$\kappa_2 = (4\pi)^{-1}\left[\frac{\omega_e^2}{\Omega_e^2} + 2\,\frac{\omega_i^2}{k_\perp b_i}\sum_{p=1}^{\infty}\frac{\gamma^2}{\gamma^2+p^2\Omega_i^2}\,\frac{(2p-1)I_{p,p-1}}{\gamma^2+(p-1)^2\Omega_i^2}\right] \tag{B.4}$$

where

$$\omega_e^2 = 4\pi\, n_i\, e^2/m_e \quad , \quad \omega_i^2 = m_i\omega_e^2/m_e \quad ,$$

$$\Omega_i = eB_o/m_i c \quad , \quad b_i = v_o/\Omega_i \quad ,$$

$$I_{p,p-1} = \frac{\delta^3}{A(\delta)}\int_0^{\infty} dx\; x\; J_p(k_\perp b_i x)J_{p-1}(k_\perp b_i x)\; \exp[-0.5\delta^2(x-1)^2]$$

$$A(\delta) = (\tfrac{\pi}{2})^{\frac{1}{2}}\left\{(1+\delta^2)[1+\mathrm{erf}(\delta/\sqrt{2})] + (\tfrac{2}{\pi})^{\frac{1}{2}}\delta\,\exp(-0.5\delta^2)\right\} \tag{B.5}$$

In Eq. (B.5) the parameters n_i and m_i denote the density of loss cone ion species i and the mass of a single particle of loss cone ion species i, respectively. The ordinary Bessel function of the first kind and order p is represented by J_p. The parameters v_o, v_i, and $\delta = v_o/v_i$ are associated with the assumed form for the loss cone ion distribution function,

$$f_i(\vec{v}) = \frac{\delta^3 v_\perp}{2\pi\, v_o^3\, A(\delta)} \exp\left(\frac{(v_\perp - v_o)^2}{2v_i^2}\right) g(v_\parallel) \quad . \tag{B.6}$$

Here $v_\perp$ and $v_\parallel$ are the perpendicular and parallel velocities to the magnetic field, respectively. The precise functional form of $g(v_\parallel)$ is unimportant for the flute modes being considered.

The wave electric field potential is nonzero only if the dispersion relation is satisfied:

$$0 = 1 + 4\pi\,(\kappa_1 + \kappa_2) \quad . \tag{B.7}$$

The new feature of this dispersion relation, which has not been considered previously for the barium cloud environment, is the contribution of the ambient plasma.

The significance of the background plasma upon the linear dynamics of the purely growing finite ion-gyroradius flute modes arises because such modes tend to be quasineutral for ionospheric parameters and the ion dynamics in response to the wave fields are much more profound than the weaker electron polarization currents. Quantitatively,

$$\omega_i^2/\Omega_i^2 \gg \omega_e^2/\Omega_e^2 \gg 1 \quad ,$$

$$\sum \omega_{jo}^2/\Omega_j^2 \gg \omega_{eo}^2/\Omega_e^2 \quad . \tag{B.8}$$

Hence, a very good approximation to the dispersion relation is:

$$0 \approx \sum_j \frac{1}{k_\perp^2 b_j^2} \frac{m_j n_{jo}}{m_i n_i} \sum_{p=1}^{\infty} \frac{p^2 \Omega_j^2}{\gamma^2 + p^2 \Omega_j^2} I_p(k_\perp^2 b_j^2)$$

$$\cdot \exp(-k_\perp^2 b_j^2) + \frac{\Omega_i^2}{k_\perp b_i} \sum_{p=1}^{\infty} \frac{\gamma^2}{\gamma^2 + p^2 \Omega_i^2}$$

$$\cdot \frac{(2p-1)\, I_{p,p-1}}{\gamma^2 + (p-1)^2 \Omega_i^2} \quad . \tag{B.9}$$

Examination of Eq. (B.9) demonstrates that the background ions always promote stability because these ions introduce a positive definite contribution to the dispersion relation while the fast ion portion of the dispersion relation can be positive or negative but is always finite. Indeed, the numerical evaluation of Eq. (B.9) also indicates that for a specified value of $k_\perp b_i$ and loss cone ion density, growth rate is reduced as background ion density is increased. Hence, lack of solution at marginal stability,

$$0 < \frac{\bar{\rho}}{\rho_i} + \frac{2 I_{1,0}}{k_\perp b_i} \quad , \tag{B.10}$$

is sufficient to assure no growing solutions are possible for a specified $k_\perp b_i$ and background plasma density. In deriving Eq. (B.10), the identity

$$\exp(z) = I_0(z) + 2 \sum_{p=1}^{\infty} I_p(z) \tag{B.11}$$

has been used while

$$\bar{\rho} = \sum_j m_j n_{jo} [1 - I_0(k_\perp^2 b_j^2) \exp(-k_\perp^2 b_j^2)] / k_\perp^2 b_j^2 \quad , \quad \rho_i = m_i n_i \quad . \tag{B.12}$$

A final simplification to the dispersion relation can be made by noting that the weighted ambient background mass density, $\bar{\rho}$, reduces to the actual ambient mass density when $b_j \to 0$ (i.e., $\bar{\rho} \xrightarrow{b_j \to 0} \sum_j n_{jo} m_j$). This approximation can be very reasonable for high velocity ions (particularly heavy ions like barium) within the ambient ionosphere because

$$b_j/b_i << 1 \quad ; \tag{B.13}$$

however, care must always be taken in applying the $b_j \to 0$ approximation since positive growth rate solutions to Eq. (B.9) are characterized by:

$$2.5 < k_\perp b_i \quad . \tag{B.14}$$

A general statement, deduced from Eqs. (B.10) and (B.12), is that maximum stabilization by the ambient plasma takes place when the background is sufficiently cold so that the $k_\perp b_j << 1$ approximation is valid and $\bar{\rho}$ has its largest possible magnitude for given loss cone and background ion density. Physically, this most effective stabilization arises because the background plasma current in the potential fluctuations is largest when $k_\perp b_j \to 0$ and is optimally able to short-circuit the tendency for wave potential growth associated with the loss cone ions. However, when the thermal spread in the background ion distribution function is large, background ion current is reduced and higher background density is required for stability. Ultimately, stability for $k_\perp b_j$ large is caused by the reduction of the net destabilizing positive slope for the total (i.e., loss cone plus background) ion distribution function.

B-3. RESULTS

Results from the quantitative evaluation of the dispersion relation, Eq. (B.9), are presented in Table B.1 and Figures B.1 and B.2. As noted in Reference B9, there are under ideal conditions with $\delta \to \infty$, a very large but finite number of possible unstable zones in $k_\perp b_i$ which correspond to negative $J_1(k_\perp b_i)J_0(k_\perp b_i)$. In the first column of Table B.1, the zones with $k_\perp b_i < 26$ are listed. For each zone of instability in $k_\perp b_i$, the value of $k_\perp b_i$ which is most difficult to stabilize with cold background ions is given in the second column and the corresponding minimum value of $\bar{\rho}/\rho_i$ required for stability is shown in the third column.

The key features of Table B.1 are that instability is not possible for $\bar{\rho}/\rho_i > 0.059$ and that smaller values of $\bar{\rho}/\rho_i$ are required for stability as the value of $k_\perp b_i$ in column 2 increases. These results are consistent with those of Reference B7 for a monoenergetic ion population. Mathematically, this reduction comes about because the maximum amplitude of Bessel function oscillations decreases with argument. Physically, the polarization drift of the background ions in the waves most easily stabilize fluctuations requiring the highest degree of coherence between ions and waves (i.e., waves with large $k_\perp b_i$). A corollary remark is that instability with sizeable $k_\perp b_i$ requires δ large in order that the ion motion within the wave has the necessary coherence.

Curves for the marginally stable values of $\bar{\rho}/\rho_i$ versus $k_\perp b_i$ are plotted in Figures B.1a - B.1c for $\delta = 5$, 10, and ∞, respectively. These cases are not quantitatively analyzed in Reference B7. In Figure B.1a only the $2.5 < k_\perp b_i < 3.8$ instability is shown because for $\delta = 5$ it is the only zone in $k_\perp b_i$ which permits instability. For $\delta = 10$ and ∞, other unstable zones in $k_\perp b_i$ are possible, but for clarity only the first two are illustrated in Figures B.1b and B.1c.

The curves in Figures B.1a - B.1c characteristically have a maximum magnitude and decrease on both sides of this point. The rate of decrease is most rapid for $k_\perp b_i$ near the values for which $J_0(k_\perp b_i)\, J_1(k_\perp b_i) = 0$. Only $\bar{\rho}/\rho_i$ below the curves permit instability. In particular, as the magnitude of $\bar{\rho}/\rho_i$ increases, only those $k_\perp b_i$ which are not too close to the $J_0(k_\perp b_i)$

Table B.1. Ranges of $k_\perp b_i$ which can be unstable with $\delta \to \infty$, the value of $k_\perp b_i$ most difficult to stabilize for each range, and the minimum value of $\bar{\rho}/\rho_i$ required to completely stabilize the instability for each range.

$k_\perp b_i$ RANGE	$k_\perp b_i$ VALUE MOST DIFFICULT TO STABILIZE	MINIMUM $\bar{\rho}/\rho_i$ REQUIRED FOR STABILITY
2.5 - 3.8	3.0	5.9×10^{-2}
5.6 - 7.0	6.2	1.5×10^{-2}
8.7 - 10.1	9.4	6.8×10^{-3}
11.8 - 13.3	12.5	3.9×10^{-3}
15.0 - 16.4	15.7	2.5×10^{-3}
18.1 - 19.6	18.8	1.7×10^{-3}
21.3 - 22.7	22.0	1.3×10^{-3}
24.4 - 25.9	25.1	9.8×10^{-4}

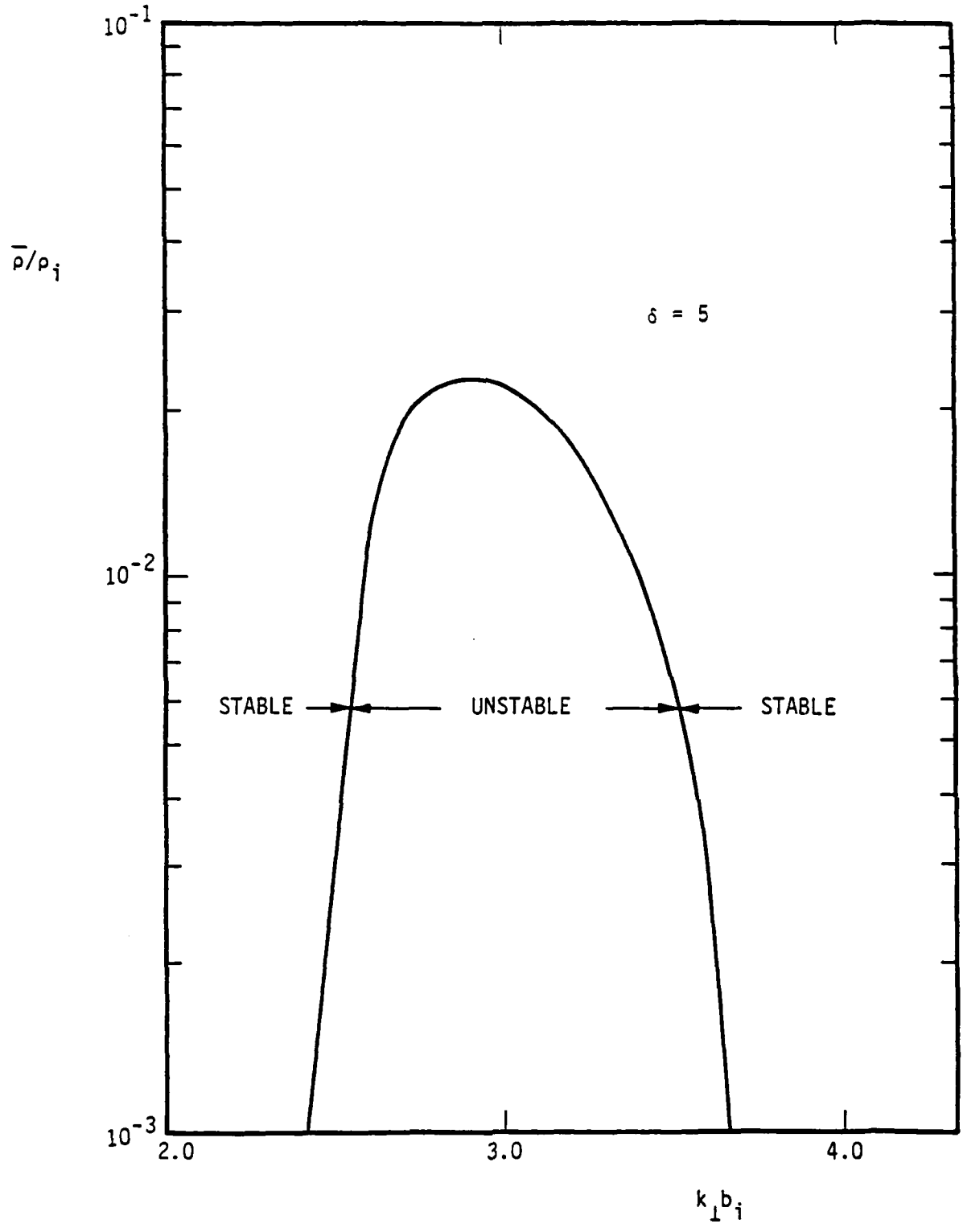

Figure B.1a. $\bar{\rho}/\rho_i$ versus $k_\perp b_i$ for $\delta = 5$. The illustrated curve gives the marginal stability condition. For values of $\bar{\rho}/\rho_i$ below the curve, instability is possible, but above the curve modes are stable.

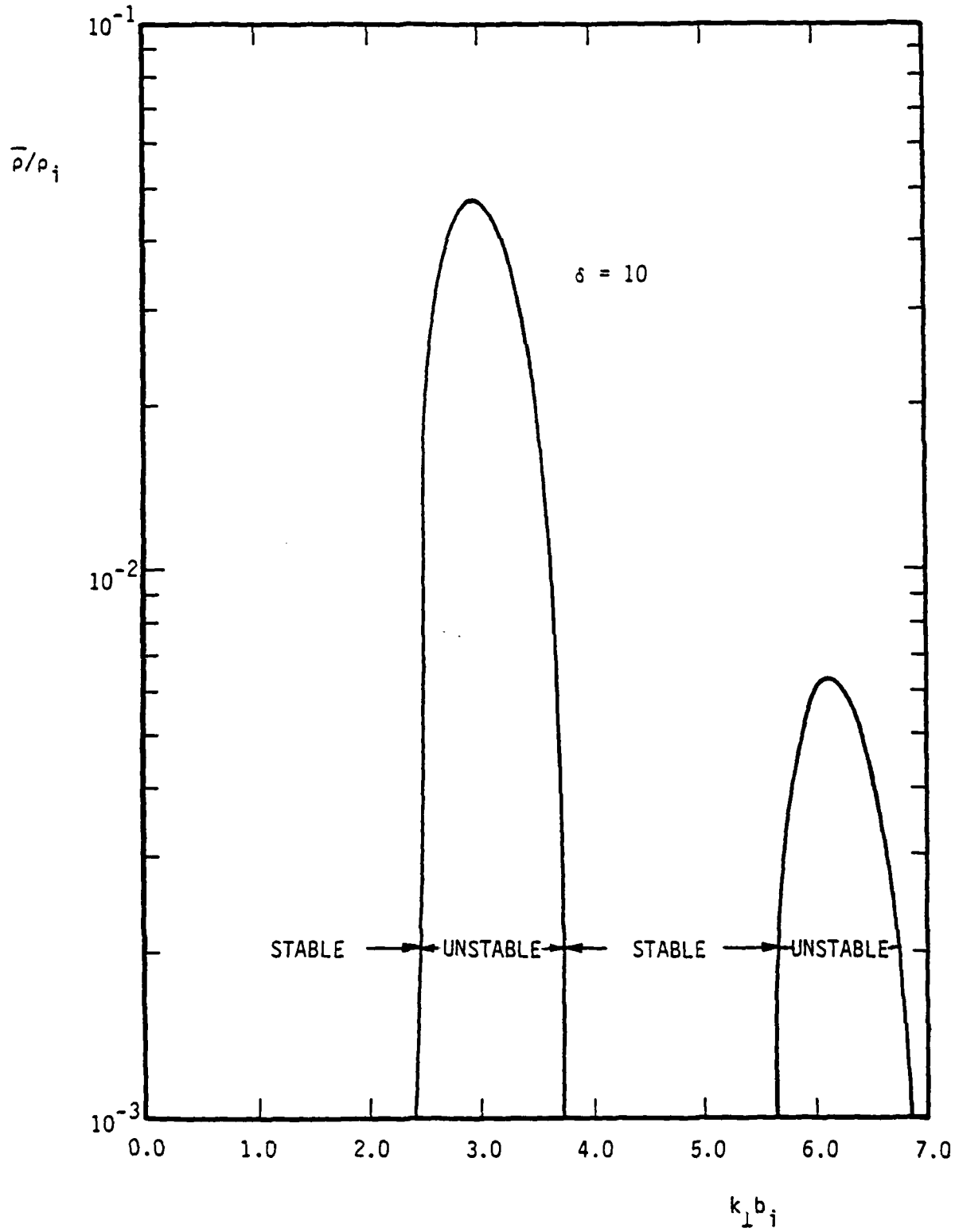

Figure B.1b. $\bar{\rho}/\rho_i$ versus $k_\perp b_i$ for δ = 10. The illustrated curves give the marginal stability condition. For values of $\bar{\rho}/\rho_i$ below the curves, instability is possible, but above the curves modes are stable.

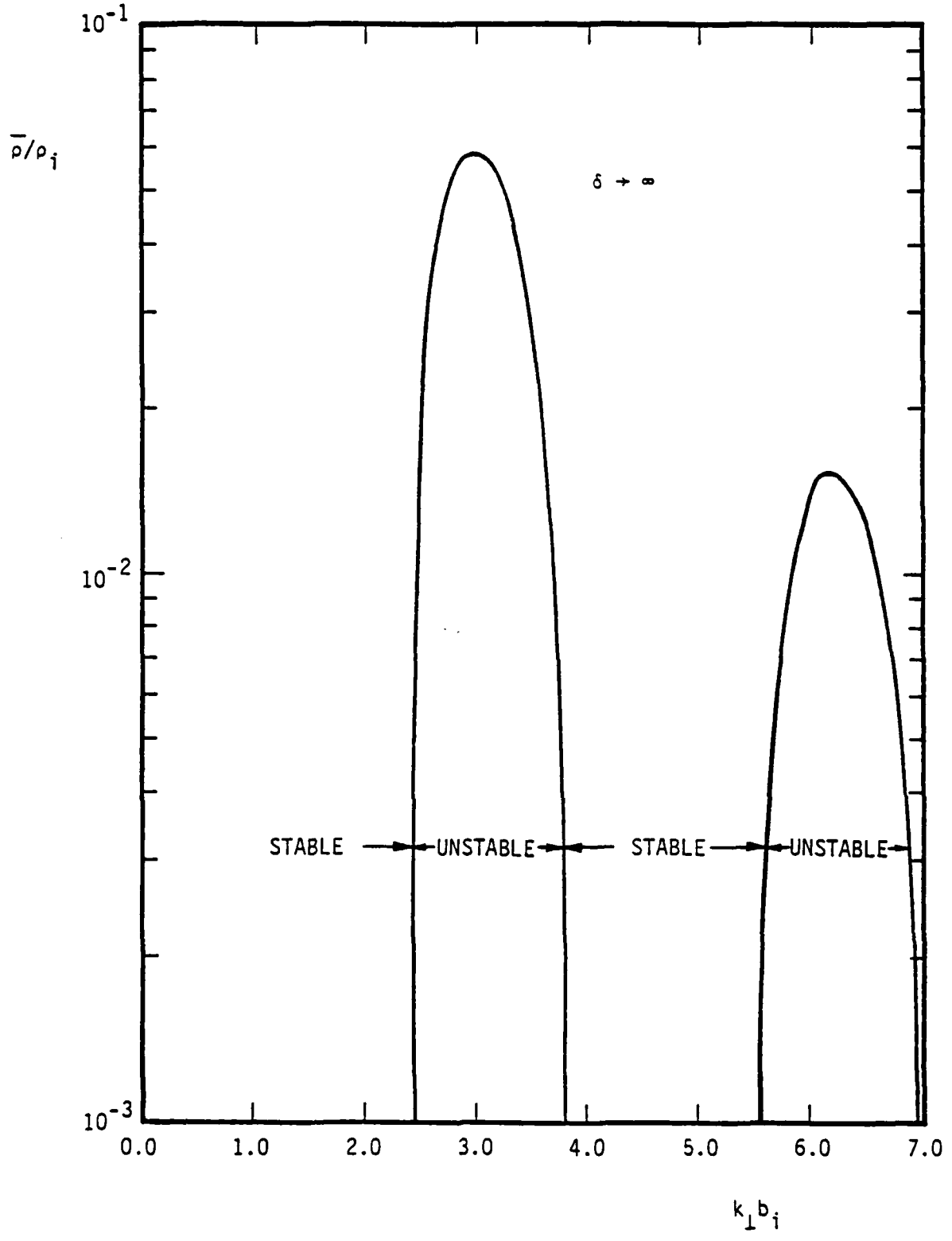

Figure B.1c. $\bar{\rho}/\rho_i$ versus $k\, b_i$ for $\delta \to \infty$. The illustrated curves give the marginal stability condition. For values of $\bar{\rho}/\rho_i$ below the curves, instability is possible, but above the curves modes are stable.

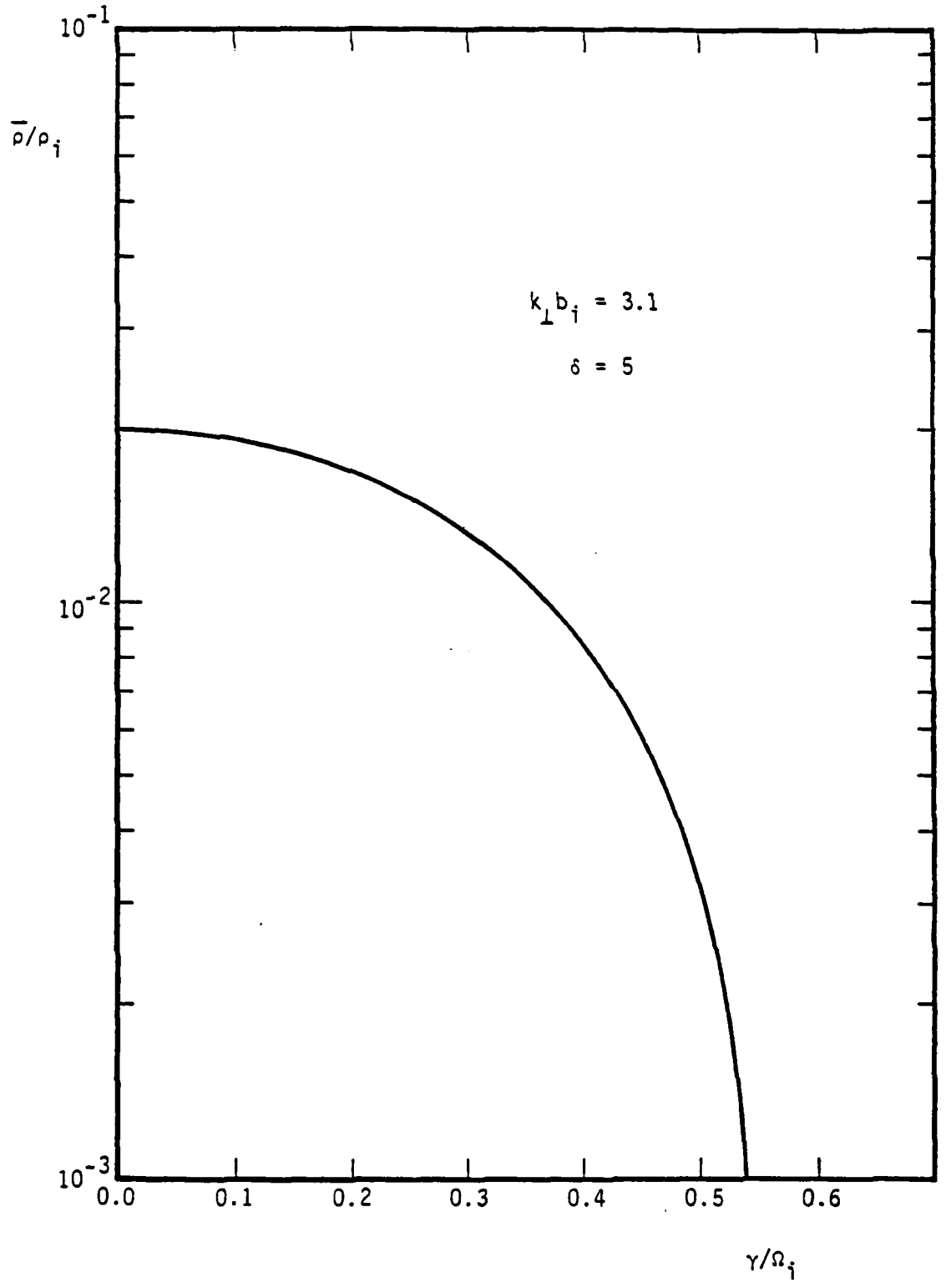

Figure B.2. $\bar{\rho}/\rho_i$ versus γ/Ω_i for $k_\perp b_i = 3.1$ and $\delta = 5$.

$J_1(k_\perp b_i) = 0$ points can be unstable. For example in Figure B.1b, $\bar{\rho}/\rho_i = 0.03$ implies that instability can occur only if $2.6 \lesssim k_\perp b_i < 3.4$. For values of $\bar{\rho}/\rho_i$ above the curves the criterion given by Eq. (B.10) is satisfied and there is stability. The three figures demonstrate that instability is possible for larger values of $\bar{\rho}/\rho_i$ if δ increases.

In Reference B6 a barium cloud with $\delta = 5$ was considered. Figure B.2 is a plot of $\bar{\rho}/\rho_i$ versus γ/Ω_i for the corresponding most unstable purely growing mode in the absence of background ion density (i.e., $\gamma/\Omega_i \approx 0.55$ and $k_\perp b_i \approx 3.1$). Given a value for $\bar{\rho}/\rho_i$, the corresponding solution to the dispersion relation is found at the intersection with the plotted curve. It is evident that with a finite background ion density the growth rate is reduced below what it would be if $\bar{\rho}/\rho_i \to 0$. Assuming a background electron density of $n_{eo} = 3 \times 10^4$ cm^{-3}, a barium ion density of $n_i = 4 \times 10^5$ cm^{-3},[B6] and singly ionized monatomic oxygen, then $\gamma \approx 0.39\ \Omega_i$. Although this value for the growth rate is still a sizeable fraction of the ion-gyrofrequency, the background density has resulted in a 30% reduction in growth rate. Complete stabilization by background ion density is not achieved in Buaro. Figure B.2 indicates that a background monatomic oxygen density in excess of 6.9×10^4 cm^{-3} would be required to totally stabilize the $k_\perp b_i = 3.1$ and $\delta = 5$ instability. From Figure B.1a total stabilization for $\delta = 5$ and all $k_\perp b_i$ is possible for monatomic oxygen densities larger than 8×10^4 cm^{-3}. This density is less than the barium density and readily occurs in the ionosphere.

The theoretical model and the application to Buaro have neglected magnetic field strength and plasma spatial variations. Reference B6 shows that Buaro density gradients perpendicular to the magnetic field only weakly modify the infinite and homogeneous analysis of the purely growing loss cone instability, but no comments are made about effects associated with inhomogeneities parallel to the background magnetic field. Now, a local approximation for mode characteristics is reasonable if the plasma permits modes with very long wavelengths parallel to the magnetic field. In particular, the dispersion relation, Eq. (B.2), is asymptotically valid if:[B9]

$$\lambda_{\parallel} >> 2(2)^{\frac{1}{2}}\ \pi\ v_i/\Omega_i \qquad \text{(B.15)}$$

where $\lambda_{\parallel}$ is the parallel wavelength. For Buaro parameters, Eq. (B.15) implies $\lambda_{\parallel} >> 0.8$ km. Also, from Figure 3 of Reference B6, it is clear that the longitudinal dimensions of the barium cloud are well in excess of 10 kilometers. Hence, a calculation using local values of density and magnitude field strength is justified to lowest order.

B-4. SUMMARY AND DISCUSSION

Purely growing, finite ion-gyroradius, flute instabilities generated because of an ion loss cone distribution function can be stabilized by the ions of a sufficiently high density ambient ionosphere. Since the electron polarization currents in the waves are much smaller than the ion currents, electrons do not contribute in a significant way to the wave dynamics.

The purely growing finite ion-gyroradius flute instabilities have characteristic scale lengths and growth times which are much smaller than those typical of EXB gradient drift instabilities. Hence, the finite ion-gyroradius instabilities provide a lower limit on striation scale length in the ionosphere than can be predicted from EXB gradient drift theory and can be the dominant mechanism producing striations when operative (i.e., with the background plasma density low enough).

For the parameters of the Buaro shaped barium release,[B6] the local approximation for the instability has been justified and it has been demonstrated that the instability exists albeit with a linear growth rate reduced by the background plasma. The theory with background plasma dynamics included does indicate that if the ambient ion density (assumed to be primarily monatomic oxygen) had been larger than 8×10^4 cm^{-3} rather than the measured value of 3×10^4 cm^{-3}, the finite ion-gyroradius flute modes would not have been unstable and small scale length prompt striations produced by these modes would not have been observed.

The theory and results presented in this paper suggest two experiments to test the theory. First, shaped barium releases similar to Buaro but with higher background ion density (e.g., greater than 8×10^4 cm^{-3} for monatomic oxygen) should not result in striations with scale lengths characteristic of the finite ion-gyroradius flute instabilities. Second, if a shaped barium release is followed in approximately five seconds by one which is not shaped, the theory predicts that the striations should first appear, if the background density is low enough, but should eventually disappear in conjunction with ionization of the second barium release. Specifically, the Buaro striations would have been completely stabilized by modest values of thermal barium ion

density (i.e., greater than 9×10^3 cm^{-3}). Since for both experiments the finite ion-gyroradius instability is or becomes inoperative, ionosphere striation structure formed must "freeze" at a larger scale length typical of more fluid-like modes such as the EXB gradient drift instability.

REFERENCES

B1. Dory, R. A., Guest, G. E., and Harris, E. G., "Unstable Electrostatic Plasma Waves Propagating Perpendicular to a Magnetic Field," Phys. Rev. Lett., 14, p. 131, 1965.

B2. Post, R. F. and Rosenbluth, M. N., "Electrostatic Instabilities in Finite Mirror-Confined Plasmas," Phys. Fluids, 9, p. 2353, 1966.

B3. Coensgen, F. H., Cummins, W. F., Logan, B. G., Molvik, A. W., Nexson, W. E., Simonen, T. C., Stallard, B. W., and Turner, W. C., "Stabilization of a Neutral-Beam-Sustained, Mirror-Confined Plasma," Phys. Rev. Lett., 35, p. 1501, 1975.

B4. Berk, H. L. and Stewart, J. J., "Quasi-linear Transport Model for Mirror Machines," Phys. Fluids., 20, p. 1080, 1977.

B5. Myer, R. C. and Simon, A., "Nonlinear Saturation of the Drift Cyclotron Loss-cone Instability," Phys. Fluids., 23, p. 963, 1980.

B6. Simons, D. J., Pongratz, M. B., and Gary, S. P., "Prompt Striations in Ionospheric Barium Clouds Due to a Velocity Space Instability," J. Geophys. Res., 85, p. 671, 1980.

B7. Swift, D. W., "Turbulent Generation of Electrostatic Fields in the Magnetosphere," J. Geophys. Res., 82, p. 5143, 1977.

B8. Goldman, S. R., Baker, L., Ossakow, S. L., and Scannapieco, A. J., "Striation Formation Associated with Barium Clouds in an Inhomogeneous Ionosphere," J. Geophys. Res., 81, p. 5097, 1976.

B9. Stix, T. H., "The Theory of Plasma Waves," McGraw-Hill, New York, 1962.

B10. Sperling, J. L. and Krall, N. A., "Electron-ion Collision Effects on the Formation of Prompt Striations in the Ionosphere," J. Geophys. Res., 86, p. 5726, 1981.

APPENDIX C

ELECTROMAGNETIC EFFECTS IN THE ANALYSIS OF PROMPT STRIATIONS

ABSTRACT

In a number of barium injection experiments in the ionosphere, field aligned structures have been observed to develop on the ion-cyclotron time scale. These structures, called prompt striations, have been attributed to plasma jetting across the ambient magnetic field and have previously been analyzed in the electrostatic limit. The electrostatic analysis is reasonable for experiments in which the directed ion kinetic energy per unit volume is much smaller than the magnetic field pressure; however, for higher altitude experiments in which the ambient magnetic field strength is weaker, justification for the electrostatic treatment fails and the full electromagnetic dispersion relation must be examined. It is demonstrated that electromagnetic effects inhibit the growth of the linear instability considered to be the source of prompt striations in the earlier experiments. Consistent with the electrostatic analysis, cold background plasma and thermal spread in the ion loss cone distribution function tend to stabilize the instability in the full electromagnetic treatment. The theory suggests that prompt striations in the magnetosphere can form from ion jets only if the plasma density is sufficiently tenuous so that electromagnetic stabilization is not complete.

C-1. INTRODUCTION

Structures with magnetic field aligned geometry have been observed on a time scale comparable to the ion-gyrotime and have been associated with plasma jetting across the ambient magnetic field.[C1,C2] Called prompt striations in Reference C1, the linear analysis of these structures has previously been examined for an ion loss-cone velocity distribution function in the electrostatic limit.[C1,C3-C5] Reference C1 showed that the ion velocity distribution function attributed to the Buaro barium release was consistent with the linear growth of a purely growing, finite ion-gyroradius flute instability. Later, it was demonstrated that electron-ion collisions and cold background plasma always tend to stabilize the linear instability, but for the particular case of Buaro, were of insufficient magnitude to provide complete stability.[C4,C5]

In the ionosphere and magnetosphere, the ambient magnetic field strength can vary over a wide range. For example, in Buaro the ion kinetic pressure was much smaller than the magnetic field pressure; however, if a Buaro-like plasma had been injected into the magnetosphere the ion kinetic pressure would be larger than the magnetic field pressure. From a theoretical viewpoint the difference between the magnetic field strength in the ionosphere and magnetosphere implies that electromagnetic effects on waves are much more significant in the magnetosphere.

The purpose of this appendix is to include full electromagnetism into the linear analysis of purely growing, finite ion-gyroradius, flute instabilities. It is demonstrated that electromagnetic effects reduce the growth rate from the values calculated in the electrostatic limit. Stabilization by cold background plasma and thermal spread in the ion distribution function persists in the electromagnetic limit. The theory implies that a Buaro-like plasma injected into the magnetosphere may lead to prompt striation formation but only after the plasma has become sufficiently tenuous.

Subsequent portions of this appendix are divided in the following way. Section C-2 gives the calculation model. Section C-3 presents results from the numerical evaluation of the electromagnetic dispersion relation, and Section C-4 describes application of the theory to the ionosphere and magnetosphere. Section C-5 contains concluding remarks.

C-2. MODEL

As the basis for the calculation, an infinite and homogeneous quasi-neutral plasma model is assumed. Cold electrons and one singly ionized ion species constitute the plasma. Two different ion velocity distribution functions are permitted simultaneously in the plasma. The first assumes that ions are cold, while the second assumes a loss cone distribution of the following form:[C1,C4,C5]

$$f_i(\vec{v}) \equiv g(v_\perp)\, h(v_\parallel) = \frac{v_\perp\, \delta^3}{2\pi\, v_1^3\, A(\delta)} \exp\left(-\frac{(v_\perp - v_1)^2}{2v_{i1}^2}\right) h(v_\parallel) \quad (C.1)$$

with

$$A(\delta) = \left(\frac{\pi}{2}\right)^{\frac{1}{2}} \left\{(1 + \delta^2)\,[1 + \mathrm{erf}(\delta/\sqrt{2})] + \left(\frac{2}{\pi}\right)^{\frac{1}{2}} \delta \exp(-0.5\delta^2)\right\} ,$$

$$\delta = v_1/v_{i1} \quad . \quad (C.2)$$

In Eqs. (C.1) and (C.2), $v_\perp$ and $v_\parallel$ are the perpendicular and parallel velocities, respectively. The parameters v_1 and v_{i1} are constants. Because the present analysis deals with flute modes having no variation along the magnetic field, the dispersion relation is not sensitive to the precise form of the function, $h(v_\parallel)$, provided the integral of $h(v_\parallel)$ over parallel velocity is equal to one. Hence, the function, $h(v_\parallel)$, is left unspecified, and

$$1 = 2\pi \int_0^\infty dv_\perp\, v_\perp \int_{-\infty}^{\infty} dv_\parallel\, f_i(\vec{v}) \quad . \quad (C.3)$$

The wave electric fields are assumed to have the plane wave form appropriate for the flute approximation:

$$\vec{E}(x,y,z,t) = \vec{E}\,\exp[i(kx - \omega t)] \quad . \tag{C.4}$$

In Eq. (C.4) the x denotes the coordinate perpendicular to the background magnetic field and parallel to the wavenumber, k. The coordinate z lines in the magnetic field direction and the time is designated by t. The wave frequency is ω and $\vec{E}$ is a constant vector.

For the indicated plasma model, modes on the extraordinary branch of the dispersion relation with frequencies well below the electron-cyclotron of the dispersion relation satisfy:[C6]

$$0 = \begin{pmatrix} \varepsilon_{xx} & \varepsilon_{xy} \\ \varepsilon_{yx} & \varepsilon_{yy} - k^2c^2/\omega^2 \end{pmatrix} \begin{pmatrix} E_x \\ E_y \end{pmatrix} \tag{C.5}$$

with

$$\varepsilon_{xx} = 1 + \frac{\omega_{eo}^2 + \omega_{e1}^2}{\Omega_e^2} - \frac{\omega_{io}^2}{\omega^2 - \Omega_i^2} - \frac{\omega_{i1}^2}{\Omega_i^2}\, I_{xx}$$

$$\varepsilon_{xy} = -\varepsilon_{yx} = i\,\frac{\omega_{eo}^2 + \omega_{e1}^2}{\omega\Omega_e} - i\,\frac{\omega_{io}^2\,\Omega_i}{\omega(\omega^2 - \Omega_i^2)} - \frac{\omega_{i1}^2}{\Omega_i^2}\, I_{xy}$$

$$\varepsilon_{yy} = 1 + \frac{\omega_{eo}^2 + \omega_{e1}^2}{\Omega_e^2} - \frac{\omega_{io}^2}{\omega^2 - \Omega_i^2} - \frac{\omega_{i1}^2}{\Omega_i^2}\, I_{yy}$$

$$\omega_{eo}^2 = 4\pi n_o^2/m_e \quad , \quad \omega_{e1}^2 = (n_1/n_0)\omega_{eo}^2 \quad , \quad \omega_{io}^2 = 4\pi n_o^2/m_i \quad ,$$

$$\omega_{i1}^2 = (n_1/n_0)\omega_{io}^2 \quad , \quad \Omega_e = -eB/m_e c \quad , \quad \Omega_i = eB/m_i c$$

$$\begin{pmatrix} I_{x,x} & I_{x,y} \\ I_{y,x} & I_{y,y} \end{pmatrix} = 2\pi \frac{\Omega_i^2}{\omega} \int_0^\infty dv_\perp \, v_\perp^2 \frac{d[g(v_\perp)]}{dv_\perp} \sum_{p=-\infty}^{\infty}$$

$$\frac{1}{p\Omega_i - \omega} \begin{pmatrix} p^2 J_p^2(b_i)/b_i^2 & ip \, J_p(b_i) \, J_p'(b_i)/b_i \\ -ip \, J_p(b_i) \, J_p'(b_i)/b_i & J_p'(b_i) \, J_p'(b_i) \end{pmatrix}$$

$$b_i = kv_\perp/\Omega_i \quad . \tag{C.6}$$

In Eqs. (C.5) and (C.6), the x- and y-directed electric field amplitudes are represented by E_x and E_y, respectively. Subscripts o, 1, e, and i denote cold background, fast ion, electron and ion quantities, respectively. Various parameters influencing the dispersion relation are density (n), speed of light (c), magnitude of electron charge (e), background magnetic field strength (B), and mass (m). Bessel functions of the first kind and order p [i.e., $J_p(b_i)$] and their derivatives with respect to argument [$J_p'(b_i)$] play a significant role for the modes described by the dispersion relation.

The eigenvalue condition is obtained by setting the determinant of the matrix of coefficients in Eq. (C.5) equal to zero:

$$0 = \varepsilon_{xx}(\varepsilon_{yy} - k^2c^2/\omega^2) - \varepsilon_{yx} \, \varepsilon_{xy} \quad . \tag{C.7}$$

For purely growing modes with linear growth rate γ (i.e., $\omega = i\gamma$) and Alfven speeds much smaller than the speed of light, the dispersion relation can be rewritten as:

$$0 = \left[(1 + \bar{\rho}) \frac{m_e}{m_i} + \frac{\bar{\rho}}{1 + x^2} - I_{xx}\right]$$

$$x \left[(1 + \bar{\rho}) \frac{m_e}{m_i} + \frac{\bar{\rho}}{1 + x^2} - I_{yy} + \frac{k^2 c^2}{\omega_{i1}^2 x^2}\right]$$

$$+ \left[\frac{\bar{\rho}}{x(1 + x^2)} - \frac{1 + \bar{\rho}}{x} - I_{xy}\right]^2 \qquad \text{(C.8)}$$

with

$$\bar{\rho} = n_0/n_1 \quad , \qquad x = \gamma/\Omega_i \quad ,$$

$$\begin{pmatrix} I_{xx} & I_{xy} \\ I_{yx} & I_{yy} \end{pmatrix} = 4\pi \int_0^\infty dv_\perp \, v_\perp^2 \, \frac{d[g(v_\perp)]}{dv_\perp} \sum_{p=0}^{\infty} \frac{1}{p^2 + x^2}$$

$$\begin{pmatrix} p^2 J_p^2(b_i)/b_i^2 & ip^2 J_p(b_i) J_p'(b_i)/b_i x \\ -ip^2 J_p(b_i) J_p'(b_i)/b_i x & J_p'(b_i) J_p'(b_i) - 0.5 J_o'(b_i) J_o'(b_i) \delta_{p,o} \end{pmatrix} \qquad \text{(C.9)}$$

In Eq. (C.9), the symbol $\delta_{p,o}$ is equal to one for p=0 and is zero otherwise.

In the electrostatic limit with cold background plasma, the dispersion relation depends upon only four dimensionless parameters, $\bar{\rho}$, x, δ, and $kb_1 = kv_1/\Omega_i$. Equation (C.8) indicates that electromagnetic effects introduce a fifth dimensionless quantity, kc/ω_{i1}, into the dispersion relation and also shows that the electrostatic approximation is valid for:

$$0 = \varepsilon_{xx} \quad , \quad kc/\omega_{i1} \to \infty \quad . \tag{C.10}$$

It is useful to rewrite the dimensionless quantity found in electromagnetic but not electrostatic dispersion relations in the following way:

$$(kc/\omega_{i1})\ (\frac{\Omega_i}{kv_1}) = \left(\frac{B^2}{4\pi\ n_1 m_i v_1^2}\right) \equiv (\frac{1}{\beta_1})^{\frac{1}{2}} \quad . \tag{C.11}$$

Equation (C.8) can now be rewritten as:

$$\beta_1 = - b_1^2 \ \frac{(1 + \bar{\rho})\ \frac{m_e}{m_i} + \frac{\bar{\rho}}{1 + x^2} - I_{xx}}{\left(\frac{\bar{\rho}}{1 + x^2} - 1 - \bar{\rho} - xI_{xy}\right)^2 + x^2 \left[(1 + \bar{\rho})\ \frac{m_e}{m_i}\right.}$$

$$\left. + \frac{\bar{\rho}}{1 + x^2} - I_{xx}\right] \left[(1 + \bar{\rho})\ \frac{m_e}{m_i} + \frac{\bar{\rho}}{1 + x^2} - I_{yy}\right] \quad . \tag{C.12}$$

Equations (C.10) and (C.12) demonstrate that the electrostatic approximation is appropriate in the limit when the ion kinetic energy per unit volume is much smaller than the magnetic pressure (i.e., $\beta_1 << 1$).

Because it is aligned in the wavenumber direction, the E_x amplitude is associated with an electrostatic field component. However, E_y is a consequence of an inductive electric field. From Eq. (C.5) the electrostatic and electromagnetic electric field amplitudes are related by the expression:

$$E_x/E_y = -\varepsilon_{xy}/\varepsilon_{xx} \quad . \tag{C.13}$$

In addition to the x- and y-directed electric fields, Faraday's law implies the presence of a z-directed inductive magnetic field with amplitude

$$B_z = -i(kc/\gamma)\, E_y \quad . \tag{C.14}$$

C-3. RESULTS

To determine the effect of finite β_1 on purely growing finite ion-gyroradius flute instabilities, the dispersion relation, Eq. (C.12), has been evaluated in terms of the critical parameters, x, kb_1, δ, and $\bar{\rho}$. Results of the explicit evaluation are summarized in Figures C.1 - C.4.

Figures C.1a and C.1b are plots of maximum values for β_1 versus δ for different values of $\bar{\rho}$. The numerical calculations indicate that solutions for positive β_1 are possible only if $\epsilon_{xx} < 0$, which requires that $J_0(kb_1) J_1(kb_1) < 0$. The difference between Figures C.1a and C.1b arises because they correspond to the first interval of negative J_0J_1 (i.e., $2.5 \lesssim kb_1 < 3.8$) and the second interval of negative J_0J_1 (i.e., $5.6 < kb_1 < 7.0$), respectively. The value of $(\beta_1)_{max}$ depends on kb_1. For Figures C.1a and C.1b, it occurs for $kb_1 \sim 3.0 - 3.2$ and $6.2 - 6.4$, respectively.

Both Figures C.1a and C.1b demonstrate that cold background plasma decreases the maximum beta permitting instability. Specifically, there is complete stability for the conditions given by Figure C.1a for $\bar{\rho} \gtrsim .06$ and in Figure C.1b for $\bar{\rho} \gtrsim .02$. This result is consistent with the cold plasma stabilization found in the electrostatic limit.

Figures C.1a and C.1b also show that for specified values of $\bar{\rho}$ the maximum value of β_1 which permits instability increases with δ. Because larger values of δ imply that the loss cone ion distribution function is more peaked and more free energy is available for instability, this result suggests that finite β_1 decreases the tendency for instability. Indeed, the numerical calculations show that for fixed kb_1, δ, and $\bar{\rho}$, growth rate decreases as β_1 increases. Maximum growth rate occurs in the electrostatic limit with $\epsilon_{xx} = 0$, while at marginal stability the maximum β_1 consistent with solution of the dispersion relation is obtained. This property of the solutions is clearly illustrated in Figure C.2 which is a plot of maximum β_1 versus γ/Ω_i for $\bar{\rho} = 0$, $kb_1 = 3.2$, and for three different values of δ.

Thus far the numerical evaluation of the full electromagnetic dispersion relation has demonstrated that electromagnetic effects along with cold plasma tend to stabilize purely growing, finite ion-gyroradius, flute

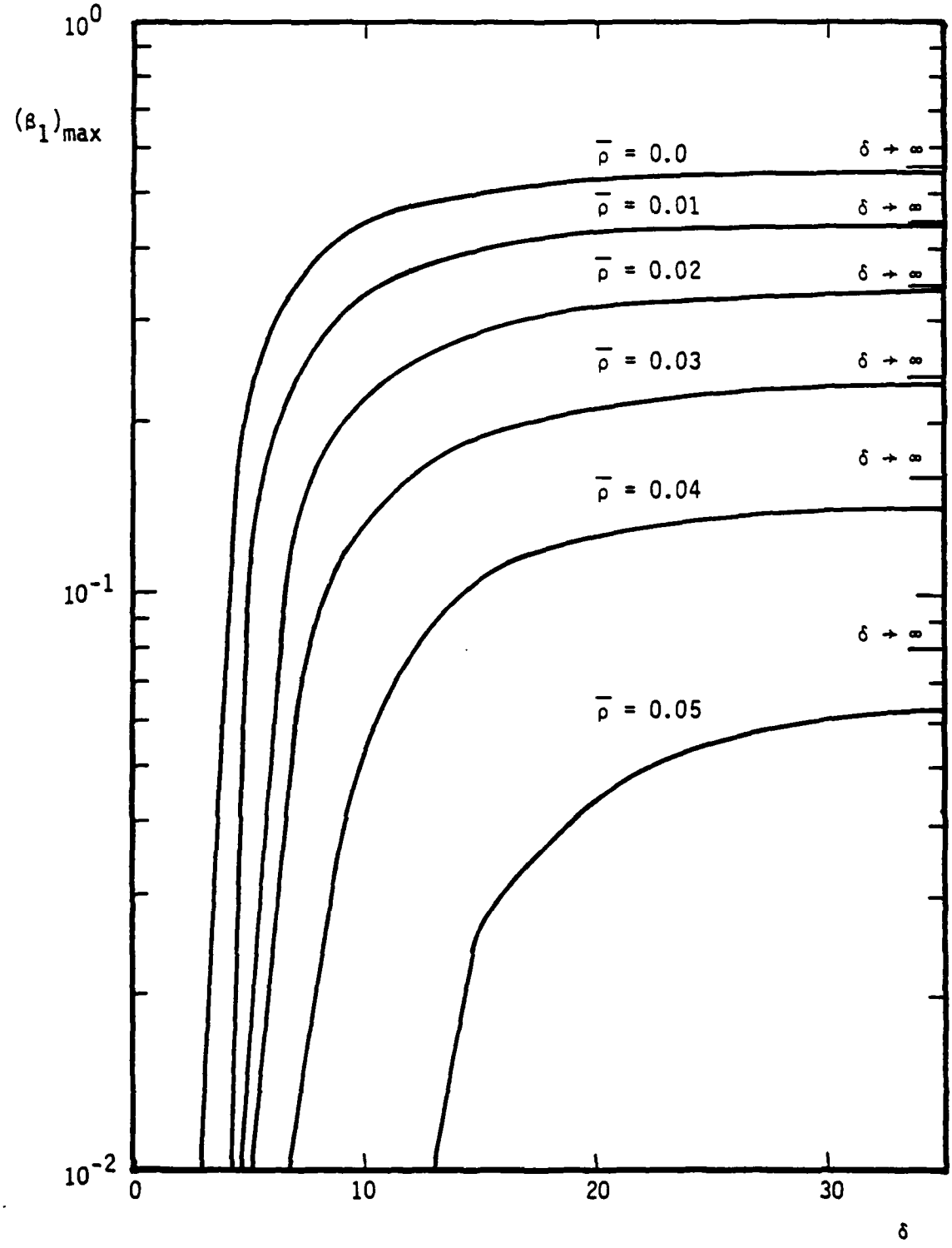

Figure C.1a. $(\beta_1)_{max}$ versus δ for various values of $\bar{\rho}$ and $2.5 \lesssim k_\perp b_i \lesssim 3.8$. $(\beta_1)_{max}$ for $\delta \to \infty$ is shown on the right-hand portion of each curve.

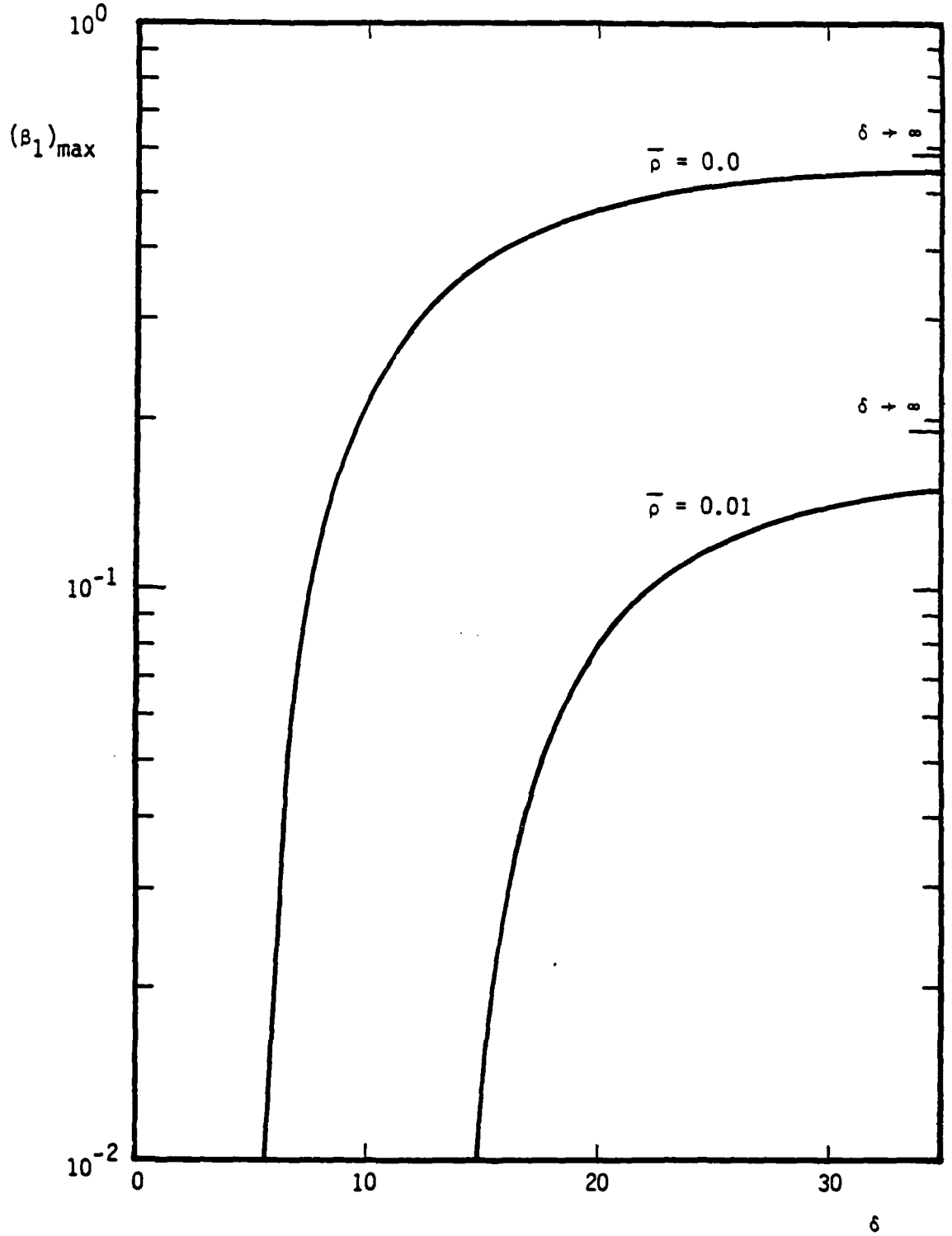

Figure C.1b. $(\beta_1)_{max}$ versus δ for various values of $\bar{\rho}$ and $5.6 \lesssim k_\perp b_i \lesssim 7.0$. $(\beta_1)_{max}$ for $\delta \to \infty$ is shown on the right-hand portion of each curve.

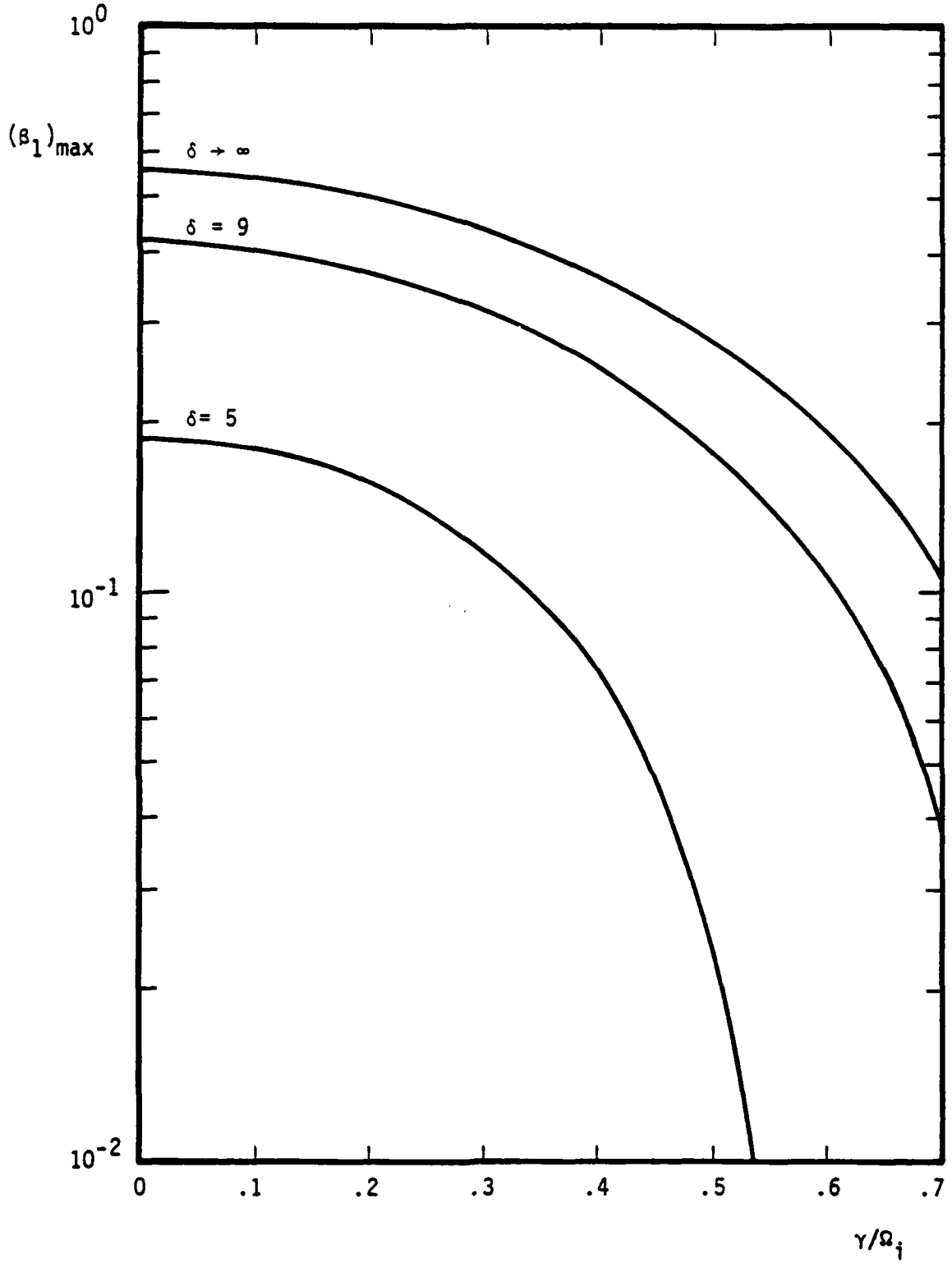

Figure C.2. $(\beta_1)_{max}$ versus γ/Ω_i for $\bar{\rho} = 0.0$, $kb_1 = 3.2$, and $\delta = 5$, 9, and ∞.

instabilities. However, the relationship between the inductive and electrostatic electric fields needs to be quantified in order to ascertain whether or not electromagnetic effects appreciably modify the wave electric field polarization. Mathematically, Eq. (C.13) must be evaluated as a function of $\bar{\rho}$, x, kb_1, and δ. A typical result of the calculation is presented in Figure C.3, which is a plot of the maximum ratio of the magnitude of E_y/E_x (i.e., $|E_y/E_x|_{max}$) versus δ for three values of $\bar{\rho}$ and $2.5 < kb_1 < 3.8$. The qualitative features of the instability for other ranges of kb_1 permitting $\varepsilon_{xx} < 0$ are similar to the results being presented. The figure shows that even though electromagnetic effects are included in the dispersion relation, the wave electric fields associated with the instability are of a dominantly electrostatic character (i.e., $|E_y/E_x|_{max} \lesssim 0.015$). Moreover, this property of the modes becomes more apparent as the instability becomes less vigorous either because cold plasma density increases or δ decreases.

Figure C.4 is a plot of $|E_y/E_x|_{max}$ versus γ/Ω_i for $\delta = 5$, $\bar{\rho} = 0.0$, and $kb_1 = 3.2$. The figure illustrates a typical feature of the instability, i.e., peak values of $|E_y/E_x|_{max}$ occur for a growth rate intermediate between marginal instability and the maximum possible growth rate for specified δ, $\bar{\rho}$, and kb_1. The physical reason for this characteristic of the instability solutions is twofold. First, near marginal stability ion and electron "polarization" currents are much smaller than the electron EXB current (i.e., $|\varepsilon_{xy}| >> |\varepsilon_{xx}|$). Second, at the maximum growth rate for specified δ, $\bar{\rho}$, and kb_1, the instability is purely electrostatic and $\varepsilon_{xx} = 0$.

Having demonstrated that the instability electric fields are of primarily electrostatic character, it becomes evident from Eq. (C.14) that:

$$1 << |B_z/E_y| = (\omega_{i1}/\Omega_i)\, kb_1 (x\beta_1)^{-1} \quad . \tag{C.15}$$

So the most significant implication of electromagnetic effects on wave fields is to permit the B_z field. Associated with this wave magnetic field is the instability nature to persist for a range of finite β_1, albeit with a reduced growth rate as compared to the purely electrostatic instability.

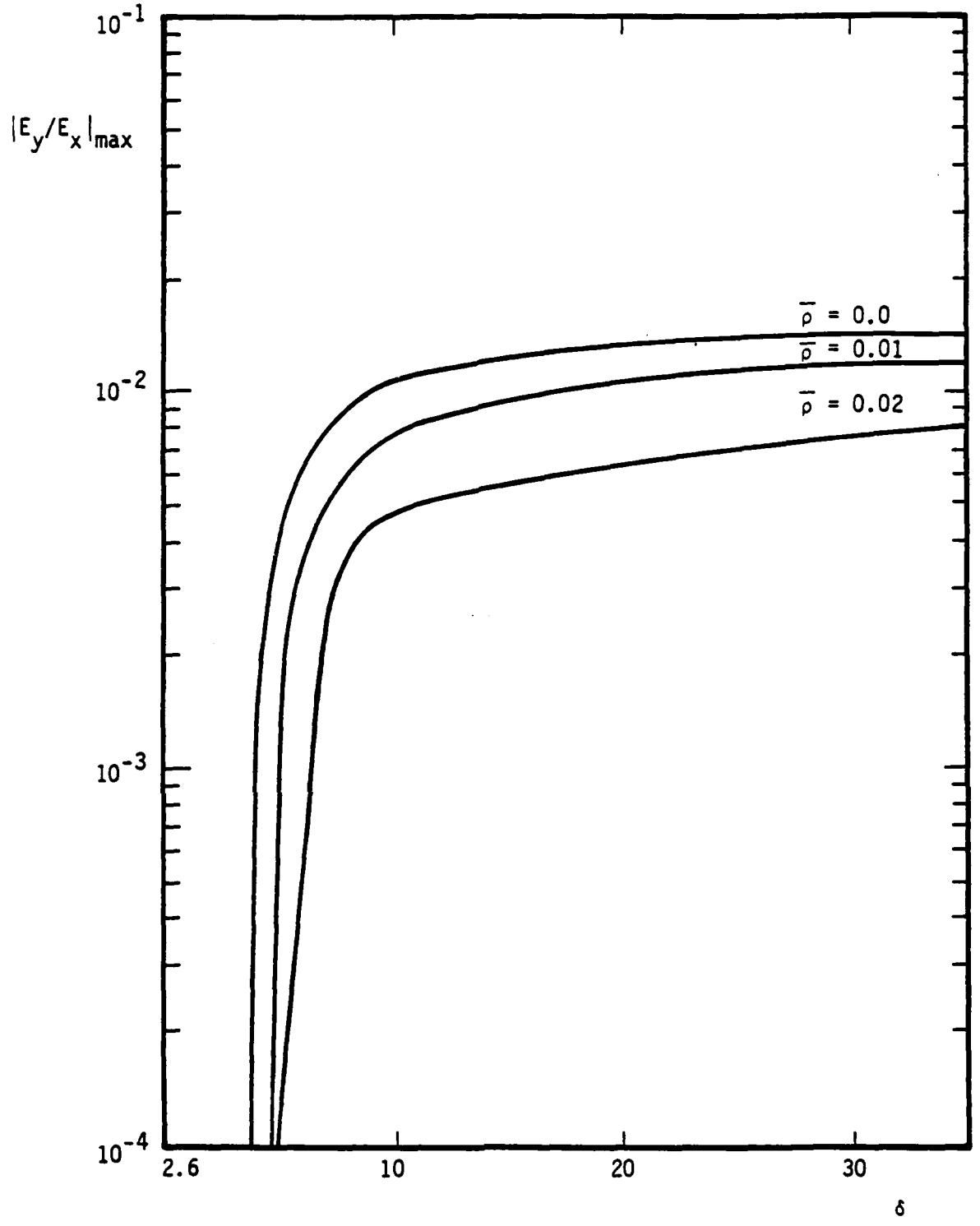

Figure C.3. $|E_y/E_x|_{max}$ versus δ for $2.5 < kb_1 < 3.8$ and $\bar{\rho}$ = 0.0, 0.01, and 0.02.

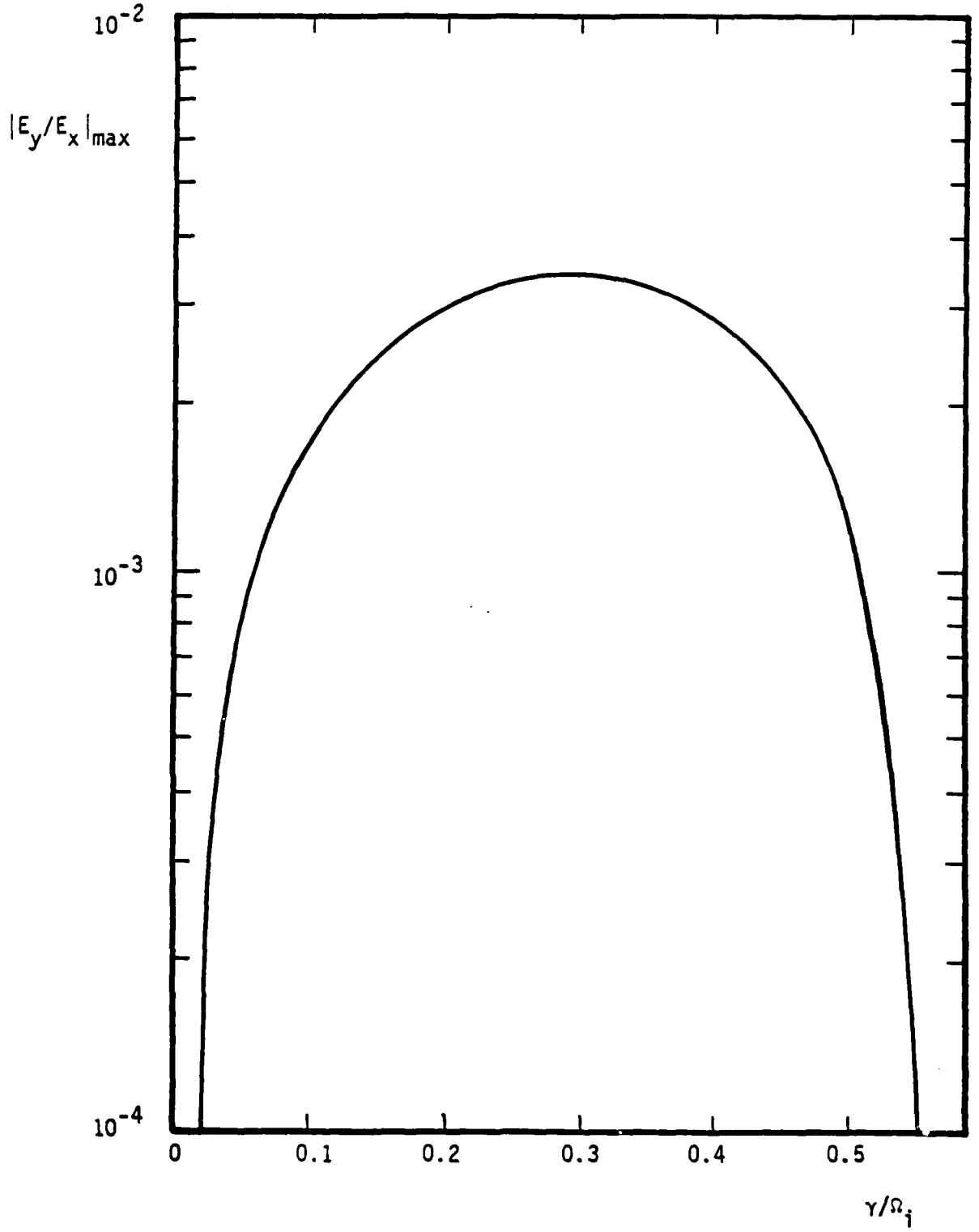

Figure C.4. $|E_y/E_x|_{max}$ versus γ/Ω_i for $kb_1 = 3.2$, $\delta = 5$, and $\bar{\rho} = 0.0$.

C-4. APPLICATION OF THE THEORY

Injection of plasma across the magnetic field in the ionosphere can lead to the formation of field aligned structures (striations) with dimensions transverse to the magnetic field which are smaller than the inverse ion-gyroradius. In particular, the Buaro shaped barium release at 400 kilometers altitude demonstrated that these prompt striations can be formed on a time scale comparable to the barium ion-gyrotime.[C1] The electrostatic approximation is well justified for the Buaro experiment because $n_1 \approx 4 \times 10^5$ cm^{-3}, $\delta = 5$, $\bar{\rho} \approx .009$, $v_1 \approx 1 \times 10^6$ cm/sec, and $B \approx .32$ gauss implies that $\beta_1 \approx 0.01$ which is an order of magnitude smaller than the maximum value of β_1 (i.e., 0.1), permitting instability for $\delta = 5$ and $\bar{\rho} = 0.01$ (see Figure C.1a).

It is instructive to calculate the minimum altitude at which complete electromagnetic stabilization of the loss cone mode would take place for Buaro plasma parameters. For this estimate it is assumed that the earth, with an approximate radius of 6.38×10^3 km, has a pure dipole magnetic field with a dipole moment of 8×10^{25} gauss-cm^3.[C7] Now Figure C.1a shows that complete electromagnetic stabilization of the flute mode for $\delta = 5$ occurs if $\beta_1 \gtrsim 0.2$. For the Buaro plasma parameters and the model dipole field, this stabilization corresponds to $B \lesssim 0.08$ gauss at equatorial altitudes above 3.6×10^3 kilometers. It follows that shaped barium injection with plasma parameters comparable to Buaro will not permit the formation of striations by the finite ion-gyroradius, purely growing, flute instability in most of the magnetosphere.

Although the purely growing instability may not develop initially for shaped barium injection in the magnetosphere, it could develop later as the plasma density decreases. For example, consider shaped barium injection across a magnetic field with strength, 1.6×10^{-3} gauss, at an altitude of 3.15×10^4 km. (The indicated parameters are those of an earlier magnetospheric release[C8].) Assuming that $\delta = 5$ and $v_1 \approx 1.0 \times 10^6$ cm/sec, the maximum barium density which permits kinetic flute mode growth is $n_1 \approx 1.8 \times 10^2$ cm^{-3}. For a background proton density of 16 cm^{-3},[C8] $n_1 \approx 1.8 \times 10^2$ cm^{-3} implies $\bar{\rho} < .001$ and stabilization by background plasma is ineffective.

C-5. CONCLUDING REMARKS

Purely growing, finite ion-gyroradius, flute modes have been postulated to be the cause of prompt striations in a shaped barium release across the magnetic field in the ionosphere.[C1] Electromagnetic effects have been included in the stability analysis of the flute modes in order to ascertain their impact on linear growth. Although inductive electric fields are much smaller than the electrostatic fields under all circumstances, electromagnetic effects nevertheless do modify the wave fields by introducing a parallel wave magnetic field not present in the electrostatic limit. When electromagnetic effects are appreciable, the ratio of ion inertial pressure to magnetic field pressure, β_1, is finite. Under such circumstances, the linear instability growth rate is smaller than it would be in the electrostatic limit with $\beta_1 \to 0$. In short, finite β_1 tends to stabilize the mode. As in the electrostatic limit, cold plasma and spread in the ion loss cone distribution function also inhibit growth.

Application of the analysis to shaped barium release in the ionosphere and magnetosphere has demonstrated that for a specific ion velocity distribution function the total ion density must be less than a specific value in order that finite beta stabilization can be circumvented. In particular, for an ion loss cone distribution function like the one in the Buaro shaped barium release, densities less than the Buaro barium ion density of 4×10^5 cm^{-3} are necessary for the kinetic flute instability to be operative in environments with $B \lesssim .08$ gauss corresponding to magnetic equatorial altitudes $\gtrsim 3.6 \times 10^3$ km. Similarly, an example appropriate to the magnetic field strength and altitude of the magnetospheric barium release[C8] has indicated that barium ion densities less than 1.8×10^2 cm^{-3} are necessary for the kinetic flute mode to be unstable. These examples suggest that in a weak magnetic field environment, the kinetic flute instability might be operative, not initially, but only later as plasma becomes more tenuous and finite beta stabilization is reduced. Moreover, even when the instability is effective, finite ion inertial effects can reduce the growth rate in a weak ambient magnetic field environment.

AD-A123 630 CERTAIN EFFECTS OF PLASMA JETTING ACROSS AND ALONG MAGNETIC FIELDS(U) JAYCOR SAN DIEGO CA J L SPERLING ET AL. 30 APR 81 JAYCOR-J510-81-028 2/2

UNCLASSIFIED DNA-5740F DNA001-79-C-0050 F/G 4/1 NL

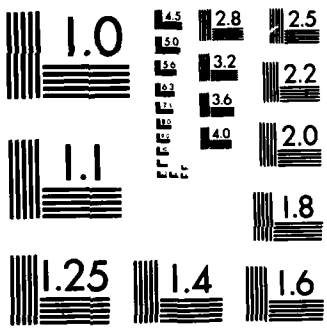

REFERENCES

C1. Simons, D. J., Pongratz, M. B., and Gary, S. P., "Prompt Striations in Ionospheric Barium Clouds due to a Velocity Space Instability," J. Geophys. Res., 85, p. 671, 1980.

C2. McDonald, B. E., Keskinen, M. J., Ossakow, S. L., and Zalesak, S. T., "Computer Simulation of Gradient Drift Instability Processes in Operation Avefria," J. Geophys. Res., 85, p. 2143, 1980.

C3. Swift, D. W., "Turbulent Generation of Electrostatic Fields in the Magnetosphere," J. Geophys. Res., 82, p. 5143, 1977.

C4. Sperling, J. L. and Krall, N. A., "Electron-ion Collision Effects on the Formation of Prompt Striations in the Ionosphere," J. Geophys. Res., 86, p. 5726, 1981.

C5. Sperling, J. L. and Krall, N. A., "Stabilization of Electrostatic, Purely Growing, Finite Ion-gyroradius, Flute Instabilities in the Ionosphere," J. Geophys. Res., 86, p. 7513, 1981.

C6. Stix, T. H., "The Theory of Plasma Waves," McGraw-Hill, New York, 1962.

C7. Brandt, J. C. and Hodge, P., "Solar System Astrophysics," McGraw-Hill, New York, Ch. 18, 1964.

C8. Mende, S. B., "Morphology of the Magnetospheric Barium Release," J. Geophys. Res., 78, p. 5751, 1973.

DISTRIBUTION LIST

DEPARTMENT OF DEFENSE

Defense Nuclear Agency
ATTN: NATD
ATTN: RAEE
ATTN: STNA
ATTN: NAFD
3 cy ATTN: RAAE
4 cy ATTN: TITL

Defense Tech Info Ctr
12 cy ATTN: DD

Field Command
Defense Nuclear Agency
ATTN: FCPR, J. McDaniel

Field Command
Defense Nuclear Agency
Livermore Br
ATTN: FC-1

DEPARTMENT OF THE ARMY

BMD Advanced Tech Ctr
ATTN: ATC-T, M. Capps

DEPARTMENT OF THE NAVY

Naval Research Laboratory
ATTN: Code 6780, S. Ossakow
ATTN: Code 7550, J. Davis
ATTN: Code 7950, J. Goodman
ATTN: Code 4700
ATTN: Code 6700
ATTN: Code 4187
ATTN: Code 4780
ATTN: Code 7500, B. Wald

Office of Naval Rsch
ATTN: Code 412, W. Condell
ATTN: Code 414, G. Joiner

DEPARTMENT OF THE AIR FORCE

Air Force Geophysics Lab
ATTN: OPR, H. Gardiner
ATTN: OPR-1
ATTN: LKB, K. Champion
ATTN: CA, A. Stair
ATTN: R. O'Neil
ATTN: PHP
ATTN: PHI, J. Buchau
ATTN: R. Babcock

Air Force Weapons Lab
ATTN: NTYC
ATTN: SUL
ATTN: NTN

Air Weather Service, MAC
ATTN: DNXP

Rome Air Development Ctr
ATTN: OCS, V. Coyne
ATTN: TSLD

OTHER GOVERNMENT AGENCY

Department of Commerce
National Bureau of Standards
ATTN: Sec Ofc for R. Moore

DEPARTMENT OF ENERGY CONTRACTORS

EG&G, Inc
ATTN: J. Colvin
ATTN: D. Wright

University of California
Lawrence Livermore National Lab
ATTN: L-389, R. Ott
ATTN: L-31, R. Hager
ATTN: Tech Info Dept Library

Los Alamos National Lab
ATTN: T. Kunkle, ESS-5
ATTN: MS 670, J. Hopkins
ATTN: C. Westervelt
ATTN: D. Simons
ATTN: J. Wolcott
ATTN: R. Jeffries
ATTN: P. Keaton
ATTN: MS 664, J. Zinn

DEPARTMENT OF DEFENSE CONTRACTORS

Berkeley Rsch Associates, Inc
ATTN: J. Workman

ESL, Inc
ATTN: J. Marshall

General Rsch Corp
ATTN: J. Ise, Jr

JAYCOR
4 cy ATTN: J. Sperling
4 cy ATTN: N. Krall

Kaman Sciences Corp
ATTN: T. Stephens

Kaman Tempo
ATTN: DASIAC
ATTN: W. Knapp
ATTN: W. McNamara

M.I.T. Lincoln Lab
ATTN: D. Towle

Mission Rsch Corp
ATTN: Tech Library
ATTN: F. Fajen
ATTN: R. Kilb
ATTN: R. Hendrick
ATTN: R. Bogusch
ATTN: S. Gutsche

Pacific-Sierra Rsch Corp
ATTN: H. Brode, Chairman SAGE

DEPARTMENT OF DEFENSE CONTRACTORS (Continued)

Photometrics, Inc
ATTN: I. Kofsky

Physical Dynamics, Inc
ATTN: E. Fremouw

R & D Associates
ATTN: H. Ory
ATTN: W. Karzas
ATTN: B. Gabbard
ATTN: R. Turco
ATTN: F. Gilmore
ATTN: M. Gantsweg
ATTN: R. Lelevier
ATTN: C. Greifinger
ATTN: W. Wright
ATTN: P. Haas

R & D Associates
ATTN: B. Yoon

Science Applications, Inc
ATTN: L. Linson
ATTN: E. Straker
ATTN: C. Smith
ATTN: D. Hamlin

DEPARTMENT OF DEFENSE CONTRACTORS (Continued)

Santa Fe Corp
ATTN: D. Paolucci

SRI International
ATTN: A. Burns
ATTN: G. Price
ATTN: R. Tsunoda
ATTN: J. Vickrey
ATTN: V. Gonzales
ATTN: D. Neilson
ATTN: R. Livingston
ATTN: J. Petrickes
ATTN: D. McDaniels
ATTN: M. Baron
ATTN: G. Smith
ATTN: W. Jaye
ATTN: W. Chesnut
ATTN: R. Leadabrand
ATTN: C. Rino
ATTN: R. Hake, Jr

Technology International Corp
ATTN: W. Boquist

END

FILMED

2-83

DTIC